**Department of Energy**
Office of Civilian Radioactive Waste Management
Yucca Mountain Site Characterization Office
P.O. Box 30307
North Las Vegas, NV 89036-0307

QA: N/A

OCT 12 2001

OVERNIGHT MAIL

C. William Reamer, Chief
High-Level Waste Branch
Division of Waste Management
Office of Nuclear Materials Safety
and Safeguards
U.S. Nuclear Regulatory Commission
Two White Flint North
Rockville, MD 20852

TRANSMITTAL OF REPORTS ADDRESSING KEY TECHNICAL ISSUES (KTI)

This letter transmits the following KTI agreement items, due to be provided to the U.S. Nuclear Regulatory Commission (NRC) in the Fiscal Year (FY) 2001, on compact disc (enclosure 1) and in hard copy (enclosure 2).

ANL-EBS-GS-000001, Analysis and Model Report (AMR) - Geochemistry Model Validation Report: Material Degradation and Release Model (CLST.5.04, ENFE.5.03, RT.4.03). The report presents the model for estimating the long-term geochemical behavior of waste packages and waste forms, specifically (1) the extent to which criticality control materials remain in the waste package, (2) the extent to which fissile material will be carried out of the waste package by infiltrating water, and (3) the chemical composition and amounts of minerals and other solids left in the waste package. This model validation report incorporates the lessons learned from the recent model validation issues raised by NRC.

ANL-EBS-GS-000002, AMR - Geochemistry Model Validation Report: External Accumulation Model (CLST.5.04, ENFE.5.03, RT.4.03). The External Accumulation Model predicts the accumulation of fissile material in fractures and voids in the rock beneath a degraded waste package. This model validation report incorporates the lessons learned from the recent model validation issues raised by NRC



NMSSOR
WM-11

List and Schedule for Model Validation Reports related to Criticality (CLST.5.04, ENFE.5.03, RT.4.03). Note that the list of scheduled reports includes the original list of 17 reports (as provided to NRC at the October 2000 Criticality Technical Exchange), the new consolidated list of reports, and the expected delivery dates of the reports to the NRC. The estimated completion dates noted in the list are subject to change as a result of future planning.

CAL-EBS-NU-000017, Calculation - Radiolytic Species Generation from Internal Waste Package Criticality (CLST.5.05). This report addresses the development of information on accelerated corrosion rates for Zircaloy due to radiolytic chemical specie generation (primarily nitric acid) during postulated static criticality events. The focus of the calculation is increased nitric acid produced by a criticality. A white paper, included as an attachment to the current calculation, addresses the issue of how the nitric acid may effect corrosion rates. Based on the amount of nitric acid produced, scavenging effects in corrosion products are expected to prevent sufficient accumulation of nitric acid to significantly affect corrosion rates. A final assessment (geochemistry evaluation) will be performed prior to license application to confirm these expectations, as per the existing agreement (CLST 5.05).

Letter Report – Excavation-Induced Failures (SDS.3.03). This report documents the U.S. Geological Survey (USGS) observations of excavation-induced fractures in the Exploratory Studies Facility and the Enhanced Characterization of the Repository Block Cross Drift.

Five additional documents due in FY 2001 have been delayed. Four of these are in final review and are expected to be available in November 2001. These include:

Crushed Tuff Hydrothermal Column Experiment Report (ENFE.2.12)

Mean vs Median Justification (SDS.1.02, SDS.2.03)

ANL-EBS-MD-000049, AMR - Multiscale Thermohydrologic Model (TEF.2.09)

USGS Regional Model (USFIC.5.09)

The remaining document, ANL-EBS-MD-000030, AMR - Ventilation Model (RDTME.3.01, TEF.2.07), has been delayed to resolve technical issues, and expected to be available in January 2002.

The above has been discussed with James W. Anderson, of your staff. Please direct any questions concerning this letter and its enclosures to Timothy C. Gunter at (702) 794-1343.

Stephan Brocoum
Assistant Manager, Office of
Licensing and Regulatory Compliance

OL&RC:TCG-0018

Enclosures:
1. CD Containing Criticality KTIs, Excavation Induced Fractures
2. Hard Copy of Enclosure 1

cc w/encl 1:
J. W. Anderson, NRC, Rockville, MD
M. M. Comar, NRC, Rockville, MD
D. D. Chamberlain, NRC, Arlington, TX
R. M. Latta, NRC, Las Vegas, NV
S. H. Hanauer, DOE/HQ (RW-2) FORS
B. J. Garrick, ACNW, Rockville, MD
Richard Major, ACNW, Rockville, MD
W. D. Barnard, NWTRB, Arlington, VA
Budhi Sagar, CNWRA, San Antonio, TX
W. C. Patrick, CNWRA, San Antonio, TX
Steve Kraft, NEI, Washington, DC
J. H. Kessler, EPRI, Palo Alto, CA
J. R. Curtiss, Winston & Strawn, Washington, DC
R. R. Loux, State of Nevada, Carson City, NV
John Meder, State of Nevada, Carson City, NV
Alan Kalt, Churchill County, Fallon, NV
Irene Navis, Clark County, Las Vegas, NV
Harriet Ealey, Esmeralda County, Goldfield, NV
Leonard Fiorenzi, Eureka County, Eureka, NV
Andrew Remus, Inyo County, Independence, CA
Michael King, Inyo County, Edmonds, WA
Mickey Yarbro, Lander County, Battle Mountain, NV
Jason Pitts, Lincoln County, Caliente, NV
L. W. Bradshaw, Nye County, Pahrump, NV
Geneva Hollis, Nye County, Tonopah, NV
Josie Larson, White Pine County, Ely, NV
Judy Shankle, Mineral County, Hawthorne, NV

cc w/encl 1: (continued)
R. I. Holden, National Congress of American Indians, Washington, DC
Allen Ambler, Nevada Indian Environmental Coalition, Fallon, NV

cc w/o encls:
N. K. Stablein, NRC, Rockville, MD
D. J. Brooks, NRC, Rockville, MD
W. L. Belke, NRC, Las Vegas, NV
L. H. Barrett, DOE/HQ (RW-1) FORS
A. B. Brownstein, DOE/HQ (RW-52) FORS
R. A. Milner, DOE/HQ (RW-2) FORS
C. E. Einberg, DOE/HQ (RW-52) FORS
N. H. Slater, DOE/HQ (RW-52) FORS
S. J. Cereghino, BSC, Las Vegas, NV
N. H. Williams, BSC, Las Vegas, NV
K. M. Cline, MTS, Las Vegas, NV
R. B. Bradbury, MTS, Las Vegas, NV
R. P. Gamble, MTS, Las Vegas, NV
R. C. Murray, MTS, Las Vegas, NV
R. D. Rogers, MTS, Las Vegas, NV
Richard Goffi, BAH, Washington, DC
G. W. Hellstrom, DOE/YMSCO, Las Vegas, NV
S. P. Mellington, DOE/YMSCO, Las Vegas, NV
R. E. Spence, DOE/YMSCO, Las Vegas, NV
V. F. Iorii, DOE/YMSCO, Las Vegas, NV
Stephan Brocoum, DOE/YMSCO, Las Vegas, NV
D. R. Williams, DOE/YMSCO, Las Vegas, NV
A. V. Gil, DOE/YMSCO, Las Vegas, NV
T. C. Gunter, DOE/YMSCO, Las Vegas, NV
C. L. Hanlon, DOE/YMSCO, Las Vegas, NV
E. T. Smistad, DOE/YMSCO, Las Vegas, NV
K. D. Lachman, DOE/YMSCO, Las Vegas, NV
D. H. Coleman, DOE/YMSCO, Las Vegas, NV
J. T. Sullivan, DOE/YMSCO, Las Vegas, NV
C. A. Kouts, DOE/YMSCO (RW-2) FORS
R. N. Wells, DOE/YMSCO (RW-60) Las Vegas, NV
OL&RC Library
Records Processing Center = " "
(ENCLS = READILY AVAILABLE)

# OFFICE OF CIVILIAN RADIOACTIVE WASTE MANAGEMENT
# REGULATORY RESPONSE REVIEW RECORD

QA:

| Project: | Department/Group: |
|---|---|
| Repository Design | Waste Pacakge Criticality |

1. Initiating Reference (e.g., E-mail, telephone call, verbal request, DOE/NRC meeting, letter from NRC, other government agency or client):
NRC/DOE Key Technical Issue agreements CLST.5.04, ENFE.5.03, and RT.4.03.

2. Scope and Description of Issue (Problem statement and key elements of the response: facts, discussion, intended actions, or BSC position):
Provide the list of model validation reports and their schedule. The model validation reports for criticality analysis are planned to be completed between FY01 and FY05. The exact dates are subject to changes in funding levels. The dates provided in the list are based on the dates in P3 as of September 14th, 2001. These dates, especially those in FY03 and beyond, are subject to change with changing budgets and funding levels. The transmittal letter for this list is to note this.

3. Documents Used in Response Development (e.g., specifications, drawings, calculations, studies, etc.):
List and Scheduleof Model Validation Reports.

| 4. Originator: | Date: | 5. Reviewer: | Date: |
|---|---|---|---|
| | 09/28/2001 | | 9.28.01 |

## 6. CONCURRENCE

| Science and Analysis | | Functional Staff | | Other | |
|---|---|---|---|---|---|
| Project Manager: | Date: | Engineering: | Date: | | Date: |
| | | Chief Science Officer: | Date: | | Date: |
| **Repository Design** | | | | | |
| Project Manager: FOR | Date: 9-28-01 | Quality Assurance: | Date: | | |
| **Program Integration** | | | | | |
| Manager: | Date: | | | | |

## 7. APPROVALS

| Project Manager: | License Application Project SME: | Project Manager, License Application Project: |
|---|---|---|
| | | |

# LIST AND SCHEDULE OF MODEL VALIDATION REPORTS

| Original List of Reports | Consolidated List | Expected Delivery Date to NRC |
|---|---|---|
| 1. Geochemistry Model Validation Report: Material Accumulation and Transport | 1.Geochemistry Model Validation Report: External Accumulation Model, Rev 0 | Sep 01 |
| | Rev 1 | Dec 03 |
| 2. Geochemistry Model Validation Report: Material Degradation and Release | 2.Geochemistry Model Validation Report: Material Degradation and Release, Rev 0 | Sep 01 |
| | Rev 1 | Sep 04 |
| 3. Configuration Generator Model Validation Report: CSNF Waste Packages | 3. Configuration Generator Model Validation Report:: Internal Configurations<br>Rev 0 (CSNF) | Jul 02 |
| 4. Configuration Generator Model Validation Report: DOE-SNF Codisposal Waste Packages | Rev 1 (DOE SNF) | Dec 03 |
| 5. Configuration Generator Model Validation Report: Immobilized Pu Codisposal Waste Packages | Rev 2 (IPWF) | Sep 04 |
| 6. Configuration Generator Model Validation Report: Near-Field/In Drift Configurations | 4. Configuration Generator Model Validation Report: External Configurations<br>Rev 1 (Near-Field/In-Drift) | Aug 04 |
| 7. Configuration Generator Model Validation Report: Far-Field Configurations | Rev 0 (Far-Field) | Apr 04 |
| 8. Criticality Model Validation Report: PWR | 5. Criticality Model Validation Report: Internal<br>Rev 0 (PWR) | Dec 02 |
| 9. Criticality Model Validation Report: BWR | Rev 1 (BWR) | Oct 03 |
| 10. Criticality Model Validation Report: DOE SNF Codisposal | Rev 2 (DOE SNF) | Jan 04 |
| 11. Criticality Model Validation Report: Immobilized Plutonium Codisposal | Rev 3 (IPWF) | Sep 04 |
| 12. Criticality Model Validation Report: External | 6. Criticality Model Validation Report: External | Apr 04 |
| 13. Isotopics Model Validation Report: PWR | 7. Isotopics Model Validation Report<br>Rev 0 (PWR) | Nov 02 |
| 14. Isotopics Model Validation Report: BWR | Rev 1 (BWR) | Dec 03 |
| 15. Steady-State Criticality Consequence Model Validation Report: Internal and External | 8. Steady-State Criticality Consequence Model Validation Report: Internal and External | Dec 02 |
| 16. Transient Criticality Consequence Model Validation Report: Internal | 9. Transient Criticality Consequence Model Validation Report<br>Rev 0 (Internal) | Dec 03 |
| 17. Transient Criticality Consequence Model Validation Report: External | Rev 1 (External) | May 04 |

OFFICE OF CIVILIAN RADIOACTIVE WASTE MANAGEMENT

ANALYSIS/MODEL COVER SHEET

*Complete Only Applicable Items*

1. QA: QA

Page: 1 of: 66

2. ☐ Analysis — Check all that apply

| | | |
|---|---|---|
| Type of Analysis | ☐ | Engineering |
| | ☐ | Performance Assessment |
| | ☐ | Scientific |
| Intended Use of Analysis | ☐ | Input to Calculation |
| | ☐ | Input to another Analysis or Model |
| | ☐ | Input to Technical Document |
| | ☐ | Input to other Technical Products |

Describe use:

3. ☒ Model — Check all that apply

| | | | | |
|---|---|---|---|---|
| Type of Model | ☐ | Conceptual Model | ☐ | Abstraction Model |
| | ☐ | Mathematical Model | ☐ | System Model |
| | ☒ | Process Model | | |
| Intended Use of Model | ☒ | Input to Calculation | | |
| | ☒ | Input to another Model or Analysis | | |
| | ☒ | Input to Technical Document | | |
| | ☒ | Input to other Technical Products | | |

Describe use:

To predict the degradation and release of radionuclides from a degrading waste package.

4. Title:

Geochemistry Model Validation Report: Material Degradation and Release Model

5. Document Identifier (including Rev. No. and Change No., if applicable):

ANL-EBS-GS-000001 REV 00

6. Total Attachments:

Three

7. Attachment Numbers - No. of Pages in Each:

I (CD-ROM), II(5), III(2)

| | Printed Name | Signature | Date |
|---|---|---|---|
| 8. Originator | Harlan Stockman, Kaveh Zarrabi, Emma Parker, and Susan LeStrange | Susan LeStrange | 9/28/01 |
| 9. Checker | Paul Domski (technical)<br>Kristine Dutton (compliance) | FOR PAUL DOMSKI<br>Kristine Dutton | 9/28/01<br>9/28/01 |
| 10. Lead/Supervisor | Susan LeStrange | Susan LeStrange | 9/28/01 |
| 11. Responsible Manager | Daniel Thomas | | 09/28/2001 |

12. Remarks:

## CONTENTS

## CONTENTS (Continued)

## FIGURES

## FIGURES (Continued)

## TABLES

## ACRONYMS AND ABBREVIATIONS

| | |
|---|---|
| AMR | Analysis and Modeling Report |
| CD-ROM | Compact Disc - Read Only Memory |
| CRWMS | Civilian Radioactive Waste Management System |
| CSNF | Commercial Spent Nuclear Fuel |
| DHLW | Defense High Level Waste |
| DOE | U.S. Department of Energy |
| DTN | Data Tracking Number |
| EDX | Energy Dispersive X-Ray |
| FFTF | Fast Flux Test Facility |
| HLW | High Level Waste |
| M&O | Management and Operating Contractor |
| MDR | Material Degradation and Release |
| QA | Quality Assurance |
| SCFT | Solid-Centered Flow-Though |
| SEM | Scanning Electron Microscope |
| TST | Transition State Theory |
| UZ | Unsaturated Zone |
| WP | Waste Package |
| XRD | X- Ray Diffraction |

# 1. PURPOSE

The purpose of this Analysis and Modeling Report (AMR) is to validate the Material Degradation and Release (MDR) model that predicts degradation and release of radionuclides from a degrading waste package (WP) in the potential monitored geologic repository at Yucca Mountain. This AMR is prepared according to *Technical Work Plan for: Waste Package Design Description for LA* (Ref. 17).

The intended use of the MDR model is to estimate the long-term geochemical behavior of waste packages (WPs) containing U. S. Department of Energy (DOE) Spent Nuclear Fuel (SNF) codisposed with High Level Waste (HLW) glass, commercial SNF, and Immobilized Plutonium Ceramic (Pu-ceramic) codisposed with HLW glass. The model is intended to predict (1) the extent to which criticality control material, such as gadolinium (Gd), will remain in the WP after corrosion of the initial WP, (2) the extent to which fissile Pu and uranium (U) will be carried out of the degraded WP by infiltrating water, and (3) the chemical composition and amounts of minerals and other solids left in the WP. The results of the model are intended for use in criticality calculations.

The scope of the model validation report is to (1) describe the MDR model, and (2) compare the modeling results with experimental studies. A test case based on a degrading Pu-ceramic WP is provided to help explain the model.

This model does not directly feed the assessment of system performance. The output from this model is used by several other models, such as the configuration generator, criticality, and criticality consequence models, prior to the evaluation of system performance.

This document has been prepared according to AP-3.10Q, *Analyses and Models* (Ref. 2), and prepared in accordance with the technical work plan (Ref. 17).

## 2. QUALITY ASSURANCE

An activity evaluation (Ref. 17, Addendum A), which was prepared per AP-2.21Q *Quality Determinations and Planning for Scientific, Engineering, and Regulatory Compliance Activities* (Ref. 1), determined that the Quality Assurance (QA) program (Ref. 45) applies to the activity under which this analysis was developed.

With regard to the development of this document, the control of the electronic management of data was evaluated in accordance with AP-SV.1Q *Control of the Electronic Management of Information* (Ref. 5). The evaluation determined that current work processes and procedures are in accordance with the controls specified in the technical work plan (Ref. 17).

# 3. COMPUTER SOFTWARE AND MODEL USAGE

## 3.1 SOFTWARE

This section describes the computer software used in the model. The software was used in a Pu-ceramic test case (Ref. 15).

Table 3-1: Computer Software Used in the Model

| Software Name | Version | Software Tracking Number (Qualification Status) | Description and Components Used | Input and Output Files [a] (Included in Attachment I) |
|---|---|---|---|---|
| EQ3/6 | 7.2b | Qualified<br>LLNL:UCRL-MA-110662<br>EQ3/6, Ref. 27 | EQ3NR: a speciation-solubility code | input: *.3i<br>pickup: *.3p<br>output: *.3o |
| | | | EQPT: a data file preprocessor | input: data0.*<br>output: data1.* |
| EQ6 | 7.2bLV | Qualified<br>10075-7.2bLV-00<br>EQ6, Ref. 31 | EQ6: a reaction path code which models water/rock interaction or fluid mixing in either a pure reaction progress mode or a time mode | input: *.6i<br>pickup: *.6p<br>output: *.6o<br>*.elem_aqu.txt<br>*.elem_min.txt<br>*.elem_tot.txt<br>*.min_info.txt<br>*.bin |
| ASPRIN | 1.0 | Qualified<br>10487-1.0-00<br>ASPRIN, Ref. 18 | ASPRIN: performs post-processing of numerical information (from an output data file created by EQ6), to calculate isotopic inventories for elements of interest | input: *.bin (from EQ6)<br>output: *.txt |
| MS EXCEL | Version 97 SR-2 | Commercial off-the-shelf software: Exempt in accordance with AP-SI.1Q Ref. 4, Section 2.1. | Excel: used in this document for graphical representation and arithmetical manipulations | input: *.elem_*.txt<br>output: *.xls |
| PP | NA | Ref. 67. Used solely for visual display or graphical representation: Exempt in accordance with AP-SI.1Q Ref. 4, Section 2.1.2. | PP: a plotting tool used for graphical representation | input: *.bin (from EQ6)<br>output: *.wmf |

[a] Files are explained in more detail in Attachment II.

In running the MDR model, EQ6 is run in the solid-centered flow-through (SCFT) mode. In this mode, an incremental amount of "fresh" water enters the WP system in each time step, displacing an equivalent volume of water out of the system.

For the test case, the software products were run on a standard personal computer, BSC Management and Operating Contractor for the Department of Energy's Office of Civilian Radioactive Waste Management Las Vegas Office, CPU # 117728. All applicable products were obtained from Software Configuration Management (SCM). The software was appropriate for

the application and was used within the range of validation in accordance with AP-SI.1Q (Ref. 4). However, some runs simulated periods of high ionic strength (1 to ~4). While EQ6 is capable of handling high ionic strengths, there is no Yucca Mountain Project (YMP)-qualified thermodynamic database with corrections for high ionic strength. To address this issue, several sensitivity tests were performed. (See Assumption 5.6).

## 3.2 MODELS

The mathematical model *Defense High Level Waste Glass Degradation* was used for degradation rate expressions for dissolution of glass immersed in water for the Pu-Ceramic test case. Both the earlier version of the model (Ref. 33 and Equations 7 and 8) and the most recent version of the model (Ref. 39 Equations 7 and 8) were used. Even though newer degradation rates were available, the earlier version of the model was used because it provides more conservative results than the most recent version of the model with regards to external and internal criticality (Ref. 15, Section 6.8.2 and 6.8.4).

The HLW glass degradation model does not have a Model Warehouse Data Tracking Number. The use of the model is justified, since the purpose of the model is to describe the degradation of HLW glass in a flooded waste package. The equations were converted to units appropriate for input into EQ6 in 'HLW_glass REV01.xls', sheet 'rates' (Attachment I).

# 4. INPUTS

## 4.1 DATA AND PARAMETERS

Table 6-1 through Table 6-4 list the inputs used in the model for the Pu-ceramic test case. The inputs are appropriate for the model because they have been developed or measured specifically for use in modeling processes at the potential repository.

### 4.1.1 Densities and Molecular Weights of Solids

The qualified EQ6 database, 'data0.ymp' (Ref. 59), does not contain molar volumes for some of the solids that were predicted to form during the EQ6 runs. If molar volumes of any of the solids are missing from the EQ6 database, then EQ6 does not add the volumes of those solids when calculating the volume of solids formed. To get a more accurate value of the volume of solids from EQ6, the molar volumes of several minerals were added to the database. The resulting file is named 'data0.yme'. Molar volumes for the solids were calculated from the molecular weights of the solids in 'data0.ymp' and the solid densities from various sources, as noted in Table 4-1. The current version of EQ6 (Section 3.1) performs the volume calculations for the minerals formed automatically.

Table 4-1. Densities, Molecular Weights and Molar Volumes of Precipitated Solids

| Solid | Molecular Weight (g/mole) [c] | Molar Volume ($cm^3$/mole) [g] | Calculated Density ($g/cm^3$) |
|---|---|---|---|
| Anatase ($TiO_2$) | 79.866 | 20.450 | 3.905[a] |
| Berlinite ($AlPO_4$) | 121.953 | 46.2 | 2.64[a] |
| $CaUO_4$ | 342.105 | 45.865 | 7.459[b] |
| Cr-ettringite ($Ca_6Al_2(CrO_4)_3(OH)_{12}\cdot 26H_2O$) | 1314.888 | 726.900 | 1.809[b] |
| Cr-ferrihydrite ($Fe_4(CrO_4)(OH)_{10}$) | 509.444 | 129.000 | 3.96[f] |
| $Cu_3(PO_4)_2$ | 380.581 | 84.520 | 4.503[b] |
| $Fe_2(MoO_4)_3$ | 508.173 | 131.850 | 3.85 |
| Fluorapatite [$Ca_5(PO_4)_3F$] | 504.302 | 157.594 | 3.2[a] |
| $GdOHCO_3$ | 234.266 | 737 | 0.318[b] |
| Hydroxylapatite [$Ca_5(PO_4)_3OH$] | 502.311 | 163.088 | 3.08[a] |
| $KNpO_2CO_3$ | 368.106 | 68.160 | 5.401[b] |
| Mesolite ($Na_{0.676}Ca_{0.657}Al_{1.99}Si_{3.01}O_{10}\cdot 2.647H_2O$) | 387.783 | 171.661 | 2.259[a] |
| $Na_4UO_2(CO_3)_3$ | 542.013 | 149.305 | 3.63[b] |
| $Ni_3(PO_4)_2$ | 366.023 | 83.263 | 4.396[b] |
| $NpO_2$ | 268.999 | 24.220 | 11.11[d] |
| $PuO_2$ | 275.999 | 23.830 | 11.581[e] |
| α-Uranophane [$Ca(UO_2SiO_3OH)_2\cdot 5H_2O$] | 856.392 | 223.601 | 3.83[a] |
| $(UO_2)_3(PO4)_2\cdot 6H_2O$ | 1108.118 | 316.605 | 3.5[b] |
| $Zn_2SiO_4$ (Willemite) | 222.863 | 55.200 | 4.04[a] |

Sources: [a] Ref. 62 pp. 26 (anatase), 83 (berlinite), 289 (fluorapatite), 389 (hydroxylapatite), 547 (mesolite), 903 (α-uranophane), and 946 ($Zn_2SiO_4$).
[b] Ref. 52, JCPDS cards for $Ni_3(PO4)_2$ (38-1473), $(UO_2)_3(PO4)_2\cdot 6H_2O$ (30-1405), $CaUO_4$ (44-583), $Na_4UO_2(CO_3)_3$ (11-81), Cr-ettringite (41-218), $Cu_3(PO_4)_2$ (70-494), $GdOHCO_3$ (24-421), $KNpO_2CO_3$ (17-264).
[c] Attachment I (EQ3/6 Data base, 'data0.yme').
[d] Ref. 73 (p. B101).
[e] Ref. 46 (p.C-103).
[f] Ref. 70 (p. 386).

NOTES: [g] Calculated from the molecular weight and density.
Values for Molecular Weights may differ from those cited in the references for Calculated Density, but the difference is less than 1% and is not expected to affect the results of this calculation.

### 4.1.2 Thermodynamic Database

The thermodynamic database used for the EQ6 calculations, 'data0.yme', is a slightly altered version of the qualified database: 'data0.ymp.R0' (Ref. 59), with the following changes:

- Several Cr- and Fe-bearing minerals and an aqueous species [Cr-ettringite ($Ca_6Al_2(CrO_4)_3(OH)_{12}\cdot 26H_2O$), Cr-ferrihydrite ($Fe_4(CrO_4)(OH)_{10}$), $CaCrO_4^{aq}$, and $Fe_2(MoO_4)_3$] were added for a more complete database. The logK values were calculated in Ref. 16 (p. 15). Although unqualified, the data for the minerals that were added to the database come from the peer-reviewed literature, and consequently, the impact of any errors likely to be produced is believed to be small.
- $GdOHCO_3$ solubility was added to the database. The logK was assumed to be the same as the logK for $NdOHCO_3$ in the 'data0.ymp.R0' since Gd and Nd are both lanthanides and chemically similar (Assumption 5.15).
- The logK of $GdHPO_4^+$ was found to be incorrect in the database and changed from the value of 185 to –5.7 to match the value given in Ref. 66 (p. 39), which is the source listed in the database for that reaction.
- Molar volumes of the minerals in Table 4-1 were added to the database in order to calculate the density of the degradation products that are formed during the calculations.
- The HLW glass (composition given in Table 6-2) and the GICI glass (composition given in Table 6-10) were added to the database in order to take advantage of EQ3/6's ability to use a pH-dependent rate law, using the EQ6 transition state theory (TST) formalism to describe the degradation. Only reactants entered as "minerals" (solids contained in the database) can specify a range of degradation rates based on pH; "special reactants" (reactants not contained in the database) must have a fixed degradation rate.

## 4.2 CRITERIA

The model validation presented in this document followed the guidance of NUREG 1636, (Ref. 48).

## 4.3 CODES AND STANDARDS

None Used.

## 5. ASSUMPTIONS

5.1 It is assumed that the solutions that drip into the waste package will have the major ion composition of J-13 well water as given in Ref. 58, and that minor components in the solution can be approximated by Ref. 50 (Table 4.2) for ~ $6 \cdot 10^5$ years. The rationale for this assumption is that the groundwater composition is controlled largely by transport through the host rock, over pathways of hundreds of meters, and the host rock composition is not expected to change substantially over $10^6$ years. This assumption is justified by recent evaluations of codisposal waste packages (Ref. 25) which show that degradation of the waste package materials (specifically, HLW glass and steel) overwhelms the native chemistry of the incoming water. (Figures 5-2 through 5-20 of Ref. 25 show pH variations of 3 to 10 in the waste package.) This assumption is used in Section 6.2.1 (Step 8) and 6.2.2.

5.2 The assumption that the water entering the waste package can be approximated by the J-13 well water implicitly assumes that any effects of contact with the engineered materials in the drift will be minimal after a few thousand years. For a few thousand years after waste emplacement, the composition may differ because of perturbations resulting from reactions with engineered materials and from the thermal pulse. These are not taken into account in this calculation because the outer shell and inner liner are not expected to breach until after that perturbed period. Therefore, the early perturbation is not relevant to the calculations reported in this document. This assumption is used in Section 6.2.1 (Step 8).

5.3 It is assumed that an aqueous solution fills all voids within the waste package and circulates freely in the partially degraded waste package so that all degraded solid products will react with each other through the aqueous solution medium. The rationale for this assumption is that sufficient decay heat will be retained within the waste package over the time of interest to cause convective circulation and mixing of the water inside the waste package (Ref. 22, Att. VI). Additionally, this assumption provides the maximum aqueous degradation of waste package components (with the potential for precipitation of radionuclides within the waste package) or the flushing of radionuclides from the waste package, and is therefore conservative. This assumption is used in Section 6.1.

5.4 It is assumed that the density of the incoming water is 1.0 g/cm$^3$. The rationale for this assumption is that for dilute solutions, the density is extremely close to that of pure water, and that any differences are insignificant in respect to other uncertainties in the data and calculations. Moreover, this value is used only initially in EQ3/6 to convert concentrations of dissolved substances from parts per million to molalities. This assumption is used in Section 6.2.1 (Step 8).

5.5 It is assumed that 25°C thermodynamic data can be used for the calculations. The rationale for this assumption is two-fold. First, though the initial breach of the WP may occur at 10,000 years, when the WP contents are at temperatures ~50°C (Ref. 36, Figure 4.6-2, p. F4-49), at times > 25,000 years, the WP temperatures are likely to be close to 25°C. Second, the assumption is conservative with respect to loss of the Gd, the internal criticality control material. Gd phosphates are likely to be the solubility-limiting solids for the Gd. Since the solubility of gadolinium phosphate decreases with increases in

temperature (Ref. 49, Tables IV and V), use of the lower-temperature database is likely to be conservative. Additionally, the solubilities of actinides decrease with temperature, which is likely to be conservative for internal criticality (Ref. 47). This assumption is used in Section 6.2.1 (Step 13).

5.6 It is assumed that the EQ3/6 results generated using the B-dot activity model for solutions with ionic strength greater than 1 molal (M) are sufficiently accurate for the current calculation. (It is accepted that the B-dot activity model is accurate for ionic strengths *less* than 1 M.) The rationale for this assumption is that experimental data (a sensitivity test comparing EQ3/6 results with experimental results in sulfate, nitrate, and chloride solutions) shows that EQ3/6 results using the B-dot activity model can be used qualitatively up to an ionic strength of about 4 M to indicate the general nature of the reactions that would actually occur (Ref. 24, Appendix D). Another sensitivity test compared EQ6 results against experimental results in a carbonate system containing uranium (Ref. 35, Section 5.1.2). The conclusion was that the B-dot activity model overestimated the concentration of U in solution by an order of magnitude or greater. This is conservative for external criticality because it maximizes the U loss from the waste package. It may also significantly overestimate the accumulation external to the waste package (Ref. 35, Section 5.1.2). For internal criticality calculations, it may also be conservative with respect to gadolinium loss, if the concentration of Gd in solution is calculated to be higher than it would be in reality, as is the case for uranium. For internal criticality calculations, with respect to uranium loss, it may not be conservative in all cases. However, the cases chosen for internal criticality calculations have 100% or close to 100% of the uranium retained in the waste package (because these cases have the greatest potential for criticality), so the concentration of U in solution is inconsequential. This assumption is used in Section 6.2.1 (Step 13) and Section 3.1.

5.7 In general, it is assumed that chromium and molybdenum will oxidize fully to chromate (or dichromate) and molybdate, respectively. This assumption is based on the available thermodynamic data (Ref. 59), which indicate that in the presence of air, the chromium and molybdenum would both oxidize to the VI valence state. Laboratory observation of the corrosion of Cr and Mo containing steels and alloys, however, indicates that any such oxidation would be extremely slow. In fact, oxidation to the VI state may not occur at a significant rate with respect to the time frame of interest, or there may exist stable Cr(III) solids that substantially lower aqueous Cr concentration. For the present analyses, the assumption is made that, over the times of concern, oxidation will occur. The rationale for this assumption is that by allowing the Cr and Mo to oxidize, the pH of the system will be lowered allowing for the removal of neutron absorbers. This is conservative for internal criticality since the solubility of $GdPO_4 \cdot 10H_2O$ (the expected solubility-controlling phase for Gd) increases at lower pH (Ref. 25, Section 5.3.1). The resulting transport of Gd out of the waste package will separate the neutron absorber preferentially from the fissile material. This assumption is used in Section 6.1.

5.8 It is assumed that gases in the WP solution remain in equilibrium with the ambient atmosphere outside the WP. In other words, contact of WP fluids with the gas phase in the repository is envisioned to be sufficient to maintain equilibrium with the $CO_2$ and $O_2$ present, whether or not this is the normal atmosphere in open air or rock gas that seeps out of the adjacent tuff. Moreover, the specific partial pressures of $CO_2$ and $O_2$ of the ambient repository atmosphere are set to, respectively, $10^{-3.0}$ and $10^{-0.7}$ bar. The rationale

for the oxygen partial pressure is that it is equivalent to that in the atmosphere (Ref. 74, p. F-210). The rationale for choosing the carbon dioxide pressure is to reflect the observation that J-13 well water appears to be in equilibrium with above-atmospheric carbon dioxide levels (Ref. 78, Table 7). However, it is recognized that local reducing conditions may exist within the WP. The consequences and likelihood of such conditions are discussed in Section 6.2.6, and this assumption is also used in Section 6.1 and Section 6.2.1 (Step 8).

5.9 It is assumed that precipitated solids are deposited in the WP, remain in place, and are not mechanically eroded or entrained as colloids in the advected water. The rationale for this assumption is that it conservatively maximizes the amount of potential deposits of fissile material inside the waste package. This assumption is used in Section 6.1.

5.10 It is assumed that the corrosion rates used in this calculation encompass rates for microbially assisted degradation, and that the degradation rates will not be controlled principally by bacteria (Ref. 43, p. 3-84). The rationale for this assumption is (1) steel corrosion rates measured under environmental conditions inherently include exposure to bacteria, and (2) the lack of organic nutrients available for bacterial corrosion will limit the involvement of bacteria. This assumption is used in Section 6.2.1 (Step 7).

5.11 It is assumed that the drip rate into the WP varies from 1.5 to 500 l/y. Two factors influence the WP water flux: the drift seepage rate and the number of openings in the DS/WP system. The low end of the range corresponds to a low drift seepage rate or to a higher drift seepage rate with diversion of the bulk of water. The high end of the range represents a high drift seepage rate with little WP/DS diversion. This assumption is used in Section 6.2.3.

5.12 It is assumed that the reported alkalinity in analyses of J-13 well water corresponds to bicarbonate ($HCO_3^-$) alkalinity. The assumption is justified by two factors. First, the concentrations of borate, phosphate and silicate (other contributors to alkalinity), in J-13 well water, are small compared to bicarbonate concentration. Second, in most calculations, the imposed $fCO_2$ will control the dissolved bicarbonate concentrations; that is, the initial bicarbonate concentrations will not be tied to assumptions about alkalinity. The same assumption is implicitly made in Ref. 58. This assumption is used in Section 6.2.1 (Step 8).

5.13 It is assumed that the high-level waste glass composition is as given in Ref. 28 (Attachment I, p. I-7), and that the density of the high level waste glass is 2.85 $g/cm^3$ (Ref. 12, p. 26, Fig. 2, and pp. 54-57). The rational for this assumption is that the references cited above are the most recent and comprehensive sources available to provide this information. Additionally, glass composition sensitivity studies show that large variations in glass composition had little effect on Gd loss (Ref. 29, Section 5.3.3). This assumption is used in 6.2.1, and Table 6-2.

5.14 It is assumed that freshly precipitated minerals dissolve and grow instantaneously to maintain equilibrium with adjacent fluids. The basis for this assumption is that over the long time periods considered in running the model (>100,000 years), the impact on the results is minimal. Where appropriate, a sensitivity study is performed to evaluate the effect of kinetically-limited precipitation (Section 6.3.1.3). This assumption is used in Section 6.1.

5.15 It was assumed that the logK value for $GdOHCO_3$ is the same as the logK for $NdOHCO_3$ in the 'data0.ymp.R0' and 'data0.yme' databases. The rationale for this assumption is that Gd and Nd are both lanthanides and chemically similar. Further justification for this assumption can be found in Ref. 29 (Section 5.3.1). This assumption was used in Section 4.1.2.

5.16 It is assumed that the thermodynamic behavior of hafnium (Hf) can be treated as if it were zirconium (Zr). The rationale for this assumption is the extreme similarity of the chemical behaviors of the two elements (Ref. 54 , p. 272). Thermodynamic data for many important Hf solids and aqueous species are lacking, thus Zr was substituted for Hf in the calculation. This assumption is used in Section 6.2.1.

# 6. MODEL

Based on the screening criteria provided in AP-3.15Q, *Managing Technical Product Inputs*, (Ref. 3) this AMR does not include estimates of any "Principal factors" or "Other Factors" and is thus assigned an importance level of 3 per AP-3.10Q (Ref. 2).

## 6.1 CONCEPTUAL MODEL

The conceptual model consists of aqueous solutions entering and exiting a breached WP at constant and equal rates. The aqueous solution fills all voids within the waste package (Assumption 5.3). Water circulates freely enough in the partially degraded waste package that all degraded solid products react with each other through the aqueous solution medium (Assumptions 5.3). WP component steels and fuels react with these solutions according to kinetic rate expressions, forming a variety of secondary oxide and clay phases in the process. Chromium and molybdenum oxidize fully to chromate (or dichromate) and molybdate, respectively (Assumption 5.7). Formation of secondary phases and speciation of the aqueous phase is assumed to be instantaneous (Assumption 5.14), as is equilibration with ambient carbon dioxide and oxygen (Assumption 5.8). Precipitated solids deposited in the WP, remain in place, and are not mechanically eroded or entrained as colloids in the advected water (Assumption 5.9).

## 6.2 MODEL IMPLEMENTATION

### 6.2.1 Step-By-Step Model Description

The step-by step description provides the names (in parenthesis) of example files (located in Attachment I) that demonstrate each step. The example files come from EQ6 calculations for Pu-ceramic waste packages (Ref. 15, Ref. 30, and Ref. 35).

**Step 1**—Calculate the volume and surface area of each component of the waste package. (example: folder 'Pu 1999', file 'pu-ceramic.xls', sheets 'GPC & Outer Web' and 'Magazine, Can, Rack, Disk' and folder 'Pu 2001', file 'Sleeve.xls')

**Step 2**—Calculate the void volume, where the void volume can also be thought of as the volume of water that would fill a flooded waste package. This is necessary because EQ6 calculations are based on 1 liter of solution. This is calculated by summing the volume of each component in the waste package and subtracting from the inside volume of the waste package shell. (example: folder 'Pu 1999', file 'pu-ceramic.xls', sheet 'Void&Norm')

**Step 3**—Calculate the moles of each component. EQ6 requires that the quantity of each component be expressed in moles, rather than mass. To do this, the molecular weight of the material must be defined. In the example, a mole of each component (except the aqueous displacer) is defined as 100 grams. Therefore, the mass of a component divided by 100 g/mole gives the moles of the component. (Example for combined Steps 3 and 4: folder 'Pu 1999', file 'pu-ceram.xls', sheet 'Void&Norm' and folder 'Pu 2001', file 'Sleeve.xls')

**Step 4**—Calculate the normalized moles and normalized surface area of each component by dividing the moles and surface area calculated in Steps 1 and 3 by the void volume calculated in Step 2. The normalized moles and surface area represent the moles and surface area that would

contact 1 liter of solution. The normalized values are entered into the EQ6 input file. (example for combined Steps 3 and 4: folder 'Pu 1999', file 'pu-ceram.xls', sheet 'Void&Norm' and folder 'Pu 2001', file 'Sleeve.xls')

**Step 5**—Determine surface area corrections, if any, based on expected cracking of material or based on cladding integrity. If the fuel or HLW glass is expected to be fractured, the surface area is increased. In the Pu-ceramic example, the HLW glass surface area is increased by a factor of 21 due to cracking, and the surface area of the Pu-ceramic is increased by a factor of 30 to account for radiation damage (Ref. 35, Section 5.3.1.2). For fuels with a robust cladding that may delay degradation, a factor less than 1 may be employed. In the case of Shippingport LWBR SNF (Ref. 34), the calculated surface area was reduced to 1% and 10% for sensitivity runs, to account for the corrosion-resistant Zircaloy cladding.

**Step 6**—Calculate the molar composition (based on 100 g/mole) of each material in all components and enter into the EQ6 input file. This step calculated the moles of each element in 100 grams of material. (example: folder 'Pu 1999', file 'pu-ceramic', sheet 'Compositions', rows 135-143)

**Step 7**—Determine a degradation rate or a range of degradation rates for each material in units of "moles/($cm^2$·s)"(Assumption 5.10). The best available sources are used. Tables 1 through 3 from Ref. 15 (Section 5.1.2) provide the values and the sources for the degradation rates and the compositions used for Pu-ceramic. The HLW glass degradation rate in Table 6-2 is not a constant value; it is pH-dependent. The file 'HLW Glass REV01.xls' in folder 'Pu 2001' shows how the degradation rate values for the EQ6 input file were calculated. The file also provides a plot of the degradation values used in the calculations. In order to use the pH-dependent rate, the composition of the HLW glass (Table 6-2) was entered into the database as a mineral called "GlassSRL". The database is provided in folder 'databases', file 'data0.yme'. The actual rate in which the material degrades is the product of the degradation rate (EQ6 variable: rk1) and the surface area (EQ6 variable: sk).

**Step 8**—Determine the composition of the aqueous solution entering the waste packages (Assumption 5.4). In the example case, the composition of J-13 well water was used (Assumption 5.1, 5.2, and 5.12). See Section 6.2.2 for further discussion on incoming water. The fugacity of $CO_2$ and $O_2$ are fixed at $10^{-3}$ and $10^{-0.7}$ bars in most cases (Assumption 5.8). For sensitivity tests, higher values of $CO_2$ are used (Ref. 29, Section 5.3.2), lower values of $CO_2$ are used (Ref. 29, Section 6.2), and cases where the value of $O_2$ and $CO_2$ are determined by in-package competition between diffusion and degradation (Ref. 35, Section 6.3).

**Step 9**—Determine range of drip rates for incoming water, normalize the rates based on 1 liter, and convert to units of "moles/s" for input into EQ6. In the example, the drip rates in Table 6-4 were used (Ref. 15, Table 5-7). See Section 6.2.3 for discussion on drip rate.

**Step 10**—Determine sequence of degradation. In the example, two types of sequences of degradation were used—a one stage, in which all of the components degraded simultaneously and a two stage, in which some of the components (Pu-ceramic and the stainless steel cans) were not introduced until the second stage. See Section 6.2.4 for discussion of sequence of degradation.

**Step 11**—Determine runs to perform, varying degradation rates, drip rates, and sequence of degradation. Table 6-6 and Table 6-7 provide the list of cases that were run for the example case (Ref. 15, Tables 5-8 and 5-9).

**Step 12**—Determine the minerals to suppress. See Section 6.2.5 for discussion of suppressed minerals.

**Step 13**—Choose a qualified thermodynamic database (Ref. 59). If changes are needed, document and justify changes (Assumption 5.5 and 5.6).

**Step 14**—Run EQ6 using a batch file that renames the outputs and indicates the options that are used. The following is an example batch file:

```
del elem0aqu.bin
del mwtmax.txt
copy decay.eq6.24100 decay.eq6

runeq6 yme p51rLx41.6i
  move hwsdata p51rLx41.bin
  move min_info.txt p51rLx41.min_info.txt
  move elem_aqu.txt p51rLx41.elem_aqu.txt
  move elem_min.txt p51rLx41.elem_min.txt
  move elem_tot.txt p51rLx41.elem_tot.txt

del decay.eq6
```

**Step 15**—Tabulate the losses of neutron absorbers (such as gadolinium, Gd) and actinides (Pu and U). Table 6-8 is an example table containing results from the Pu-ceramic cases (Ref. 15, Table 6-16)

**Step 16**—For internal criticality calculations, calculate the density and mass of the corrosion products as a function of time for the cases with most conservative results (high Gd loss and low actinide loss). The density and mass are calculated using the '*.elem_min.txt' output file. Table 6-9 is an example for one of the Pu-ceramic cases with high Gd loss, Case s10 (Ref. 15, Table 6-27). (example: folder 'Pu 2001', file 'density_pu-ceramic.xls', sheet 'density'.)

**Step 17**—For external criticality calculations, calculate the U enrichment fraction (molar ratio of U-235 to total U) of the aqueous solution using ASPRIN software for the cases with the most conservative results (high Pu discharged from the waste package or high Pu and U loss).

Figure 6-1 is a plot from Pu-ceramic for a case with high Pu discharged from the waste package, Case s5 (Ref. 15, Figure 6-25).

Table 6-1: Steel Compositions, Densities, and Degradation Rates

| Element | A516 Carbon Steel | | 316L Stainless Steel | | 304L Stainless Steel | |
|---|---|---|---|---|---|---|
| | (wt%)[a] | (moles)[b] | (wt%)[c] | (moles)[b] | (wt%)[d] | (moles)[b] |
| C | 0.28 | 2.3312E-02 | 0.030 | 2.4977E-03 | 0.03 | 2.4977E-03 |
| Mn | 1.045 | 1.9021E-02 | 2.000 | 3.6405E-02 | 2.00 | 3.6405E-02 |
| P | 0.035 | 1.1299E-03 | 0.045 | 1.4528E-03 | 0.045 | 1.4528E-03 |
| S | 0.035 | 1.0915E-03 | 0.030 | 9.3557E-04 | 0.03 | 9.3557E-04 |
| Si | 0.29 | 1.0326E-02 | 1.000 | 3.5606E-02 | 0.75 | 2.6704E-02 |
| Cr | 0 | 0 | 17.000 | 3.2695E-01 | 19.00 | 3.6541E-01 |
| Ni | 0 | 0 | 12.000 | 2.0446E-01 | 10.00 | 1.7039E-01 |
| Mo | 0 | 0 | 2.500 | 2.6058E-02 | 0 | 0 |
| N | 0 | 0 | 0.100 | 7.1394E-03 | 0.10 | 7.1394E-03 |
| Fe | 98.315 | 1.7604E+00 | 65.295 | 1.1692E+00 | 68.045 | 1.2184E+00 |
| Total | 100.00 | 1.8153 | 100.000 | 1.8107 | 100.00 | 1.8294 |
| | | | | | | |
| Density (g/cm$^3$) | 7.85[e] | | 7.98[f] | | 7.94[f] | |
| | | | | | | |
| Rate | (μm/y) | (moles/(cm$^2$·s))[g] | (μm/y) | (moles/(cm$^2$·s)) | (μm/y) | (moles/(cm$^2$·s)) |
| Very Low | Same as average | Same as average | 0.01[h] | 2.53E-15 | Same as low | Same as low |
| Low | Same as average | Same as average | 0.1[i] | 2.53E-14 | 0.1[i] | 2.52E-14 |
| Average | 72[j] | 1.79E-11 | 2[k] | 5.06E-13 | 34[k] | 8.55E-12 |
| High | Same as average | Same as average | 33[m] | 8.34E-12 | 208[m] | 5.23E-11 |

Sources: [a] Ref. 10 (p. 321, Table 1)
[c] Ref. 9 (p. 2, Table 1)
[d] Ref. 8 (p. 3, Table 1)
[e] Ref. 7 (p. 9)
[f] Ref. 11 (p. 7, Table XI)
[i] Ref. 23 (pp. 11-13)
[j] Ref. 57 (pp. 2.2-96 – 2.2-98) were used to derive the corrosion rate in spreadsheet 'A516_Rate.xls', sheet 'prob', (Attachment I)
[k] Ref. 38 (Figure 3-15, 50 percentile value)
[m] Ref. 38 (Figure 3-15, 95 percentile value)

NOTES: [b] The moles of each element are calculated by dividing the weight percent by the atomic weight of each element
[g] The molecular weight of each material is assumed to be 100 grams. The degradation rates in units of μm/y are multiplied by the density, divided by $10^4$ μm/cm, divided by 100 g/mole, divided by 365.25 days/y, and divided by 86,400 s/day to convert to units of moles/(cm$^2$·s).
[h] The very low rate for 316L was assumed to be 10 times lower than the low rate.

Table 6-2. Simplified Glass Composition, Density, and Degradation Rates

| Element | Moles [a] | Comment |
|---|---|---|
| O | 2.7038 | |
| U | 0.0078 | |
| Np | 0 | Merged with U (~0.1% of actinides,ceramic Np overwhelms) |
| Pu | 0 | Merged with U (Pu ~1% actinides, ceramic Pu overwhelms glass Pu). |
| Ba | 0.0011 | |
| Al | 0.0863 | |
| S | 0.0040 | |
| Ca | 0.0162 | |
| P | 0.0005 | |
| Cr | 0 | Merged with Al (overwhelmed by steel Cr; $Cr_2O_3$ similar to $Al_2O_3$) |
| Ni | 0 | Merged with Fe |
| Pb | 0 | Merged with Ba (both form insoluble $CrO_4^=$ compounds in EQ6 runs) |
| Si | 0.7765 | |
| Ti | 0 | Merged with Si (overwhelmed by ceramic Ti; $TiO_2$ similar to $SiO_2$) |
| B | 0.2912 | |
| Li | 0 | Merged with Na |
| F | 0.0017 | |
| Cu | 0 | Merged with Fe |
| Fe | 0.1722 | |
| K | 0.0752 | |
| Mg | 0.0333 | |
| Mn | 0 | Merged with Fe |
| Na | 0.5767 | |
| Cl | 0 | Removed (overwhelmed by Cl in in-dripping water) |
| | | |
| **Density [b] ($g/cm^3$)** | 2.85 | |
| | | |
| Total Rate Degradation Rate = $k_1[H+]^{0.04} + k_2[H+]^{0.6}$ ($moles/cm^2 \cdot s$) | | |
| **Average [d]** | $k_1$=8.86E-19 $liters/cm^2 \cdot s$ | $k_2$=7.98E-13 $liters/cm^2 \cdot s$ |
| **Moderately High [d]** | $k_1$=7.06E-18 $liters/cm^2 \cdot s$ | $k_2$=3.59E-12 $liters/cm^2 \cdot s$ |
| **High [d]** | $k_1$=1.08E-17 $liters/cm^2 \cdot s$ | $k_2$=4.87E-12 $liters/cm^2 \cdot s$ |
| **New Average [c]** | $k_1$=8.86E-19 $liters/cm^2 \cdot s$ | $k_2$=1.12E-11 $liters/cm^2 \cdot s$ |

Notes: [a] Simplified composition based on Ref. 28 (Assumption 5.13) as calculated in spreadsheet 'HLW_glass REV01.xls', sheet 'composition' (Attachment I). This composition was added to the 'data0.ymp' for the pseudo-mineral GlassSRL. One mole = 100g HLW glass.
[b] Based on HLW glass density in Ref. 68, p. 2.2.1.1-4 (Assumption 5.13)
[c] Ref. 39 (Equations 7 and 8); Converted to inputs for EQ6 in 'HLW_glass REV01.xls', sheet 'rates'.
[d] Ref. 33 (Equations 7 and 8); Converted to inputs for EQ6 in 'HLW_glass REV01.xls'; sheet 'rates'.

Table 6-3. Composition and Degradation Rates of Pu-ceramic

| Oxide | Composition | | |
|---|---|---|---|
| | (wt%) [a] | (moles metal) [b] | (moles oxygen) [c] |
| CaO | 10.0 | 1.78E-01 | 1.78E-01 |
| $HfO_2$ [d] | 10.6 | 5.04E-02 | 1.01E-01 |
| $UO_2$ [g] | 23.7 | 8.78E-02 | 1.76E-01 |
| $PuO_2$ | 11.9 | 4.35E-02 | 8.70E-02 |
| $NpO_2$ | 0.0 | 3.91E-04 | 7.82E-04 |
| $Gd_2O_3$ | 7.9 | 4.36E-02 | 6.54E-02 |
| $TiO_2$ | 35.9 | 4.49E-01 | 8.99E-01 |
| Total | 100.0 | 8.53E-01 | 1.51E+00 |
| | | | |
| **Density ($g/cm^3$)** | 5.5 [e] | | |
| | | | |
| **Rate** | **(moles/($cm^2$·s))[f]** | **Basis** | |
| **Average** | 8.0E-16 | Picked as factor of 10 lower than high value | |
| **High** | 8.0E-15 | Ref. 35, p. 27, based on 50°C rates for radiation-damaged ceramic from Ref. 63 | |
| **Very High** | 8.0E-14 | picked as factor of 10 higher than high value | |

Sources: [a] Ref. 56 (Table 3.1)
[e] Ref. 64 **(p. 3-4)**

Notes: [b] Moles of metal is the weight percent oxide divided by the molecular weight of the oxide.
[c] Moles of oxygen is the moles metal (calculated in the previous column) times the ratio of (moles oxygen)/(moles metal) in the formula for the oxide.
[d] Replaced by Zr in EQ6 runs, then converted back to Hf for mass calculations.
[f] One mole special reactant ≡ 100 g.
[g] The uranium is 1.69 wt% U-235, with the remainder U-238 (Ref. 64)

Table 6-4. Drip Rate Values for Input to EQ6

| Drip Rate ($m^3$/year) | Drip Rate (normalized for EQ6 input) (moles/s)[a] |
|---|---|
| 0.0015 | 1.03E-11 |
| 0.015 | 1.03E-10 |
| 0.15 | 1.03E-09 |
| 0.5 | 3.45E-09 |

NOTE: [a] The values of drip rate in units of $m^3$/year are multiplied by 1000 liters/$m^3$, divided by 1 liter/mole, divided by 365.25 days/year, divided by 86,400 s/day, and divided by 4594 liters of void volume.

Table 6-5. EQ6 Input File Elemental Molal Composition for J-13 Well Water

| Chemical Composition | | | | | |
|---|---|---|---|---|---|
| O | 5.55E+01 | Gd | 1.00E-16 | Na | 1.99E-03 |
| Al | 1.00E-16 | H | 1.11E+02 | Ni | 1.00E-16 |
| B | 1.00E-16 | C | 2.07E-03 | Np | 1.00E-16 |
| Ba | 1.00E-16 | P | 1.00E-16 | Pu | 1.00E-16 |
| Ca | 3.24E-04 | K | 1.29E-04 | S | 1.92E-04 |
| Cl | 2.01E-04 | Mg | 8.27E-05 | Si | 1.02E-03 |
| Cr | 1.00E-16 | Mn | 1.00E-16 | U | 1.00E-16 |
| F | 1.15E-04 | Mo | 1.00E-16 | | |
| Fe | 1.00E-16 | N | 1.42E-04 | | |

Sources: from Ref. 40 (Table 6), based on Ref. 58. These values are outputs from EQ3NR for input into EQ6 input file.

Table 6-6. Summary of Single-Stage EQ6 Cases for Pu-Ceramic Waste Package

| Case Number | Rates of Degradation [a] for: | | | Water Drip Rates ($m^3/y$) | Comments [b] | Case ID |
|---|---|---|---|---|---|---|
| | Steel | Glass | Pu-ceramic | | | |
| 3 | Average | Average | High | 0.0015 | 5 Pu canisters | p10_1131 |
| 5 | Average | Average | Average | 0.015 | 5 Pu canisters | p10_1122 |
| 8 | Average | High | High | 0.0015 | 5 Pu canisters | p10_1231 |
| 10 | Average | High | Average | 0.015 | 5 Pu canisters | p10_1222 |
| 14 | High | Average | High | 0.15 | 5 Pu canisters | p10_2133 |
| s1 | Average | Average | High | 0.0015 | 1 Pu canister | p51_1131 |
| s2 | Average | Average | High | 0.015 | 1 Pu canister | p51_1132 |
| s3 | Average | Average | High | 0.0015 | 2 Pu canisters | p52_1131 |
| s4 | Low | High | Very High | 0.0015 | 2 Pu canisters | p52rL241/p52sL241 |
| s4b | Low | High | Very High | 0.0015 | 2 Pu canisters | p53rL241/p53sL241 |
| s5 | Very Low | Moderately High | Very High | 0.0015 | 2 Pu canisters | p52rLx41 |
| s6 | Average | Average | High | 0.0015 | 5 Pu canisters, $GdPO_4 \cdot H2O$ is formed | p60_1131 |
| s9 | Low | Average | High | 0.015 | 2 Pu canisters | p52_L132 |
| s10 | Low | Average | Very High | 0.015 | 2 Pu canisters | p52_L142 |
| s11 | Low | Average | High | 0.15 | 2 Pu canisters | p52_L133 |
| s12 | Low | Average | Very High | 0.15 | 2 Pu canisters | p52_L143 |
| s13 | Average | Average | High | 0.015 | 2 Pu canisters | p52_1132 |
| s14 | Average | Average | Very High | 0.015 | 2 Pu canisters | p52_1142 |
| s15 | Average | Average | High | 0.15 | 2 Pu canisters | p52_1133 |
| s16 | Average | Average | Very High | 0.15 | 2 Pu canisters | p52_1143 |
| s17 | Low | New Average | Very High | 0.015 | 2 Pu canisters | p52_Ln42 |
| s18 | Average | New Average | Very High | 0.15 | 2 Pu canisters | p52_1n43 |
| s19 | Low | New Average | Very High | 0.0015 | 2 Pu canisters | p53rLn41 |
| s20 | Very Low | New Average | Very High | 0.0015 | 2 Pu canisters | p52rLn41 |
| s21 | Very Low | Moderately High | Very High | 0.0015 | 1 Pu canister | p51rLx41 |

NOTE: [a] See Table 6-1, Table 6-2, and Table 6-3 for numerical values of rates.
[b] In the single-stage runs, hematite was the iron oxide allowed to form.

Table 6-7. Summary of Multiple-Stage EQ6 Cases for Pu-Ceramic Waste Package

| Case Number | Rates of Degradation[a] for: | | | Water Drip Rates ($m^3/y$) | Comments | Case ID | Fe Oxide |
|---|---|---|---|---|---|---|---|
| | Steel | Glass | Pu-ceramic | | | | |
| 21(a) | High | High | No Ceramic | 0.5 | 5 Pu canisters | p11h2204 | Hematite |
| 21(b) | High | No Glass Present | Average | 0.015 | 5 Pu canisters | p12h2022 | Hematite |
| 22(a) | High | High | No ceramic | 0.5 | 5 Pu canisters | p11g2204 | Goethite |
| 22(b) | High | No Glass Present | Average | 0.015 | 5 Pu canisters | p12g2022 | Goethite |
| s7(a) | High | High | No ceramic | 0.5 | 1 Pu canister | p71g2204/p72g2204 | Goethite |
| s7(b) | High | No Glass Present | Average | 0.015 | 1 Pu canister | p73g2022 | Goethite |
| s8(a) | High | High | No ceramic | 0.5 | 2 Pu canisters | p81g2204 | Goethite |
| s8(b) | High | No Glass Present | Average | 0.015 | 2 Pu canisters | p82g2022 | Goethite |

NOTE: [a] See Table 6-1, Table 6-2, and Table 6-3 for numerical values of rates.

Table 6-8. Result of Sensitivity Analyses

| Sensitivity | Case ID | Root Name | Number of Pu Canisters | Years | %Gd Loss[a] | Initial Moles Pu | Moles Pu Discharged[b] | %Pu & U Loss[a] |
|---|---|---|---|---|---|---|---|---|
| Pu-Ceramic Loading | s1 | p51_1131 | 1 | 6.34E+05 | 0.05 | 112 | 14.12 | 100.00 |
| | s2 | p51_1132 | 1 | 3.97E+05 | 0.21 | 112 | 12.24 | 100.00 |
| | s3 | p52_1131 | 2 | 6.34E+05 | 0.27 | 224 | 27.21 | 100.00 |
| | s7 | p71g2204/p72g2204/ 73g2022 | 1 | 4.36E+05 | 0.15 | 112 | 0.67 | 8.98 |
| | s8 | p81g2204/p82g2022 | 2 | 6.34E+05 | 0.25 | 224 | 0.79 | 6.10 |
| Source Term | s4 | p52rL241/p52sL241 | 2 | 6.34E+05 | 33.49 | 224 | 115.92 | 69.63 |
| | s4b | p53rL241/p53sL241 | 2 | 6.34E+05 | 33.47 | 224 | 109.15 | 68.95 |
| | s5 | p52rLx41 | 2 | 6.34E+05 | 0.26 | 224 | 155.14 | 100.00 |
| | s19 | p53rLn41 | 2 | 6.34E+05 | 31.97 | 224 | 0.14 | 0.44 |
| | s20 | p52rLn41 | 2 | 6.34E+05 | 10.68 | 224 | 22.44 | 100.00 |
| | s21 | p51rLx41 | 1 | 6.34E+05 | 0.14 | 112 | 80.30 | 100.00 |
| $GdPO_4$ Hydration | s6 | p60_1131 | 5 | 6.34E+05 | 0.24 | 558 | 51.82 | 100.00 |
| Gd Loss | s9 | p52_L132 | 2 | 2.19E+05 | 45.44 | 224 | 1.69 | 1.87 |
| | s10 | p52_L142 | 2 | 2.22E+04 | 77.92 | 224 | 0.81 | 0.22 |
| | s11 | p52_L133 | 2 | 9.69E+04 | 4.87 | 224 | 3.70 | 5.69 |
| | s12 | p52_L143 | 2 | 4.93E+04 | 23.48 | 224 | 3.19 | 2.79 |
| | s13 | p52_1132 | 2 | 1.55E+05 | 0.31 | 224 | 15.53 | 85.83 |
| | s14 | p52_1142 | 2 | 1.54E+04 | 41.95 | 224 | 3.80 | 0.58 |
| | s15 | p52_1133 | 2 | 1.04E+05 | 0.28 | 224 | 8.24 | 8.46 |
| | s16 | p52_1143 | 2 | 1.52E+04 | 58.61 | 224 | 4.12 | 1.83 |
| | s17 | p52_Ln42 | 2 | 5.19E+04 | 57.20 | 224 | 0.40 | 0.46 |
| | s18 | p52_1n43 | 2 | 1.53E+04 | 53.16 | 224 | 3.79 | 1.35 |

NOTE: [a] Calculated in file 'Summary Results.xls', sheet 'Total Elem' in Attachment II of Ref. 15 for Cases s1-s8. Calculated in 'calculate loss.xls' for Cases s9-s21.
[b] Calculated in files 'p52{rs}L241 extended.xls', 'p53rL241 extended.xls', 'p52rLx41 extended.xls', 'p52rLn41.xls',and 'Pu_discharged_elem_aqu.xls' in Attachment II of Ref. 15.

# OFFICE OF CIVILIAN RADIOACTIVE WASTE MANAGEMENT
# REGULATORY RESPONSE REVIEW RECORD

QA:

| Project: | Department/Group: |
|---|---|
| Repository Design | Waste Pacakge Criticality |

1. Initiating Reference (e.g., E-mail, telephone call, verbal request, DOE/NRC meeting, letter from NRC, other government agency or client):
NRC/DOE Key Technical Issue agreements CLST.5.04, ENFE.5.03, and RT.4.03.

2. Scope and Description of Issue (Problem statement and key elements of the response: facts, discussion, intended actions, or BSC position):
Provide the list of model validation reports and their schedule. The model validation reports for criticality analysis are planned to be completed between FY01 and FY05. The exact dates are subject to changes in funding levels. The dates provided in the list are based on the dates in P3 as of September 14th, 2001. These dates, especially those in FY03 and beyond, are subject to change with changing budgets and funding levels. The transmittal letter for this list is to note this.

3. Documents Used in Response Development (e.g., specifications, drawings, calculations, studies, etc.):
List and Scheduleof Model Validation Reports.

| 4. Originator: | Date: | 5. Reviewer: | Date: |
|---|---|---|---|
| D. C. Thomas | 09/28/2001 | I. W. [illegible] | 9.28-01 |

## 6. CONCURRENCE

| Science and Analysis | | Functional Staff | | Other | |
|---|---|---|---|---|---|
| Project Manager: | Date: | Engineering: | Date: | | Date: |
| **Repository Design** | | Chief Science Officer: | Date: | | Date: |
| Project Manager: I. W. [illegible] FOR | Date: 9-28-01 | Quality Assurance: | Date: | | |
| **Program Integration** | | | | | |
| Manager: | Date: | | | | |

## 7. APPROVALS

| Project Manager: | License Application Project SME: | Project Manager, License Application Project: |
|---|---|---|
| | | |

# LIST AND SCHEDULE OF MODEL VALIDATION REPORTS

| Original List of Reports | Consolidated List | Expected Delivery Date to NRC |
|---|---|---|
| 1. Geochemistry Model Validation Report: Material Accumulation and Transport | 1.Geochemistry Model Validation Report: External Accumulation Model, Rev 0 | Sep 01 |
| | Rev 1 | Dec 03 |
| 2. Geochemistry Model Validation Report: Material Degradation and Release | 2.Geochemistry Model Validation Report: Material Degradation and Release, Rev 0 | Sep 01 |
| | Rev 1 | Sep 04 |
| 3. Configuration Generator Model Validation Report: CSNF Waste Packages | 3. Configuration Generator Model Validation Report:: Internal Configurations<br>Rev 0 (CSNF) | Jul 02 |
| 4. Configuration Generator Model Validation Report: DOE-SNF Codisposal Waste Packages | Rev 1 (DOE SNF) | Dec 03 |
| 5. Configuration Generator Model Validation Report: Immobilized Pu Codisposal Waste Packages | Rev 2 (IPWF) | Sep 04 |
| 6. Configuration Generator Model Validation Report: Near-Field/In Drift Configurations | 4. Configuration Generator Model Validation Report: External Configurations<br>Rev 1 (Near-Field/In-Drift) | Aug 04 |
| 7. Configuration Generator Model Validation Report: Far-Field Configurations | Rev 0 (Far-Field) | Apr 04 |
| 8. Criticality Model Validation Report: PWR | 5. Criticality Model Validation Report: Internal<br>Rev 0 (PWR) | Dec 02 |
| 9. Criticality Model Validation Report: BWR | Rev 1 (BWR) | Oct 03 |
| 10. Criticality Model Validation Report: DOE SNF Codisposal | Rev 2 (DOE SNF) | Jan 04 |
| 11. Criticality Model Validation Report: Immobilized Plutonium Codisposal | Rev 3 (IPWF) | Sep 04 |
| 12. Criticality Model Validation Report: External | 6. Criticality Model Validation Report: External | Apr 04 |
| 13. Isotopics Model Validation Report: PWR | 7. Isotopics Model Validation Report<br>Rev 0 (PWR) | Nov 02 |
| 14. Isotopics Model Validation Report: BWR | Rev 1 (BWR) | Dec 03 |
| 15. Steady-State Criticality Consequence Model Validation Report: Internal and External | 8. Steady-State Criticality Consequence Model Validation Report: Internal and External | Dec 02 |
| 16. Transient Criticality Consequence Model Validation Report: Internal | 9. Transient Criticality Consequence Model Validation Report<br>Rev 0 (Internal) | Dec 03 |
| 17. Transient Criticality Consequence Model Validation Report: External | Rev 1 (External) | May 04 |

Table 6-9. Composition of Corrosion Products [b] (grams) and Density in Selected Years for Case s10 (p52_L142)

| Element | Year | | | | |
|---|---|---|---|---|---|
| | 157 | 15154 | 22226 | 49918 | 630370 |
| O | 3.60E+02 | 4.87E+02 | 5.22E+02 | 6.58E+02 | 1.79E+03 |
| Al | 6.22E-02 | 5.54E-01 | 7.82E-01 | 1.67E+00 | 2.38E+01 |
| B | 0.00E+00 | 0.00E+00 | 0.00E+00 | 4.15E-14 | 0.00E+00 |
| Ba | 4.03E-03 | 3.29E-02 | 4.60E-02 | 9.71E-02 | 1.38E+00 |
| Ca | 3.31E-02 | 1.21E+00 | 1.13E+00 | 1.53E+00 | 1.54E+01 |
| Cl | 0.00E+00 | 1.90E-13 | 0.00E+00 | 0.00E+00 | 0.00E+00 |
| Cr | 0.00E+00 | 1.25E-02 | 1.74E-02 | 3.68E-02 | 0.00E+00 |
| F | 3.06E-03 | 2.22E-11 | 2.57E-19 | 0.00E+00 | 1.95E-01 |
| Fe | 8.16E+02 | 9.99E+02 | 1.07E+03 | 1.33E+03 | 2.89E+03 |
| Gd | 7.95E-02 | 3.82E+00 | 1.69E+00 | 1.69E+00 | 1.69E+00 |
| H | 3.15E-02 | 8.03E-01 | 8.90E-01 | 1.16E+00 | 6.60E+00 |
| C | 5.13E-13 | 2.71E-01 | 3.90E-13 | 0.00E+00 | 1.21E-01 |
| P | 5.58E-02 | 2.86E-01 | 3.33E-01 | 5.14E-01 | 1.56E+00 |
| K | 0.00E+00 | 2.54E-13 | 0.00E+00 | 0.00E+00 | 1.85E+00 |
| Mg | 0.00E+00 | 1.31E-12 | 2.97E-02 | 1.72E-01 | 5.74E+00 |
| Mn | 8.71E+00 | 1.41E+01 | 1.61E+01 | 2.37E+01 | 6.87E+01 |
| Mo | 1.16E-03 | 1.40E+00 | 1.44E+00 | 1.35E+00 | 9.61E-02 |
| N | 0.00E+00 | 1.45E-12 | 3.04E-18 | 0.00E+00 | 0.00E+00 |
| Na | 0.00E+00 | 8.53E-13 | 3.99E-17 | 0.00E+00 | 9.42E+00 |
| Ni | 0.00E+00 | 1.15E+01 | 1.31E+01 | 1.47E+01 | 1.85E+02 |
| Np | 0.00E+00 | 5.66E-02 | 3.33E-02 | 0.00E+00 | 0.00E+00 |
| Pu | 7.33E-02 | 7.46E+00 | 6.08E+00 | 2.73E+00 | 0.00E+00 |
| S | 9.38E-04 | 5.58E-11 | 0.00E+00 | 0.00E+00 | 0.00E+00 |
| Si | 3.04E+00 | 1.10E+01 | 1.44E+01 | 2.80E+01 | 3.01E+02 |
| Ti | 2.50E-01 | 2.41E+01 | 2.41E+01 | 2.41E+01 | 2.41E+01 |
| U | 2.84E-01 | 2.72E+01 | 2.87E+01 | 3.25E+01 | 4.87E+01 |
| Hf(Zr)[a] | 5.33E-02 | 5.13E+00 | 5.13E+00 | 5.13E+00 | 5.13E+00 |
| | | | | | |
| **Total (kg)** | 5459 | 7330 | 7827 | 9757 | 24727 |
| **Density (g/cm$^3$)** | 5.27 | 5.21 | 5.16 | 5.10 | 4.59 |
| **%Gd loss** | 0.0 | 49.4 | 77.9 | 77.9 | 77.9 |
| **%U + PU loss** | 0.03 | 0.2 | 0.2 | 0.5 | 6 |
| **%Pu-ceramic left** | 99.0 | 0.0 | 0.0 | 0.0 | 0.0 |
| **%Glass left** | 99.8 | 98.6 | 98.1 | 95.9 | 41.9 |
| **%316NG WP Liner left** | 100.0 | 97.5 | 96.3 | 91.7 | 0.0 |

NOTES: [a] Hf was converted to Zr for EQ6, then converted back to Hf for mass and density calculations (See Assumption 5.16).

[b] Mass of each element is based on 1 liter aqueous fluid. To obtain total grams of each element in waste package, multiply by total system volume of 4594 liters.

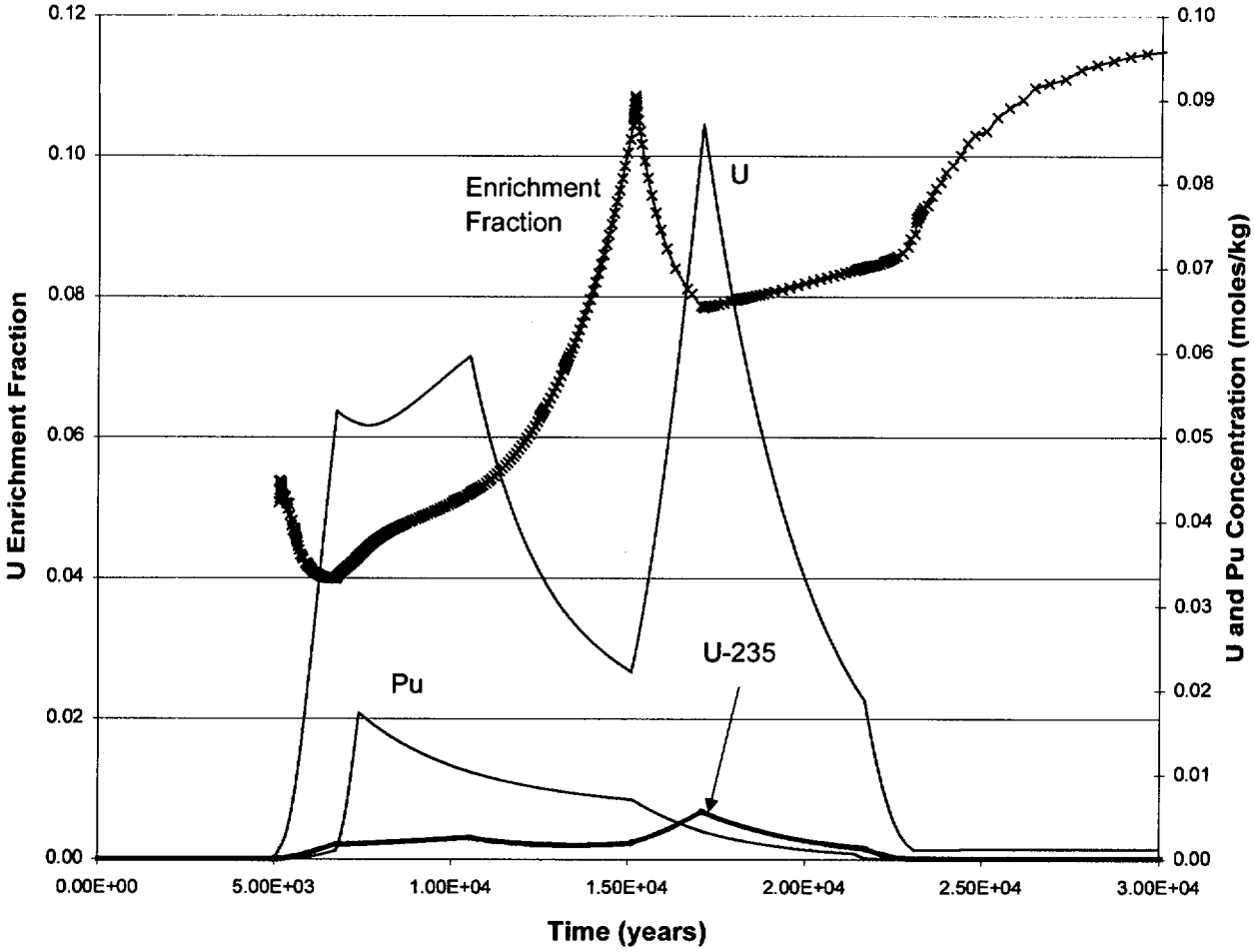


Figure 6-1: Case s5: Uranium Enrichment Fraction and Total Aqueous U and Pu

### 6.2.2 Incoming Water Composition

The water composition likely to enter the waste package cannot be predicted accurately ahead of time, but it most likely will be similar to some combination of the water found in the unsaturated zone today and saturated zone J-13 well water (Ref. 58). For the current application, we assume the chemical composition of the incoming water will have the major ion composition of J-13 well water (Assumption 5.1). Recent evaluations of codisposal waste packages (Ref. 14, Figures 7 and 8) and Pu-ceramic waste packages (Ref. 29, Figures 6-17 and 6-19) show that degradation of the waste package materials overwhelms the native chemistry of the incoming water, causing wide pH variations. A recent document (Ref. 16, Section 4.1.2) studied the impact of using alternate compositions for incoming water (evaporated J-13 water and simulated pore water). For degrading waste packages containing Fast Flux Test Facility (FFTF), Ref. 25, SNF or commercial SNF (CSNF), the pH profiles varied only slightly with the composition of the incoming water. The sensitivity of the incoming water composition to the output pH was insignificant compared to the effects of changing the drip rate or surface area of the fuel (Ref. 16, Section 6.2).

### 6.2.3 Drip Rate of Incoming Water

It is assumed (Assumption 5.11) that the drip rate onto a waste package is the same as the rate at which water flows through the waste package. (This rate is called the mean seep flow rate). The drip rates selected for this report correspond to reasonable percolation flux values as shown in Figure 3.2-15 of Ref. 36. A range of drip rates was chosen. Specifically, values of 0.0015, 0.015, and 0.15 $m^3$/year were used for most cases, corresponding to percolation fluxes ranging from about 10 mm/year to 80 mm/year. The value of 10 mm/year corresponds to a high infiltration rate for the present-day climate and 80 mm/year corresponds to about twice the high infiltration rate for the glacial-transition climate (Ref. 36, Table 3.2-2). [Table 3.2-2 of Ref. 36 gives values of net infiltration rate, rather than percolation flux; however, they are equal at the potential repository level (Ref. 36, Section 3.2.3.4, p. 3-33)]. For a few runs, the range of allowed drip rates included an upper value of 0.5 $m^3$/yr, which represents about 100 mm/year percolation flux.

### 6.2.4 Sequence of Degradation Scenarios

The rationale for selecting a particular scenario for degradation sequence for the EQ6 simulations is to provide conservative assessments of solubility and transport of criticality control materials (Gd and Hf, the neutron absorbers) and fissile materials (i.e., U and Pu compounds) in the waste package. For internal criticality, conservative conditions are those that maximize the loss of Gd from the waste package, while maintaining a high level of U and Pu within the waste package. For external criticality, conservative conditions must maximize the loss of Pu and U and minimizes the loss of neutron absorbers from the waste package and maintain a high aqueous concentration of U and Pu. It is important to maintain a high aqueous concentration of U and Pu to allow precipitation in the fractures and lithophysae beneath the degrading waste package. For external criticality, a high uranium enrichment (molar ratio of U-235 to total U) of the aqueous phase is also considered conservative.

The degradation scenarios are divided into two general categories. The first category comprises single-stage cases, in which all reactants (steels, HLW glass, and fissile materials) are exposed simultaneously to the water in the waste package. Because the reaction rates of the materials in the waste package may vary greatly, the materials do not necessarily coexist for the entire span of the EQ6 calculation. For example, the carbon steel support structure may be completely corroded within the first few hundred years, whereas stainless steel components, and the more durable fuel types, may remain, largely uncorroded, for ~$10^4$ to $10^5$ years. The second category comprises two types of two-stage runs, referred to as Scenario I and Scenario II. For an example of a Scenario I two-stage run, consider the case of a Pu-ceramic waste package. The first stage involves exposing the A516 outer web (basket) and the GPCs (HLW glass and 304L steel) to water first, until the HLW glass is completely degraded and its alkalinity largely flushed out of the system. In the second stage, the 304L cans, magazines, rack, and Pu-ceramic disks are added as reactants. The aim of this two-stage run is to force a "conservative" condition of high acidity, by degrading the HLW glass rapidly, before all the acid-producing steel is degraded. For an example of a Scenario II two-stage run, consider the case of a Melt and Dilute codisposal waste package (Ref. 14, Section 5.2.2). The first stage involves an early breach of the 316L DOE canister containing the Melt and Dilute ingots, with everything degrading except the HLW glass. When the ingots degrade in this low pH environment, the uranium minerals are favored to form over the Gd minerals, and the Gd released from the ingots is flushed out of the package. In the second stage, the 304L canisters holding the HLW glass are allowed to breach.

### 6.2.5 Suppressed Minerals

The following minerals were suppressed (not allowed to form) in many of the EQ6 runs: quartz, tridymite, muscovite, celadonite, dolomite, dolomite-dis, dolomite-ord, annite, and phlogopite. The dolomites, micas (muscovite, annite, and phlogopite), and celadonite were suppressed because they are extremely unlikely to form at low temperatures. The more stable quartz and tridymite were suppressed because the J-13 water is supersaturated with them (Ref. 16, p. 12). In some cases, the log K value of minerals are adjusted for sensitivity studies ($Pu(OH)_4$ in Ref. 35, Section 5.1.3; $CaUO_4$ in Ref. 14, Section 6.2.3). In addition, in some cases the more stable iron and aluminum minerals are suppressed, such as hematite and diaspore, such that less stable goethite and gibbsite are formed.

### 6.2.6 Consequences of Lowered $fO_2$

Several sensitivity studies have shown that lowered $fO_2$ can dramatically reduce the loss of either actinides or Gd. For example, section 2 in Ref. 29 assessed the effect of simply lowering the $fO_2$ to $10^{-10}$ bars, from the default of $10^{-0.7}$ (0.2) bars. As shown in that calculation, $10^{-10}$ bars is not that "low" and is easily achievable in a natural, near-surface environment. The lowered $fO_2$ dropped calculated Gd loss from 20.45 to 1.3%, for a Pu-ceramic package, but had no significant effect on the Pu or U loss. Since the retention of Gd decreased the chance of internal criticality, use of atmospheric $fO_2$ (0.2 bars) was conservative. The cause of the reduced Gd loss was indirect. The lower $fO_2$ reduced acidity of the aqueous phase in the WP, by reducing the rate of acid production via oxidation of Cr (in steel) to $CrO_4^{=}$. Since $GdOHCO_3$ is the major Gd-containing solid phase in the simulations, reduction of acidity decreased the loss of Gd from the WP.

A more mechanistic analysis of $fO_2$ variation was used in Ref. 35. It was recognized that some of the most aggressive chemical environments, as modeled by EQ6, occurred when either steel or glass degraded very rapidly. However, under such conditions, the buildup of corrosion products should also be fast, and should provide a diffusive barrier to oxygen. Since the corrosion of steel or reduced actinides consumes oxygen, it is easy to achieve a state where the competition between corrosion and diffusion limits the local $fO_2$.

Figure 6-2, reprised from Section 6.3 of Ref. 35, compares the aqueous U and Pu concentrations for a run in which the $fO_2$ is fixed at 0.2 bars (case 1), versus a run in which a diffusive boundary layer is allowed to limit oxygen ingress (case 2). For the latter case, a very modest boundary layer thickness of 1 cm was assumed. This boundary thickness is considered to be very conservative, since the calculation predicts corrosion products amounting to ~20% of the entire package void space within $\sim 2.10^3$ years. (20% corresponds to particle volume; the actual sedimented volume of clay-like material, including porosity, could be much higher). When the oxygen ingress is limited by diffusion through the boundary layer, the aqueous Pu and U concentrations are 6 to 9 orders of magnitude lower in the early part of the calculation. The concentrations rise only after the supply of reducing materials (steels and reduced actinides) is consumed. Thus for the initial $\sim 3.10^4$ years, the case 2 conditions generate a much lower "source term" for external criticality calculations.

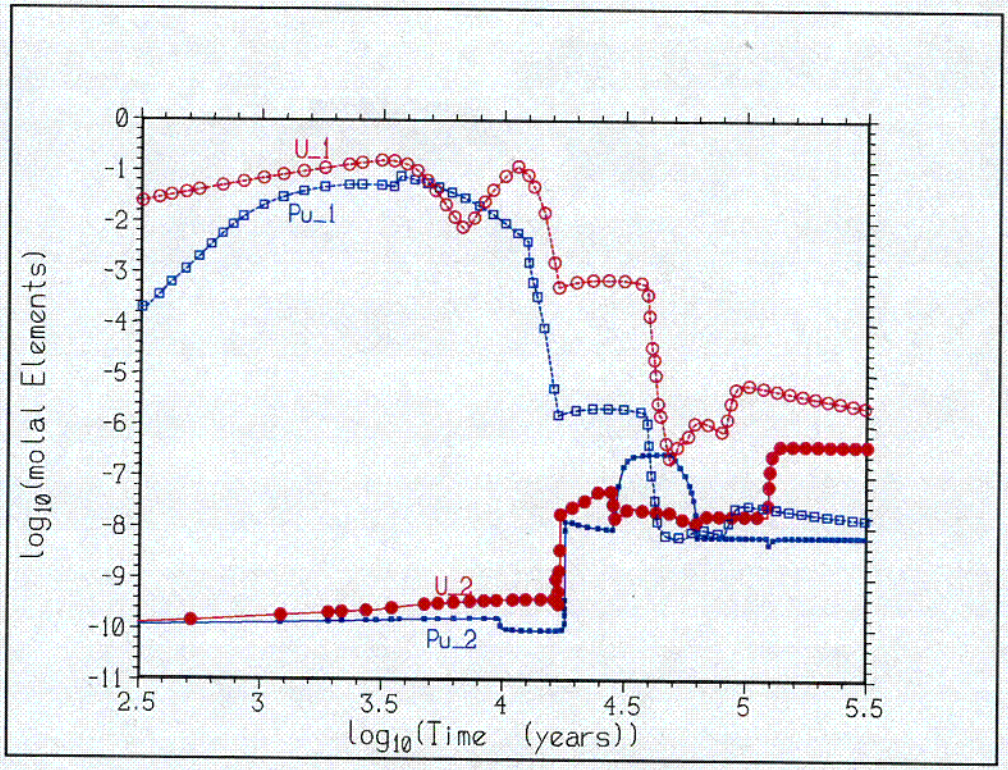


(U_1 and Pu_1) model with fixed system $fO_2$=0.2

(U_2 and Pu_2) model with fO2 determined by competition between diffusion (through a 1-cm boundary layer) and corrosion.

Figure 6-2: Aqueous U and Pu concentrations in the WP

C01

## 6.3 MODEL VALIDATION

The MDR model is a combination of simpler sub-models for the corrosion behavior of DHLW glass, actinide ceramics (such as spent fuel), and steels. The corrosion sub-models depend, in turn, on accurate thermodynamic data to describe the stabilities of the corrosion products, and on reasonable kinetic data for the corrosion mechanisms. Confidence in the MDR model can be increased, if the corrosion sub-models of the individual components can be validated. Validation consists of showing that the methodology used in the MDR sub-models, when applied to controlled experiments or well-studied analogues, correctly predicts the sequence of corrosion products, or the concentrations of solutes in the coexisting aqueous phases.

In this section, the EQ6 simulations for glass and fuel degradation are validated. The focus on glass and fuel modeling is in response to the findings of the DOE-NRC technical exchange (Ref. 60). Specifically, subissues 3 and 4 addressed the need to validate fuel and glass corrosion models.

The corrosion chemistry of steels, under oxidizing conditions, is well studied, and is not discussed further in this document. Steel corrosion shows little dependence on $fCO_2$, at least for near-atmospheric levels (Ref. 6, p. 536). In the pH range of 4 to 10, the corrosion rate of iron depends little on pH, but the rate has a significant dependence on oxygen availability (Ref. 6, p. 515). Thus the validation of steel corrosion models, under varying $fO_2$, will be covered in upcoming calculations and analyses that focus on WP degradation under varied $fO_2$ conditions.

### 6.3.1 Glass Degradation Sub-Model

Studies of archeological stained glass (Ref. 20 and Ref. 19) were chosen to validate the glass corrosion sub-model. In these studies, Cooper and Cox estimated glass degradation rates from both MCC-4 lab experiments (Ref. 69) and examination of 450 year-old glass exhumed from soils near the River Ouse, in York, England (Ref. 53). Several aspects of the archeological glass studies make them suitable for validation, such as:

(1) Some MCC-4 experiments were of sufficiently low temperature (85.5 °C) and sufficiently simple composition, to allow modeling via EQ6 at the same temperature. The glass had low corrosion resistance, and high alkali and alkaline-earth content, and is therefore more similar to waste glass than are natural analogues involving rhyolitic or basaltic glasses.

(2) The tests did not reach saturation with amorphous silica, and therefore were unaffected by the $(1 - (Q/K))$ affinity term (where Q is the ion activity product, and K is an effective equilibrium constant (Ref. 39). Many glass dissolution tests are performed such that the affinity term is significant; however, the EQ6 simulations do not include an affinity term, so those tests are difficult to model.

(3) The MCC-4 tests involve a flushed reactor, directly analogous to the SCFT model used in the MDR model. Ref. 20 reported that the initial agreement between the experiments and EQ6 was "not very encouraging;" however, they did not use a version of EQ6 with the SCFT capability, and did not attempt to include a pH dependence in the model.

(4) The 450 year-old glass had significant corrosion crusts, and was likely in a state of constant dampness and constant contact with clay minerals, during its burial period. These conditions are reasonably analogous to those predicted for the MDR model. Measured pH (7.6, from Ref. 20) approximates values measured in wells from the proposed repository (Ref. 58).

(5) The compositions and mineralogy of alteration products in both MCC-4 tests, and the buried archeological samples, are well documented; in most glass laboratory studies, the crusts are too thin, or too amorphous, for characterization.

(6) The 450 year-old samples appear to have degraded faster than expected, based on MCC-4 and static Dickson autoclave experiments, suggesting a mechanism that must be explained to justify conservatism and the use of experimental results. The authors suggested a pH mechanism for increasing degradation rates, which is testable with EQ6.

(7) The longevity of glass in the presence of clays has been questioned by Vernaz and Godon (Ref. 72, p. 30). This issue is relevant to the WP models, in which glass is expected to coexist with massive quantities of Fe-rich Si-poor nontronite clays. The Ouse region soils consist of clays, silts and limestone fragments (Ref. 53), and the interaction with clay was suggested as a cause of high corrosion rates by Ref. 20.

One disadvantage of the Cooper and Cox study is the lack of pH monitoring in the MCC-4 tests. However, simple mass-balance strongly constrains the pH of the solutions; and the pH is determined principally by the Na and K contents and the input rate for the MCC-4 tests. As will be shown, a variety of calculations converges on the same predicted pH.

#### 6.3.1.1 Metrics for Validation

The first and most important metric is a comparison of model predictions with the types and amounts of minerals formed in the MCC-4 tests at 85.5 °C, and on the 450 year-old archeological samples. For the second metric, the EQ6 simulations should predict the anomalous, high degradation rates claimed for the buried glasses. Because of the uncertainties in the natural degradation environment, the prediction is really a defensible explanation of the causes for rate variations. The third metric is the prediction of Mg concentrations in the MCC-4 tests. This test is subject to substantial uncertainties, so the principal aim of the model is to show that with reasonable assumptions, the approximate Mg concentration will be estimated, within the uncertainty of rate and surface area estimates. The prediction of Na, K, Ca and Si aqueous concentrations is not a strong test, as these elements are not strongly controlled by alteration minerals, and the prediction would involve little more than a consistency check on rates reported in the journal article. Furthermore, Cooper and Cox (Ref. 20) provide Mg and Ca concentrations, but do not provide explicit measurements of aqueous Na, K and Si for the 85.5 °C tests.

The purpose of the glass models, as used for in-package criticality, is to provide reasonable constraints on the effects of glass degradation on in-package chemistry. In particular, the models bound the types and mass of degradation minerals and the alkalinity and pH of the aqueous solutions that coexist with degrading glass. The literature abounds with detailed models for prediction of glass behavior (Ref. 39); we do not attempt to validate such detailed models, but rather to validate the bulk chemical evolution of the glass-water system. The minerals predicted by EQ6 runs are taken to represent the alteration crusts that form in experiments and in analogues; however, the EQ6 simulations do not consider explicitly the physical location of the crusts.

The EQ6 simulations do not consider an affinity effect for three reasons:

(1) it is generally conservative to ignore the affinity effect, and analyses have determined that the effect is unreliable as a means to slow glass degradation (Ref. 39)

(2) studies show that the affinity effect may be ephemeral, because clay nucleation may cause a return to high rates and low solution silica contents (Ref. 72)

(3) EQ6 does not provide a means to control the affinity term with an arbitrarily-selected set of aqueous species (e.g., $SiO_2$). In EQ6, the affinity term must use the full equilibrium constant K for the solid, and this constant is particularly meaningless for controlling glass degradation.

### 6.3.1.2 Methods: MCC-4 Models

Test 4a was selected (Table 2 in Ref. 20) because of its low temperature and comparatively long reaction time (i.e., long relative to the other low-T experiments). The temperature of this test (85.5 °C) is below the 100 °C limit of the current qualified thermodynamic database (Ref. 59). The MCC-4 tests involved continuous flow through a heated reactor vessel, and were modeled with the SCFT capability of EQ6 (Ref. 31). The authors specified that the test was run with deionized, distilled water; EQ3NR was used to provide an initial water composition (file stain00.3i), containing trace Na, K, Mg, Ca, P, and Si, and equilibrated to atmospheric $CO_2$ ($10^{-3.5}$ bar, Ref. 74, p. F-210) at 85.5 °C. This initial water was added to the model system as a "displacer" reactant, pushing an equal volume out of the vessel with each timestep. The vessel volume was taken as 80 $cm^3$ (Ref. 19, p. 527), the glass density as 2.62 $g/cm^3$, the surface area as 4.5 $cm^2$, and the water addition rate as 0.08 $cm^3$/minute (Ref. 20). These physical quantities were scaled to a standard EQ6 system with an aqueous volume of 1000 $cm^3$, via spreadsheet 'glass_archeol.xls' (folder 'glass', Attachment I).

The GICI glass composition from Table 1 of Ref. 20 was normalized to a molecular weight of 100 g in spreadsheet 'glass_archeol.xls', and presented in Table 6-10. A pseudo-mineral, GlassGICI, was created from this composition, and placed in the EQ6 database 'data0.yme' (Section 4.1.2). The glassGICI mineral was given a $\log_{10}K = 50$ for dissolution, which assures that the solid phase will never be stable under WP conditions. The pseudo-mineral was created purely to allow assignment of a TST rate law to the glass under EQ6.

Table 6-10: Simplified GICI Glass Composition

| Element | Moles |
|---|---|
| O | 2.5798 |
| Na | 0.0974 |
| Mg | 0.1845 |
| Al | 0.0315 |
| Si | 0.7711 |
| P | 0.0991 |
| K | 0.2966 |
| Ca | 0.3369 |
| Mn | 0.0241 |

Table 1 of Ref. 20, as simplified in 'glass_archeol.xls' (Attachment I)

Three types of EQ6 simulations, of increasing complexity, were used to simulate the MCC-4 test.

The first (Model A) employed a fixed glass dissolution rate, independent of pH, and equal to the normalized Na release rate given in Table 6 of Ref. 20; the conversion to EQ6 units is performed in spreadsheet 'glass_archeol.xls'. The input file used for this model is 'stain00A.6i'. However, it is apparent that the dissolution of the glass must have a dramatic effect on the system pH (Figure 6-5).

The second (Model B) used a pH-dependent glass dissolution rate, based on the functional form given by Ref. 39 (Section 6.1.1, equations 1 and 2, and Section 6.2.1.1) for the pH coefficients.

$$\text{Rate at low pH} = S.k_1 \,.\, 10^{-0.6.pH} \,.\, \exp(\_E_a/RT) \qquad \text{Equation 1}$$

$$\text{Rate at high pH} = S.k_2 \,.\, 10^{0.4.pH} \,.\, \exp(\_E_a/RT) \qquad \text{Equation 2}$$

where S is the surface area and the rate is given in mols/($cm^2$.s), $E_a$ is the activation energy in J/mole, and R is the gas constant in J/(mole.K). The $k_1$ and $k_2$ were obtained by successively incrementing the Ref. 39 values until the final, total dissolution rate matched the steady-state rate reported by Ref. 20. The files used for the incremental testing are named 'staine?a.6i', where ? is a number from 1 to 6 ('staine6a.6i' was the file that matched the observed steady-state glass rates).

Both Models A and B allow instantaneous precipitation of minerals (corrosion products) that achieve saturation. It is expected that these models will produce a rapid and unrealistic drop in the aqueous Mg concentration, due to precipitation of Mg-rich saponites.

Model C pursues a more realistic simulation of aqueous Mg, by deriving TST precipitation rates from the smectite dissolution rates determined by Ref. 51, (Abstract and p. 402). Three choices were tested for the effective surface area of the precipitating smectite.

For Model C1, the baseline area was taken as the glass surface area. Micrographs of the corrosion crusts (e.g. Figure 2 in Ref. 20) show that the platy alteration minerals tend to grow with the plate surfaces roughly perpendicular to the glass surface, and the plate edges exposed sub-parallel to the glass surface. The input file for Model C1 was 'staine6s.6i'.

Model C2 uses a surface area of 1/5 the glass surface area, and is motivated by the observation of Turner and Pabalan (Ref. 71, p. 377) that the grain edges are the significant sorption sites on most clays. If the clay particles are oriented with the platy surfaces perpendicular to the glass surface, it is very unlikely that the edges will exceed the total surface area of the substrate (Turner and Pabalan suggest 10% of the total surface area is grain edges). The input file for Model C2 was 'stai_e6s.6i'.

On the other extreme, model C3 uses ten times the glass geometric surface area, and was chosen to assess the possibility that Huertas et al. (Ref. 51, p. 403) underestimated the activation energy (hence the 85.5 ∘C dissolution rate). The input file for Model C3 is 'stai!e6s.6i'.

### 6.3.1.3 Results: MCC-4 Models

All models show an initial rise, followed by a plateau, for aqueous Na, K, Ca, Si and pH (Figure 6-5, Figure 6-3, and Figure 6-4); calculated in spreadsheet 'elem_stain00a_staine6a _stai_e6s.xls' (Attachment I). While Cooper and Cox (Ref. 20) refer to "initial and long-term" release rates, it is important to recognize that with the MCC-4 tests, the initial fast rise in concentration is largely unrelated to a change in the glass degradation mechanism.

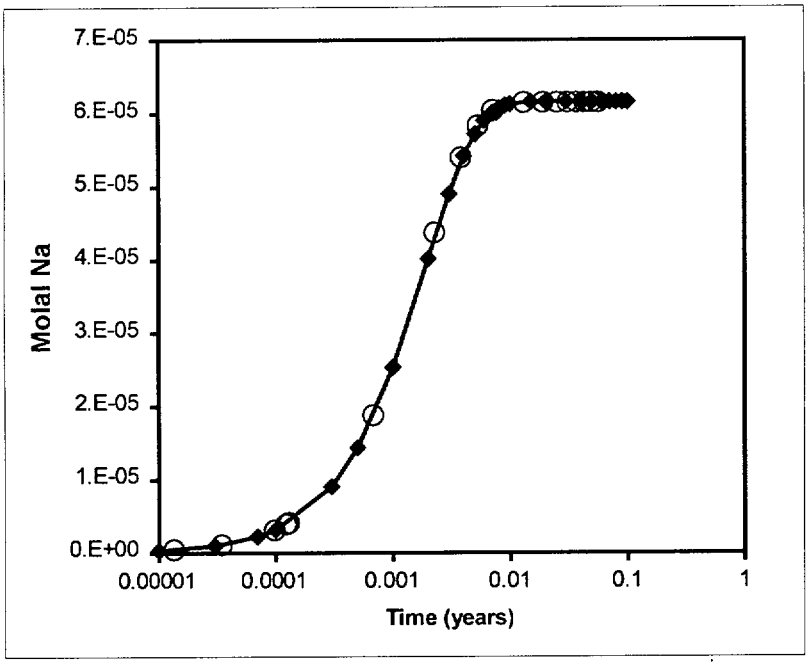


The diamonds and continuous curve represent the analytical solution Equation 3and Equation 4;

The open circles show the results from MCC-4 Model A (file 'stain00A.6i').

Figure 6-3: Molal Na vs Time for Analytical Solution vs Model

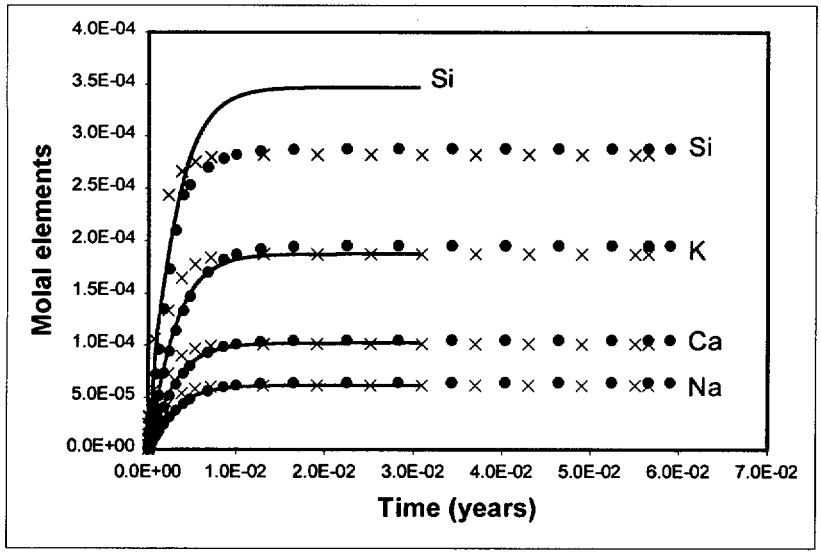


Model A (× symbols), Model B (•) and Model C2 (solid line).

Figure 6-4: Predicted Si, K, Ca and Na Variations for MCC-4

Consider a model with a constant glass degradation rate, for elements such as Na and K (which are largely uninvolved in precipitation reactions, so long as the solutions are kept dilute by high flow rates). The aqueous molarity, is determined by the competition between glass dissolution and removal by flushing. The equation to describe the evolution of molarity, in such a system, is:

$$dM/dt = (S \cdot f \cdot k)/V - M \cdot (dV/dt)/V$$

Equation 3

where t is time in seconds, S is the total surface area of the glass in $cm^2$, f is the number of mols of the element per mol of glass, k is the dissolution rate in (mols glass)/($cm^2$·s), dV/dt is the rate of water flushing through the MCC-4 test ($cm^3$/s), and V is the test vessel volume in $cm^3$. Equation 3 is derived by simple mass balance. For such dilute solutions, molarity is approximately equal to molality. It is easily verified, by substitution, that the solution to Equation 3 is:

$$M = ((S \cdot k \cdot f)/(dV/dt)) \cdot [1 - \exp(-(t \cdot dV/dt)/V)]$$

Equation 4

Thus there will be an initial rise in the aqueous concentration, followed by a plateau to M = ((S·k·f)/(dV/dt)) at long times, even though the glass corrosion rate is unchanging. Figure 6-3 compares Na concentrations predicted by Equation 4, to the results of Model A (EQ6 run 'stain00A.6i'). The excellent agreement indicates that the SCFT model in EQ6 is implemented correctly.

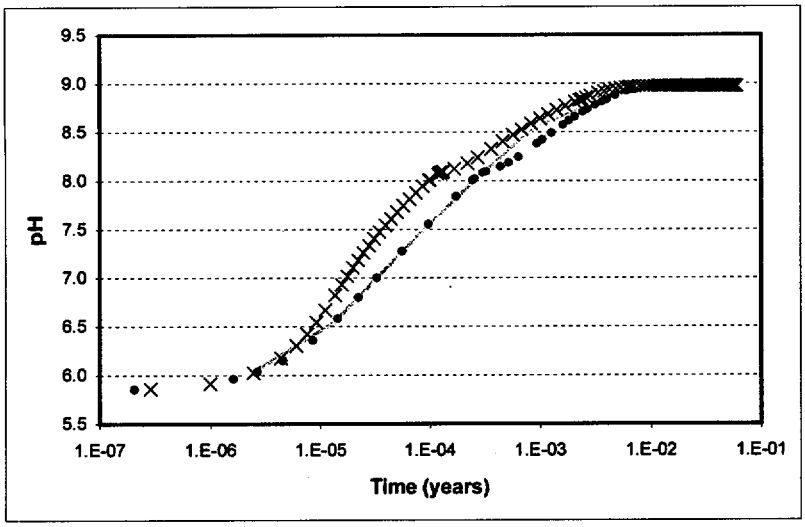


Model A (× symbols), Model B (•) and Model C2 (solid line)

Figure 6-5: Predicted pH Variations for MCC-4.

Figure 6-4 shows the predicted behavior of aqueous Na, Ca, K and Si. All models produce substantially similar results; the slight exception is the plateau Si content for Model C3, for which the aqueous Si is ~20% higher. For Model C2, the higher Si is due to the inhibition of Mg-smectite precipitation, which normally serves as a sink for silica. Figure 6-5 shows the evolution of pH for Models A, B and C. All models show a rapid rise to essentially the same pH (~9 at 85.5 °C). Because of the log time scale, Figure 6-5 emphasizes differences at early times; however, the various models produce nearly identical pH for the final 90% of the simulation time.

Figure 6-6 and Figure 6-7 show the predicted evolution of minerals assemblages (corrosion crusts) for Models A and C2, respectively. In both models, the dominant alteration phases are saponite (an Mg-smectite), apatite, and $MnO_2$, in molar proportions ~ 1 : 0.55 : 0.40. The observed minerals (Ref. 20) were Mg-smectite and apatite in the proportions ~ 1 : 0.33, with no explicit observation of $MnO_2$. However, in the Cox and Ford 1993 study, $MnO_2$ dendrites were observed in the corrosion crusts of similar glasses (Ref. 21, Figure 2 in original article). In the 1996 study, it may have been extremely difficult to identify an amorphous $MnO_2$ phase by the methods used. Cooper and Cox (Ref. 20, p. 513) characterize the smectite as $Mg_{(2-x)}Mn_x[(Si_{(4-y)}Al_y)O_{10}](OH)_2 \cdot nH_2O$, where x varies from 0 to 0.4 and y from 0.1 to 0.4; this formula requires the Mn be in the (IV) state for charge balance. Since Mn(IV)-smectites are not well-known, it seems possible that the clay observed by Cooper and Cox is actually an intergrowth of smectite and amorphous $MnO_2$. Thus, the agreement between the observed and predicted mineral assemblages is reasonably good.

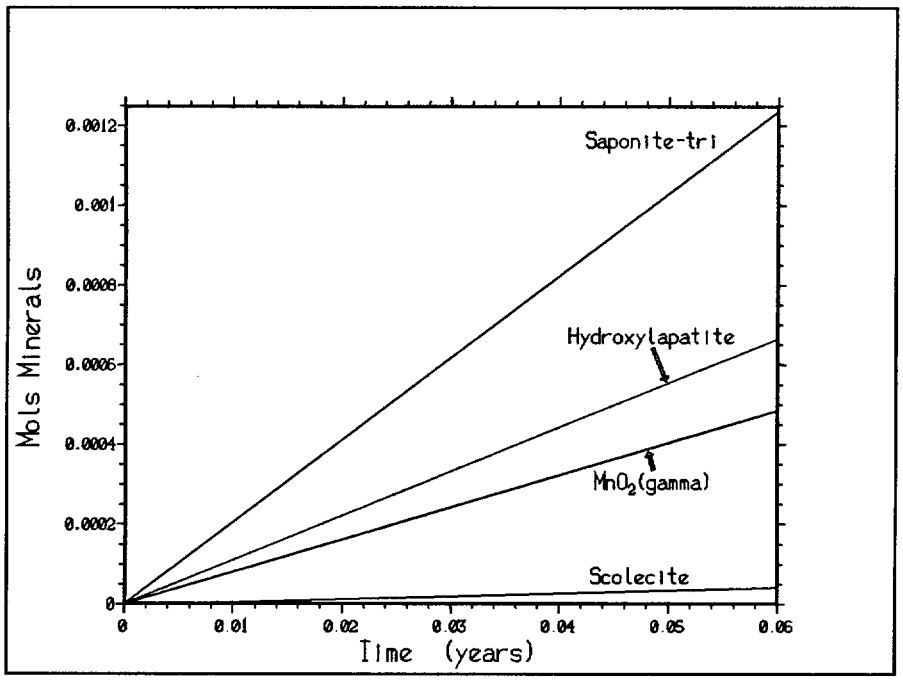


Figure 6-6: Corrosion Minerals Predicted for MCC-4 Model A

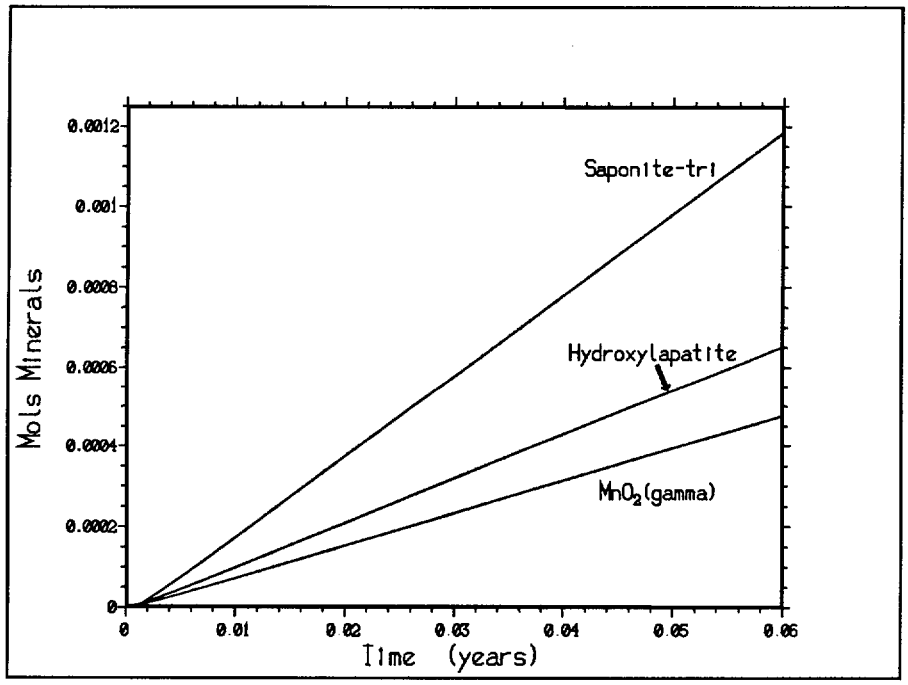


Figure 6-7: Corrosion Minerals Predicted for MCC-4 Model C2

The predicted volume of all corrosion products for Model C2, is 0.02148 $cm^3$. The observed crust thickness is 10 to 40 microns, corresponding to 0.00450 to 0.01800 $cm^3$, with an average of 0.01125. Thus, the model predicts roughly twice the "average" observed volume. Given the

approximate nature of the observed thicknesses, and the uncertainty in the rates and effective surface areas, this agreement is considered reasonably good.

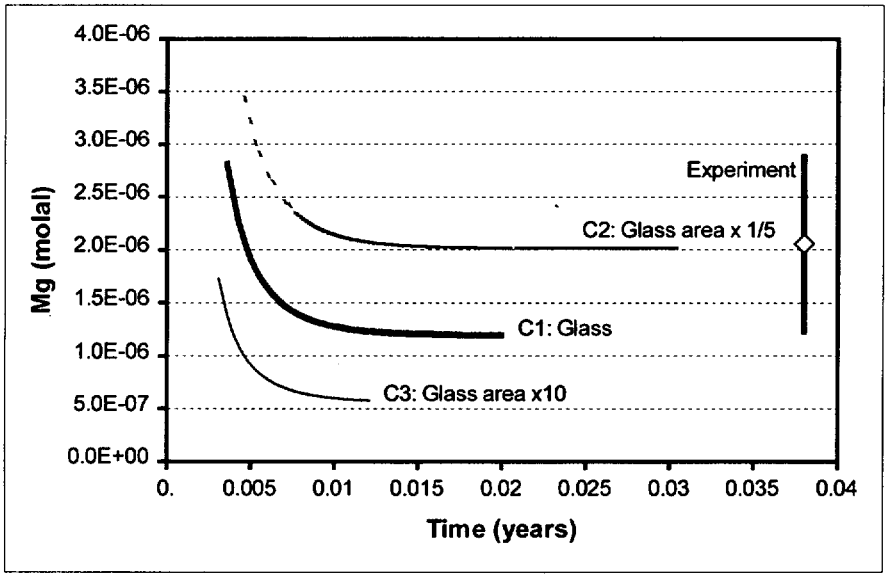


Note: Spreadsheet 'Mg_stain_glass_expt.xls'.

Figure 6-8: Experimentally Observed (error bar) Aqueous Mg Concentrations, and Concentrations Predicted for Models C1, C2 and C3

Figure 6-8 gives the Mg concentrations observed in the MCC-4 test (at steady-state), and the concentrations predicted by Models C1, C2 and C3. Despite the 50-fold variation in the surface area used in the models, the plateau Mg concentration varies by just a factor of four. The C2 Model predicts Mg concentrations close to the observed mean, and the C1 Model is just outside the observed Mg concentration range. The agreement between the models and observation is good, given the uncertainties in the effective surface areas, rates, and the approximation inherent in deriving a TST precipitation law from dissolution studies.

### 6.3.1.4 Methods: Archeological Models

The degradation of glass shards in soil, for up to 320 years, was modeled in a two-step process. First, water was equilibrated at 25 °C with illite and calcite at $fO_2$=0.2, based on the observations that the Yorkshire soils contain clays and limestones (Ref. 53, p. 325), and that calcite is observed within or adjacent to the altered glass (Ref. 20, p. 513). The $CO_2$ fugacity of this initial solution was varied until the equilibrium pH matched the observed soil pH of 7.6 (Ref. 19, p. 525). The final $fCO_2$ was ~ $10^{-2.22}$. The input files for the process were 'clay!h2o.3i' and 'clay!h2o.6i' (folder 'glass' in Attachment I). The solids were removed from this fluid, and the fluid (hereafter called "soil water") was used as a "displacer" reactant in the second stage of the model. The second stage represents the flow of soil water past a buried glass shard; the $fCO_2$ and $fO_2$ were not fixed in the second stage, but were controlled by the gases dissolved in the soil water, and the interaction with the degrading glass.

Two variations on the archeological model (hereafter called I and II) were considered. Model I

is intended to represent a glass shard in an environment that washes the surface efficiently, via the downward flux of water from rainfall. The input file for Model I was 'gla!cly0.6i'. For the EQ6 simulation, the aqueous volume around the shard is defined by the shard length and width, and by the effective diffusion thickness (calculated in spreadsheet 'glass_archeol.xls', sheet 'comp&size'; Figure 6-9).

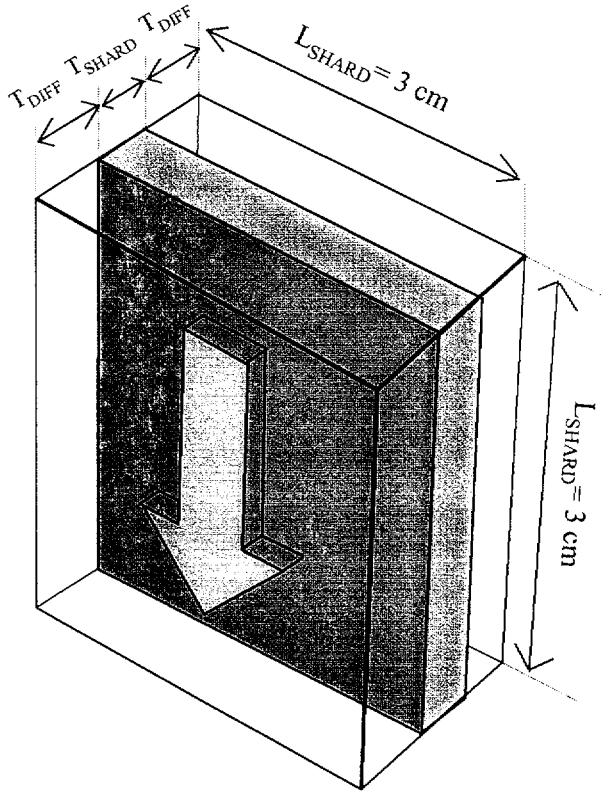


NOTE: Flow of soil water is in the direction of the large arrow. The thickness of the diffusion zone ($T_{DIFF}$) is defined in spreadsheet 'glass_archeol.xls'. The shard length is $L_{SHARD}$, and the fluid volume for the EQ6 calculation is $2 \cdot L_{SHARD}^2 \cdot T_{DIFF}$.

Figure 6-9: Geometry for Archeological Glass Corrosion Models I and II

The diffusion thickness is the approximate distance solutes would diffuse into the surrounding porous soil, during the length of time it would take a packet of recharge water to flow the length of the shard. The recharge rate is taken as 100 cm/year; this is an upper estimate, exceeding the observed average precipitation rate of 90.6 cm/yr for the Upper Yorkshire catchment basin (Ref. 53, p. 325). (Rainfall provides an overestimate of true recharge, because some of the precipitation is lost to evaporation and uptake by plant roots. Moreover, in a clay-rich soil, there may be regions of very low permeability, and locally low fluence of water.) With the dimensions of the EQ6 volume, the presumed recharge rate defines a flux of soil water into the system. Model I is not intended to be a realistic depiction of the soil water system, but a plausible upper bound on the flushing experienced by the glass shards. Model II is identical to Model I, except the total flux of soil water through the system is dropped by a factor of ten, to

represent a system with more limited flushing, such that the fluid near the glass surface will have a higher probability of accumulating alkali metals from glass degradation. Model I was run out to 65 years, at which point the calculation reached a steady-state, and iteration became prohibitively slow. Model II was run to 320 years, again limited by the decreasing size of the EQ6 time steps. The input file for Model II was 'gla!cly2.6i'.

### 6.3.1.5 Results: Archeological Models

The difference in behavior, between the two models, is striking, and provides a simple explanation for the observation of Cooper and Cox (Ref. 20) that the soil glass appeared to have corroded more rapidly than would be predicted by the MCC-4 experiments.

Figure 6-10 and Figure 6-11 show the pH, and amount of glass remaining, for Models I and II. For Model I, the pH plateaus at 7.84, only slightly above the initial soil water value of 7.6, and the glass degradation rate is sufficiently slow to ensure that some of the shard will remain at the end of 450 years. In Model II, the pH rapidly reaches a plateau of 11.1, which greatly increases the degradation rate, so that no glass remains after ~26 years. The high pH is achieved by two factors. First, the lower flushing rate allows more alkali to build up near the surface of the shard, which raises the pH; and in turn, the increased pH further increases the degradation rate (via Equation 2), producing a positive feedback. Thus, the speculation of Cooper and Cox (Ref. 20, p. 518) that in the soils, "the pH at the glass surface may be very high" appears justified.

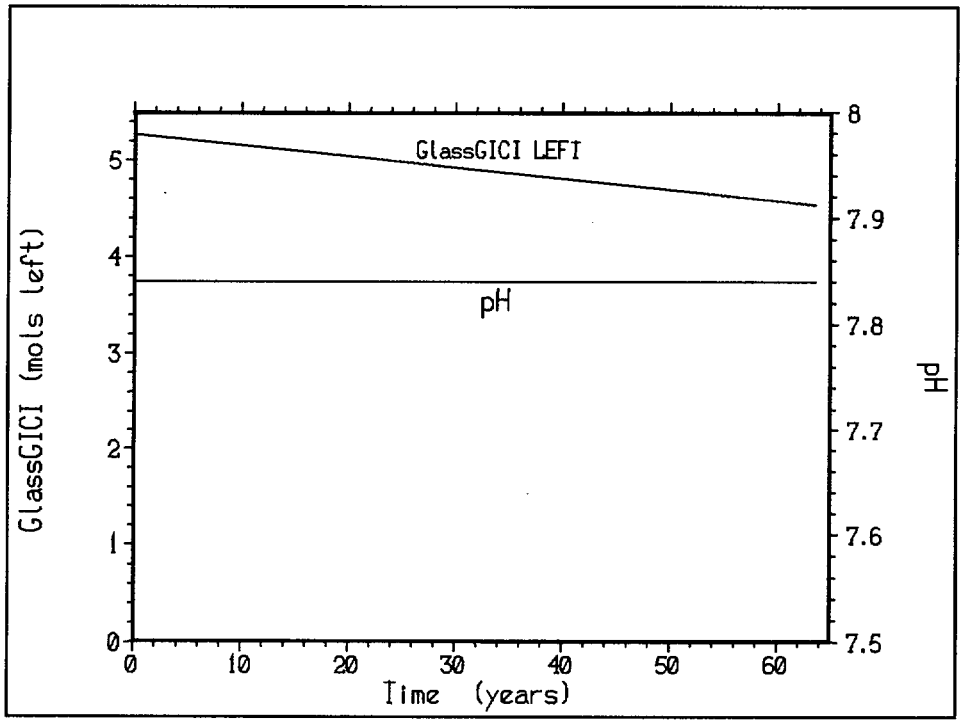


Figure 6-10: pH and Glass Consumption for In-Soil Corrosion Model, Model I

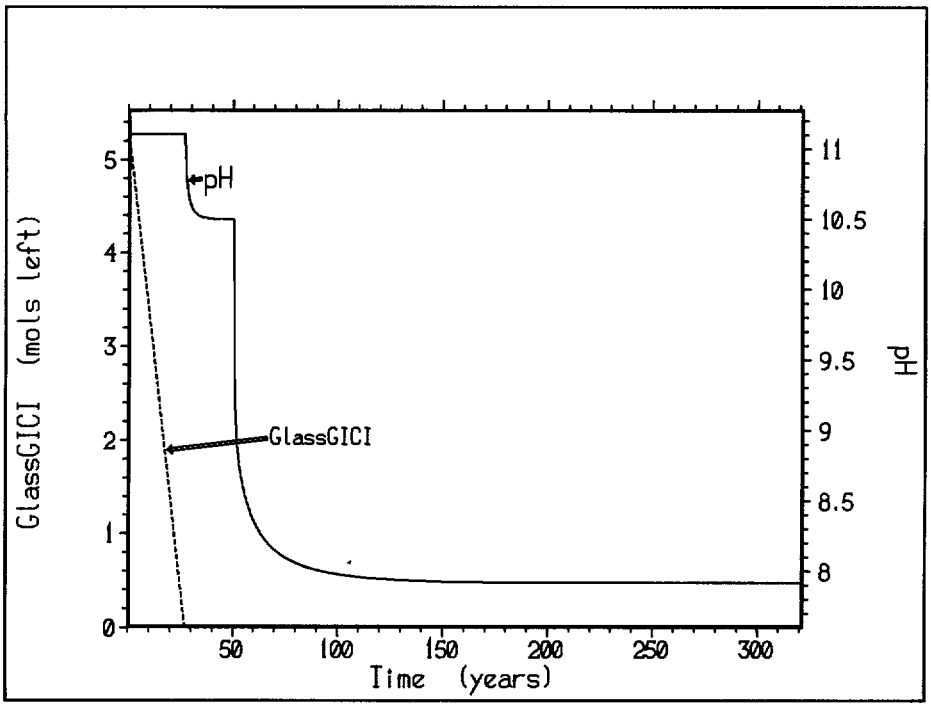


Figure 6-11: pH and Glass Consumption for In-Soil Corrosion Model, Flow Rate Dropped by 10x, Model II

Figure 6-12 and Figure 6-13 show the minerals predicted for Models I and II. In both models, calcite ($CaCO_3$), silica (here modeled as chalcedony, or cryptocrystalline quartz), apatite and $MnO_2$ dominate. For the archeological corrosion crusts, the observed phases are: a porous silica "gel," Ca-phosphate, $CaCO_3$ and $MnO_2$. Thus if the chalcedony is associated with the porous silica "gel," the match between model and observation is quite good. Presumably, silica gel is a thermodynamically less stable than chalcedony; however, the "gel" may be stabilized, relative to chalcedony, by residual alkali (Ref. 41, pp. 345-346).

### 6.3.2 Summary of Glass Modeling

The MCC-4 and archeological models meet the proposed metrics. The MCC-4 models match the types and amounts of experimentally observed phases, given the uncertainties in the experiments and the subsequent chemical analyses. The aqueous Mg concentration is matched with varying success, depending on the estimate of surface area. For the two lower surface areas, Mg concentrations either match well, or nearly within the experimental uncertainty; while for the highest surface area, the predicted values are ~$1/4^{th}$ the observed value. Given the factor 50 rate variation implicit in this test, the overall match is considered good. The archeological model provides a plausible explanation for the accelerated dissolution rates (local high pH from slow rates of recharge), and also matches the product phase assemblages.

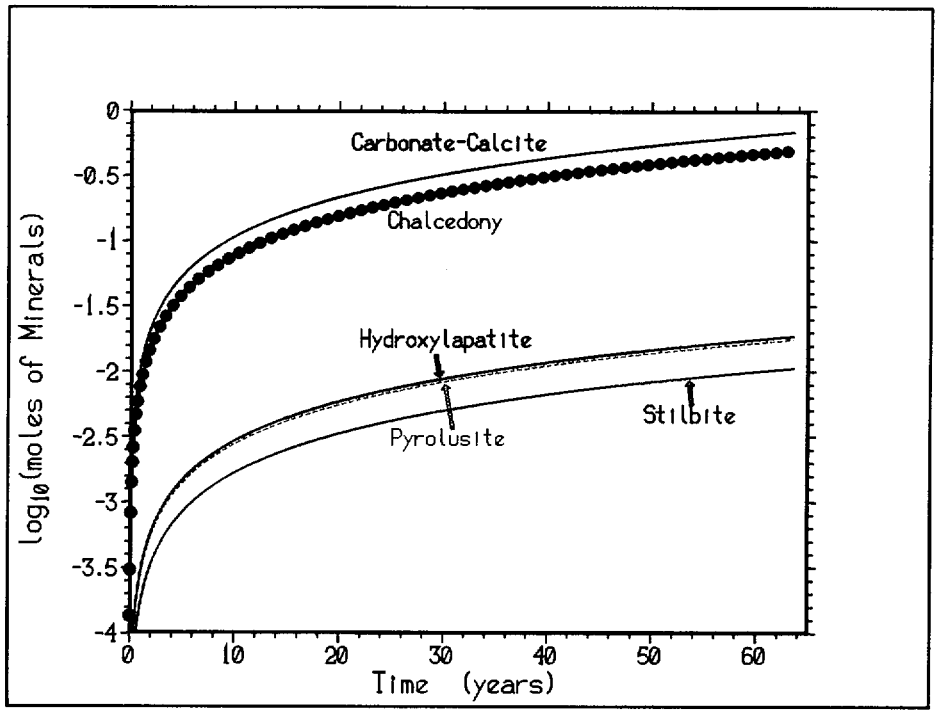


Figure 6-12: Minerals Predicted for In-Soil Corrosion Model, Model I

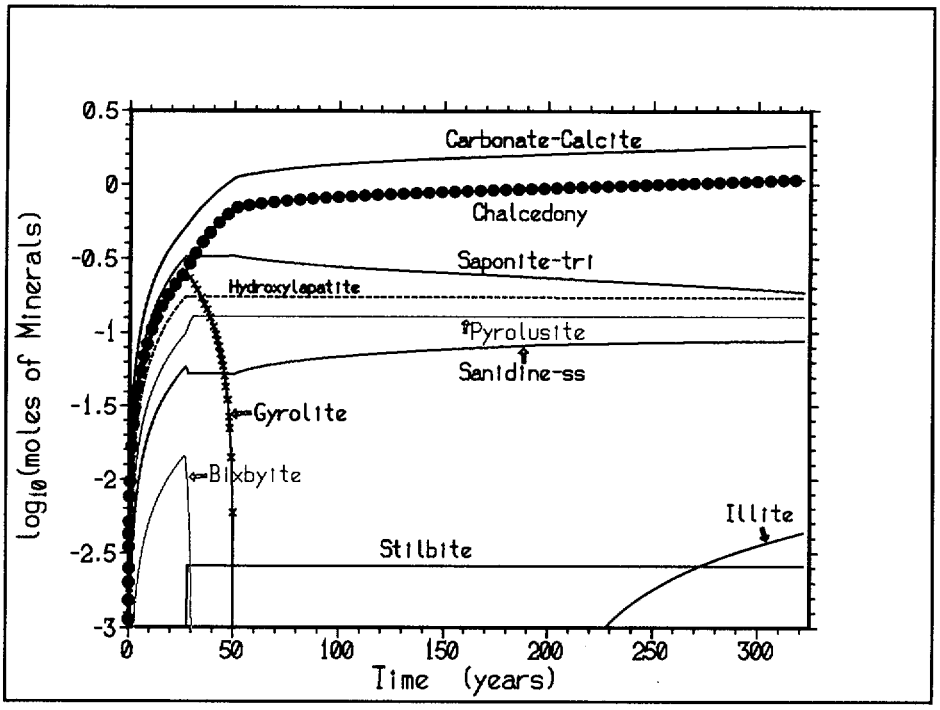


Figure 6-13: Minerals Predicted for In-Soil Corrosion Model, Flow Rate Dropped by 10x, Model II

### 6.3.3 Fuel Degradation Sub-Model

The fuel degradation sub-model can be validated by comparison with laboratory experiments. In particular, confidence in the model is increased if the model predicts the minerals formed in the experiments, and also predicts some quantitative aspect of the experimental chemistry, such as aqueous concentrations of actinides. To be suitable for such a comparison, the experiments must meet the following conditions:

(1) Thermodynamic data must be available, or easily extrapolated, for the experimental conditions. In the current, qualified EQ6 database Ref. 59, thermodynamic data for most actinide solids and aqueous species are limited to 25°C. Thus it is necessary to use experiments conducted at low temperature.

(2) The experimental work should provide chemical composition, the amount, total surface area, and the rate of degradation for each component, so that a quantitative model can be constructed.

(3) The experiments should involve materials and conditions similar to those expected in the WP; these conditions include the composition of the in-dripping aqueous phase.

(4) The experiment should be of as long duration as possible, to increase confidence in the extrapolation to the time scales of WP degradation.

The HBR-3-25 experiments of Wilson (Ref. 75) and Wilson and Bruton (Ref. 76) were chosen for validation of the EQ6 fuel degradation sub-model. These experiments meet the criteria outlined above; the tests were conducted at 25°C, the solutions were analyzed periodically for actinide concentration, the material used was an actual spent fuel in J-13 water, in a stainless-steel vessel; and the tests were run for up to a year. The radiation environment was undoubtedly more severe in the experiments, than would be expected for a WP breached after $10^4$ years, since the spent fuel used in the experiments contained significant activity of short-lived fission products.

#### 6.3.3.1 Preliminary Fuel Model 1 and $PuO_2$ Solubility Sensitivity

Fuel Model 1 is based on the calculations provided by Wilson and Bruton (Ref. 76). The template for the Fuel Model 1 is the standard EQ6 test file 'j13wsf.6i' (Ref. 77, p. 297, called 'j13wwsf.6i' in original manual). This test file simulates the reaction of 100 g of spent $UO_2$ fuel into 1000 g J-13-like water at $\log_{10}(f(CO_2)) = -3.5$. Fuel Model 1 differs from the original Wilson and Bruton calculations in two ways: (1) Fuel Model 1 uses the qualified 'data0.ymp' database, vs. the older data0.com used by Wilson and Bruton, and (2) Fuel Model 1 uses the "closed system" option, as opposed to the "titration" option, to ensure that the calculation runs until all the fuel is reacted and near-steady-state aqueous concentrations are achieved. The Fuel Model 1 input file is denoted 'j13wsf_.6i' and is located in folder 'j13wsf'.

Figure 6-14 compares the experimentally measured Pu concentrations with the EQ6 predictions of Fuel Model 1 (indicated by 'data0.ymp'), and the EQ6 predictions of Wilson and Bruton. Wilson and Bruton give two values, based on the assumptions of equilibrium with amorphous $Pu(OH)_4$ versus equilibrium with crystalline $PuO_2$. Clearly, the Fuel Model 1 predictions are much closer to the experimental results, than are the original Wilson and Bruton predictions. The better match is due principally to the updated thermodynamic data for $PuO_2$. However, the Fuel Model 1 result is still ~ 1.3 orders higher than the experimental observations. To better

match the experimental values, the stability constant in the thermodynamic database, logK, for $PuO_2$ was reduced by 1.3 units, via the EQ6 "augmentk" input file parameter (folder 'j13wsf', file 'j13wsf13.6i'). Not surprisingly, the result is a close match between the predicted Pu concentrations with the experimental values (folder 'j13wsf', file 'j13wsf_.xls'). Figure 6-14 shows the "augmentk=-1.3" line matches exactly with the experimental value.

Using Pu concentrations that are higher than expected is conservative for external criticality concern, but not conservative for internal criticality concerns. To determine the sensitivity to the value of the logK for $PuO_2$ on losses from the waste package, a case from a recent calculation (Ref. 15, Case s10) was rerun, using the database as it is ('data0.yme') and using a $PuO_2$ logK value that was lowered by 1.3. The cumulative losses of Gd, Pu, and U were calculated (folder 'j13wsf', file 'j13wsf_.xls') and are listed in Table 6-11. The loss of Pu and U was only slightly higher for the case that uses the 'data0.yme' database.

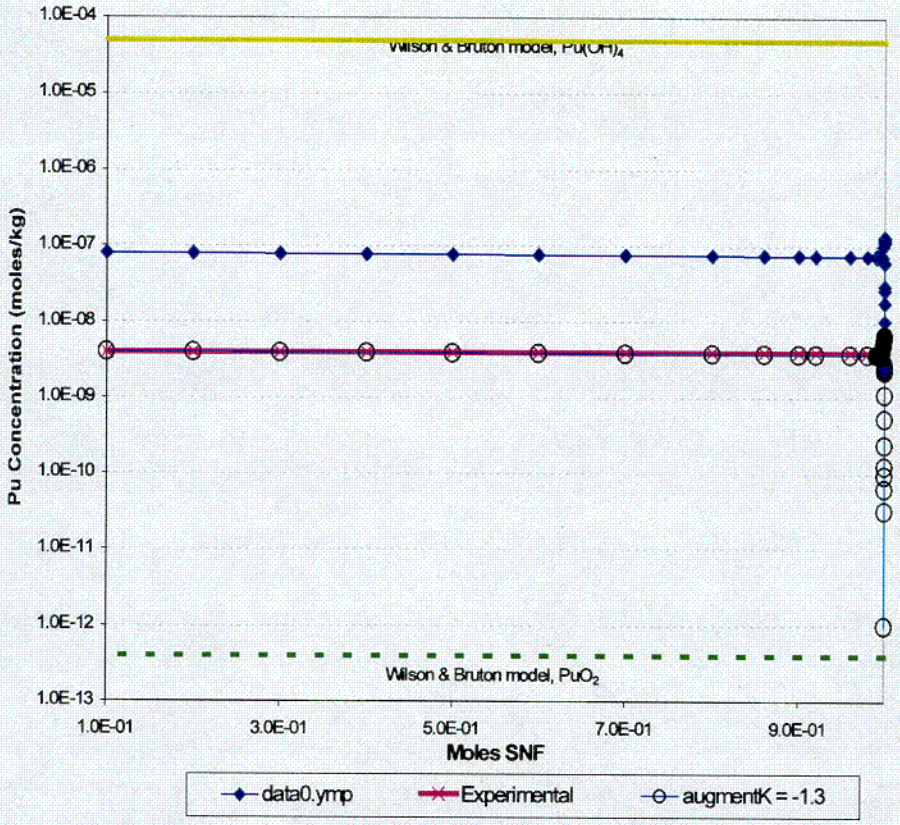


Figure 6-14. Simulated Versus Experimental Pu Concentration

C02

Table 6-11. Comparison of Results with Reduced $PuO_2$ LogK Values

| Case ID | Root Name | LogK $PuO_2$ | Years | %Gd Loss[a] | %Pu & U Loss |
|---|---|---|---|---|---|
| s10 | p52_L142 | -4.2197 ('data0.yme') | 2.22E+04 | 53.35 | 0.45 |
| s10a | p52aL142 | -5.5197 (augmentk = -1.3) | 2.22E+04 | 53.36 | 0.39 |

For aqueous uranium, the agreement between experiments and the Fuel Model 1 is significantly worse. Fuel Model 1 predicts an aqueous U concentration of $\sim 10^{-4}$ M. For cycle 3 of HBR-3-25 (the "cleanest" subset of the experiment, in which the high-surface area fines had been removed), the observed aqueous U is $\sim 10^{-6}$ M, two orders of magnitude lower. However, there are obvious limitations in Fuel Model 1. First, the model is non-kinetic. Given the limited amount of silica in the J-13 water, the long-term U concentration will always rise to a level determined by schoepite ($UO_3 \cdot nH_2O$) once all the silica is consumed. Second, the Wilson and Bruton model fixes the fugacities of $O_2$ and $CO_2$ to ambient values, while the series 2 experiments were nominally capped, and the series 3 experiments were definitely closed. The dominant aqueous U species, predicted by Fuel Model 1, are $(UO_2)_2CO_3(OH)_2$, $UO_2(CO_3)_2^{2-}$ and $UO_2(CO_3)_3^{4-}$. The equilibrium constants (Ks) for these species depend on the carbonate concentration raised to the first, second and third powers, respectively, so the U solubility is fairly sensitive to the assumptions about $CO_2$ control. (In contrast to the Wilson and Bruton experiments, the WP degradation models are inherently open to the atmosphere, thus it is more reasonable to model the WPs with fixed $CO_2$ fugacities.) The following section discusses refinements to the basic Wilson and Bruton model.

### 6.3.3.2 Degradation Fuel Model 2

Fuel Model 1 (Section 6.3.3.1) can be refined by using kinetic degradation rates, and by implementing more realistic controls on the $O_2$ and $CO_2$ fugacities. Fuel Model 2, developed in this section, is a more detailed simulation of cycle 3 of the HBR-3-25 test, as described by Wilson (Ref. 75).

Test HBR-3-25 employed bare (clad removed) SNF fuel in a sealed 304 stainless steel container at 25°C. Cycle 3 of this test was analyzed by Steward (Ref. 32, Table 28), who derived specific surface areas and degradation rates. After the reaction vessel was filled, the test was closed to the atmosphere, and involved 80.7g of fuel in 250 $cm^3$ of J-13 water. The EQ6 simulation did not buffer the $fO_2$ or $fCO_2$, but allowed the gas fugacities to drift; in contrast, Wilson and Bruton (Ref. 76) chose to fix gas fugacities to the atmospheric ambient. The details of the EQ6 simulation, including the fuel composition (molar), degradation rate (moles/$cm^2$-s), geometric surface area ($cm^2$/g), and moles of $O_2$ and $CO_2$ in the headspace are explained in file 'j13fuel_081001.xls', in folder 'Fuel2' (Attachment I). The EQ6 simulation was run for 1.0 year. Two versions of Fuel Model 2 were run. Fuel Model 2A ignored the stainless steel container (input filename: 'j13fuel.6i'), used for the HBR-3-25 test, whereas Fuel Model 2B included the steel liner of the vessel (input filename: 'j13sfuel.6i').

Figure 6-15 and Figure 6-16, respectively, show the concentration of radionuclides in solution

and the mineral assemblage, as predicted by Fuel Model 2A. The sequence of U minerals, formed from the reaction of J-13 with the corroding fuel, begins with formation of alpha-uranophane ($Ca(UO_2SiO_3OH)_2 \cdot H_2O$), followed by boltwoodite ($NaUO_2SiO_3OH \cdot 1.5H_2O$) and schoepite ($UO_3 \cdot nH_2O$). The mineralization sequence appears to follow an increase in the ratio of uranium to silicate, reflecting a decrease in concentration of silica in J-13 water.

Wilson reports the results of instrumental analysis with a Scanning Electron Microscope (SEM) equipped with an Energy Dispersive X-Ray (EDX) unit for semi-quantitative analysis of alteration-product compositions. In addition, powder X- Ray Diffraction (XRD) was performed on selected runs. The EDX spectrum (Figure 4 of Ref. 75) identified a calcium-uranium-silicate composition. The XRD patterns of the same test at higher temperature (HBR-3-85) identified uranophane and tentatively, haiweeite. In addition, precipitated silica and calcite flakes were also identified on several of the filters. Examining Figure 6-16 of the EQ6 simulation for the same period as the experiments reveals similar mineralization patterns, with formation of uranophane as the major uranosilicate mineral, and both precipitation and dissolution of calcite and chalcedony. This comparison shows reasonably good agreement between the experiments and Fuel Model 2A. Haiweeite is not predicted in Fuel Model 2A, simply because there is no entry for Haiweeite in the thermodynamic database ('data0.ymp', Ref. 59). Nonetheless, only very small quantities of haiweeite were observed in the experiments.

Quantitatively, U and Pu concentrations reported by Wilson were 0.3-0.4 μg/ml for U (Figure 6-17, cycle 3, HBR 3-25) and 80-100 pCi/ml for Pu. Wilson provides a conversion factor of 1.0ng Pu/ml = 100 pCi/ml for Pu that corresponds to a concentration of 0.8-1.0 ng Pu/ml. Conversion to molality allows a comparison of the results obtained by EQ6 simulations to those reported by Wilson. The conversion of U concentration reported by Wilson is:

$$0.3\frac{\mu g \text{ of } U}{ml \text{ soln}} \times \frac{1000ml \text{ soln}}{1L \text{ soln}} \times \frac{1L \text{ soln}}{kg \text{ soln}} \times \frac{1g \text{ soln}}{10^6 \mu g \text{ soln}} \times \frac{1 \text{ mole } U}{238 \text{ g of } U} = 1.26 \cdot 10^{-6} \frac{\text{moles } U}{kg \text{ soln}}$$

A concentration of 0.4 μg U/ ml results in a concentration of $1.68 \cdot 10^{-6}$ moles U/kg soln. In comparison, Fuel Model 2A predicts a concentration of $1.66 \cdot 10^{-6}$ moles U/ kg soln (inverse log of –5.78, Figure 6-15) which is in excellent agreement with the results obtained by Wilson.

The conversion of Pu concentration reported by Wilson is:

$$0.1\frac{ng \text{ of } Pu}{ml \text{ soln}} \times \frac{1000ml \text{ soln}}{1L \text{ of soln}} \times \frac{1L \text{ soln}}{kg \text{ soln}} \times \frac{1g \text{ soln}}{10^9 ng \text{ soln}} \times \frac{1 \text{ mole } Pu}{244 \text{ g of } Pu} = 4.1 \cdot 10^{-9} \frac{\text{moles } Pu}{kg \text{ soln}}$$

EQ6 simulation predicts a concentration of $8.91 \cdot 10^{-8}$ moles Pu/ kg soln (inverse log of –7.05, Figure 6-15). The agreement is within a factor of 5, which is significantly better than the factor 20 difference seen in Fuel Model 1. In addition, it must be considered that in the Wilson experiment, all samples were passed through a 0.45 μm filter before chemical analysis. Dissolved Pu species have a high tendency to adsorb to suspended and colloidal particles in solution. In the UZ flow and transport PMR (Ref. 37) maximum and minimum $K_d$ values for a number of elements are reported as function of rock type and main WP corrosion products (Iron Oxides) in the UZ units. Information in Table 6-12 was obtained from Ref. 37 (Table 3.11-1, p. 236). The reported Kd values reveal that Pu has a much higher sorptive properties than U. This

could contribute to higher concentration of Pu observed in simulation compared to the experimental results.

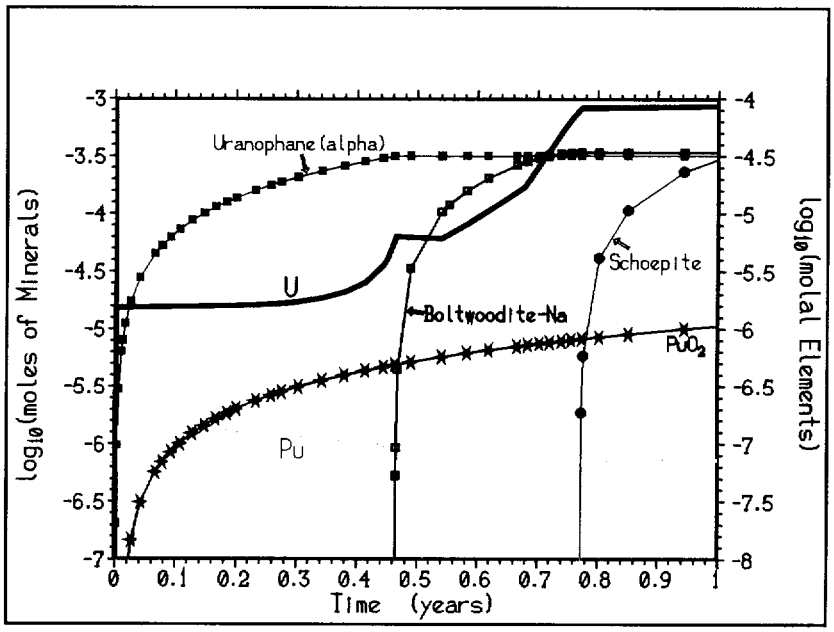


Figure 6-15: Fuel Model 2A. Concentration of Radionuclide Elements and Minerals vs. Time

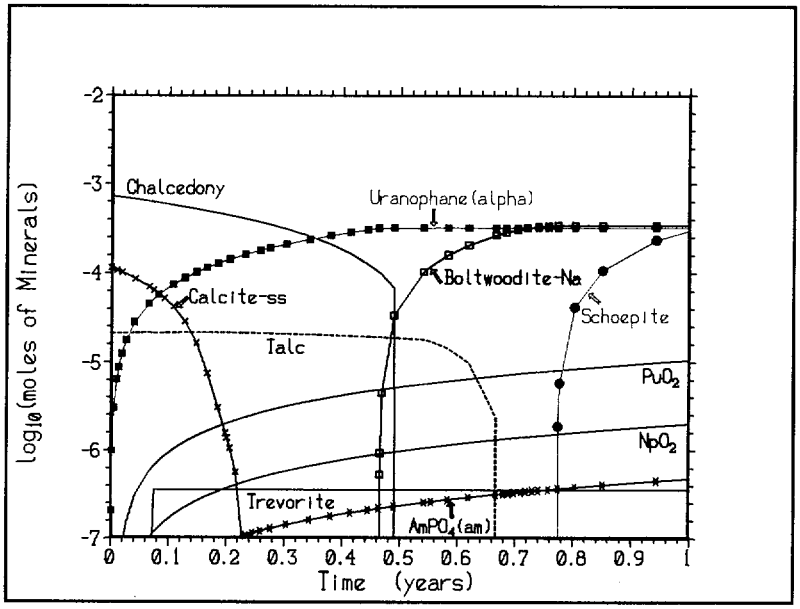


Figure 6-16: Fuel Model 2A. Moles of Minerals and Aqueous Concentrations of Pu and U vs. Time

Table 6-12: Sorption Coefficient Distributions for UZ Unite

| Element | Rock type | Min Kd (mL/g) | Max Kd (mL/g) |
|---|---|---|---|
| Pu | Devitrified | 5 | 70 |
| | Vitric | 30 | 200 |
| | Zeolitic | 30 | 200 |
| | Iron Oxide | 1000 | 5000 |
| U | Devitrified | 0 | 2 |
| | Vitric | 0 | 1 |
| | Zeolitic | 0 | 10 |
| | Iron Oxide | 100 | 1000 |

Source: Adapted from Ref. 37

Figure 6-18 shows the results of Fuel Model 2B, in which the stainless steel was allowed to corrode. The aqueous concentrations and the mineral sequences are virtually identical to those in Figure 6-15, which indicates that stainless steel had a negligible effect on the modeling.

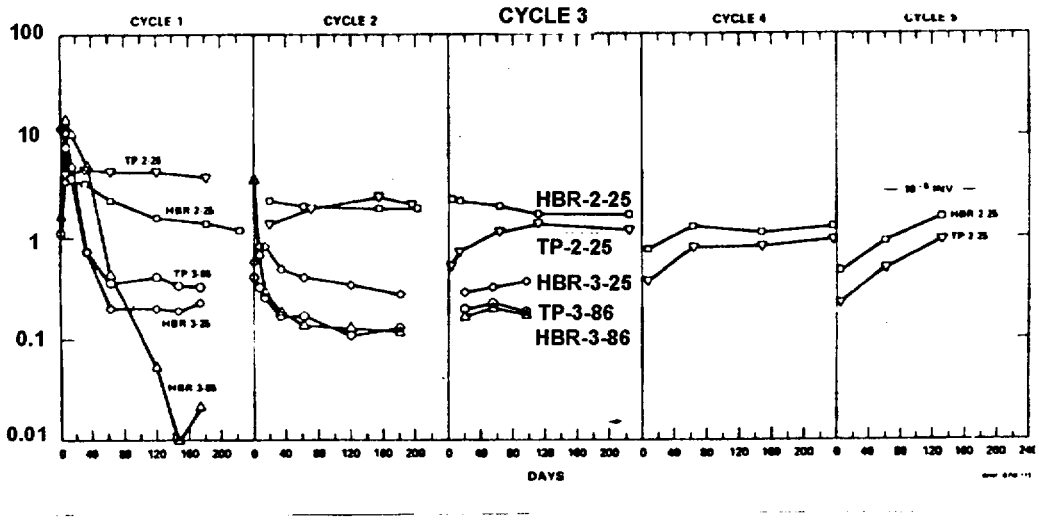


Figure 6-17: Uranium Concentration Measured in 0.4 μm Filtered Solution Sample (Wilson, Figure 2)

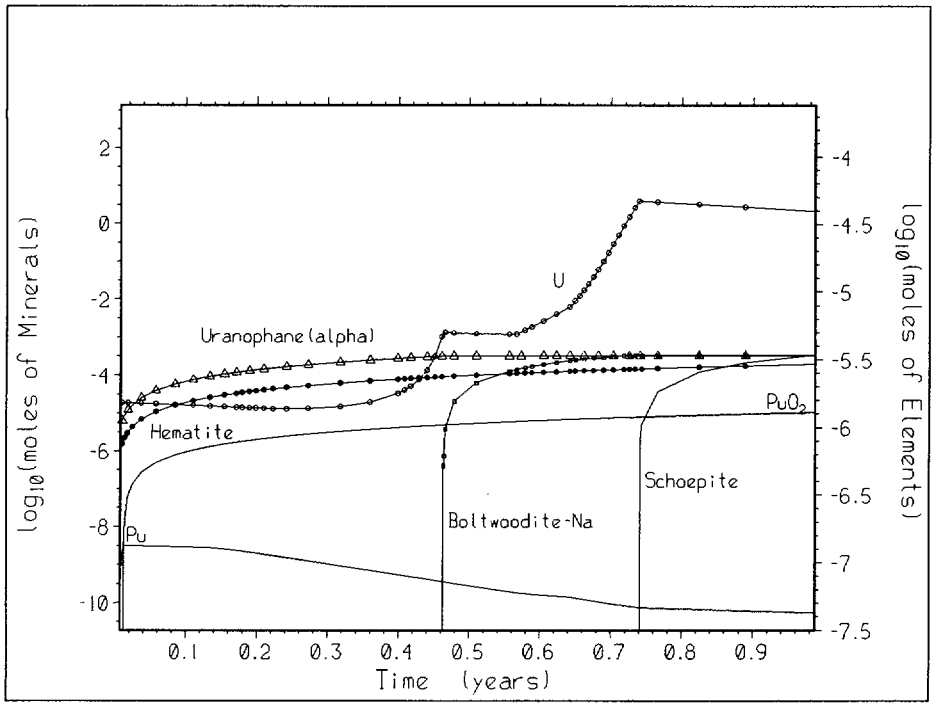


Figure 6-18: Fuel Model 2B, Moles of Minerals and Aqueous Concentrations of Pu and U vs. Time

### 6.3.4 Solubility-Limiting Uranium Phases in Mixed Glass/Fuel Systems

EQ6 simulations for degradation of codisposal packages typically predict a sequence of uranium alteration phases with relatively low Si/U. Such phases include schoepite ($UO_3 \cdot nH_2O$), soddyite ($(UO_2)_2SiO_4 \cdot 2H_2O$), uranophane ($Ca(UO_2SiO_3OH)_2 \cdot 5H_2O$), and boltwoodite ($NaUO_2SiO_3OH \cdot 1.5H_2O$), with molar Si/U ratios ranging from 0 to 1. In contrast, experimental degradation of actinide-bearing waste glasses tends to produce weeksite ($Na_2(UO_2)_2Si_5O_{13}:3H_2O$, with Si/U = 2.5) as the dominant U-bearing phase, along with lesser amounts of uranophane and haiweeite ($Ca(UO_2)_2(Si_2O_5)_3:5H_2O$, Si/U=3) (Ref. 55, p. 128). It is expected that both glass and actinide ceramics may degrade simultaneously in the WPs, so it is important to understand the apparent contradiction between predicted and observed uranium solids.

There are reasonable explanations for the discrepancy. The experiments that yield weeksite and haiweeite may have much higher silica concentrations, than are predicted for the codisposal WPs. Indeed, degradation of alkaline glass often produces an amorphous silica layer (Ref. 20), suggesting very high silica activity. However, The degraded WPs contain abundant steel corrosion products, which would be expected, through long times, to react with the corroded glass to form relatively Si-poor nontronite clays. In addition, the experiments are typically run at temperatures near 90 °C; whereas the WP models are constrained, in part by lack of thermodynamic data for U phases, to 25 °C.

It is hypothesized that the discrepancy in U solids is due principally to the controls on Si activity in the degrading glass, vs. the WP. To test this hypothesis, an FFTF (Ref. 65) model was altered to remove the steels that would potentially react with silica.

### 6.3.4.1 EQ6 File Inputs

This EQ6 simulation consisted of MOX and UOX fuel and HLW glass. The parameters for the input file are described in Table 6-13 and Table 6-14.

Table 6-13. Properties of Reactants

| | MOX[a] | UOX[a] | HWL Glass[b] |
|---|---|---|---|
| **Total Moles of Reactant** | 0.39378[c] | 0.0182[c] | 24.821[c] |
| **Chemical Composition** | O 7.397063E-01<br>U 2.746725E-01<br>Pu 9.407909E-02<br>Np 1.101603E-03 | O 7.406648E-01<br>U 3.703324E-01 | O 2.7039E+00 Si 7.7649E-01<br>U 7.8186E-03 B 2.9124E-01<br>Ba 1.0751E-03 F 1.6615E-03<br>Al 8.6298E-02 Fe 1.7221E-01<br>S 4.0071E-03 K 7.5059E-02<br>Ca 1.6224E-02 Mg 3.3327E-02<br>P 4.8866E-04 Na 5.7672E-01 |
| **Surface Area ($cm^2$)** | 1559.383[c] | 72.0726[c] | 1340.6[c] |
| **Reaction Rate ($mol/cm^2 \cdot s$)** | 1.1422E-14[d] | 1.1422E-14[d] | 1.3541E-10 (cdac 0.6)[e]<br>1.0756E-17 (cdac –0.4)[e] |

Sources: [a] The MOX and UOX chemical composition comes from 'Glass&Fuel' (Ref. 65).
[b] The glass chemical composition is based on Ref. 28 (Attachment I, p. I-7) as simplified in 'HLW_glass REV01.xls', sheet 'composition' (Attachment I). This is the composition added to 'data0.yme' (in Attachment I) for the mineral, GlassSRL.
[c] The number of total moles of reactants and surface areas come from DTN: SN9911T0811199.003: 'fftf_fuel_hws_rev04.xls', sheets 'Mols_rct'
[d] The Fuel rate comes from Ref. 65, converted in 'FFTF IA 2001.xls', sheet 'MOX,UOX' (Attachment I)
[e] The HLW Glass: (Ref. 39) Eq. 7 and 8, converted to EQ6 format in 'HLW_glass REV01.xls', sheet 'rates' (Attachment I).

Table 6-14. EQ6 Input File Elemental Molal Composition for J-13 Well Water

| Chemical Composition | | | | | |
|---|---|---|---|---|---|
| O | 5.55E+01 | Gd | 1.00E-16 | Na | 1.99E-03 |
| Al | 1.00E-16 | H | 1.11E+02 | Ni | 1.00E-16 |
| B | 1.00E-16 | C | 2.07E-03 | Np | 1.00E-16 |
| Ba | 1.00E-16 | P | 1.00E-16 | Pu | 1.00E-16 |
| Ca | 3.24E-04 | K | 1.29E-04 | S | 1.92E-04 |
| Cl | 2.01E-04 | Mg | 8.27E-05 | Si | 1.02E-03 |
| Cr | 1.00E-16 | Mn | 1.00E-16 | U | 1.00E-16 |
| F | 1.15E-04 | Mo | 1.00E-16 | | |
| Fe | 1.00E-16 | N | 1.42E-04 | | |

| Drip Rate ($m^3$/year) [a] | Drip Rate (normalized for EQ6 input) (moles/sec) [b] |
|---|---|
| 0.15 | 8.18545E-10 |

Sources: from Ref. 40 (Table 6), based on Ref. 58. These values are outputs from EQ3NR for input into EQ6 input file.

Notes: Drip rate selection is explained in Ref. 26 (Section 5.1.1.3), and were converted from $m^3$/yr to moles/sec for input into EQ6 in the 'Rates' tab of 'fftf_fuel_hws_rev4.xls' DTN: SN9911T0811199.003 (Ref. 65).

Several minerals are routinely suppressed (not allowed to form) in most EQ6 runs, including the runs for this study. These minerals are listed and explained in Section 6.2.5.

### 6.3.4.2 Method

First, a run was completed suppressing only the default minerals listed in Section 6.2.5. Weeksite did not form. The Si minerals that did form were noted, and those minerals with the lowest LogK value were suppressed one at a time in successive runs. For each run, the minerals that formed and the Log(Q/K)(saturation state) were plotted (Figure 6-19 through Figure 6-22). The Log(Q/K) for weeksite gets closer to 0 (and thus becoming more likely to form), as each Si mineral is suppressed.

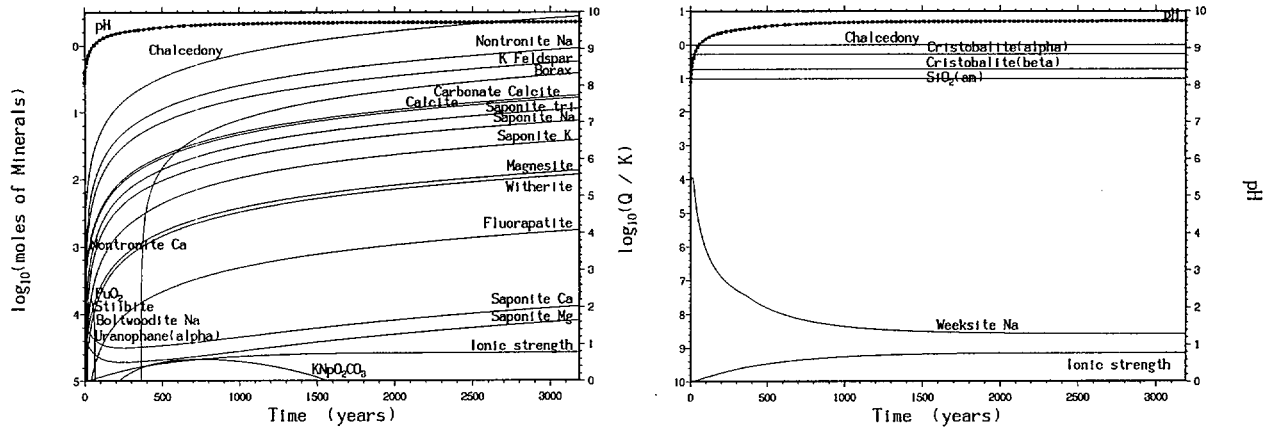


Figure 6-19: EQ6 Run with no Si Minerals Suppressed

The mineral chalcedony was suppressed first.

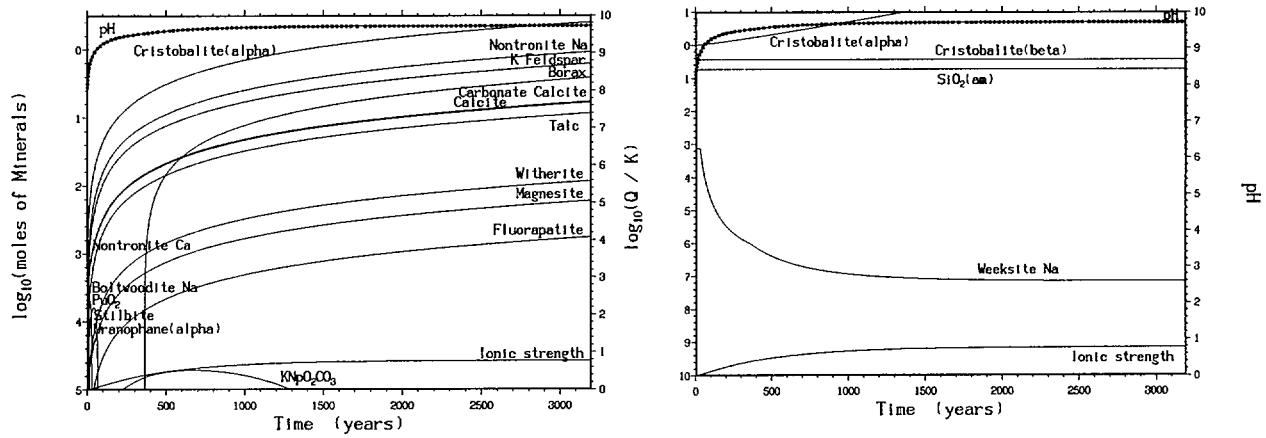


Figure 6-20: EQ6 Run with Chalcedony Suppressed

With Chalcedony suppressed, the Log(Q/K) value for weeksite at early times increases from –4 to –3, and the mineral cristobalite (alpha) formed.

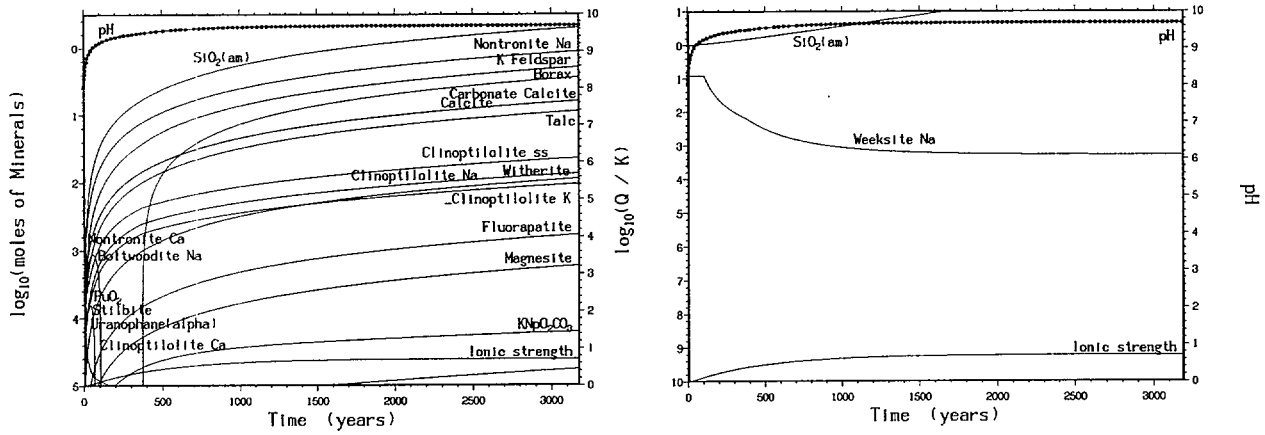


Figure 6-21: EQ6 Run with Chalcedony, Cristobalite (alpha) & (beta), and Coesite Suppressed

Suppressing two more Si minerals (cristobalite (beta) and coesite), allows the Log(Q/K) value for weeksite to jump up to –1, but $SiO_2$(am) is still forming and taking all of the available Si.

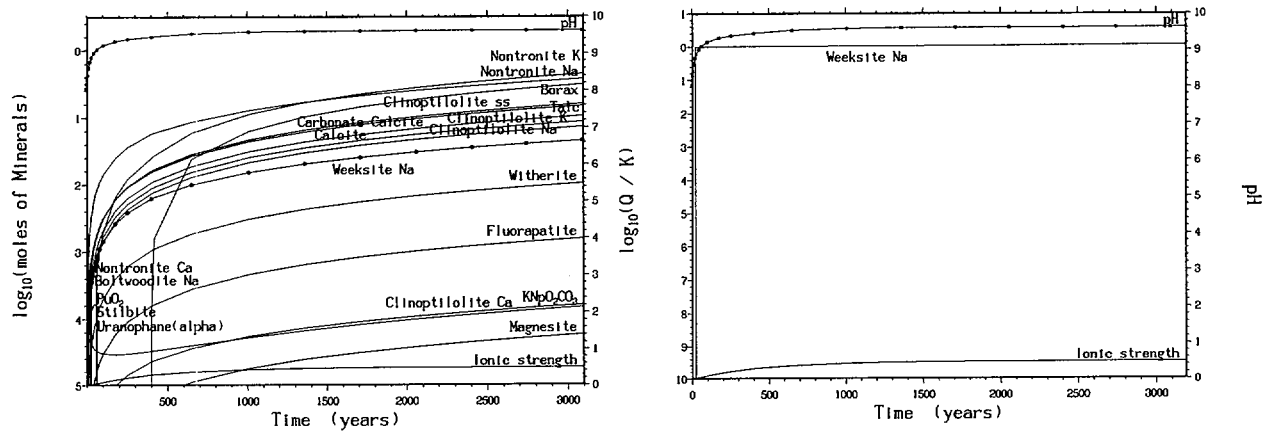


Figure 6-22: EQ6 Run with All Five Si Minerals Suppressed

Suppressing $SiO_2$(am) allows weeksite to form, and its Log(Q/K) goes to 0.

### 6.3.4.3 Summary

Once weeksite forms, it only stays around for the first 20,000 years while the pH is high due to the degradation of the glass. As the pH decreases with the influx of J-13, the weeksite goes back into solution.

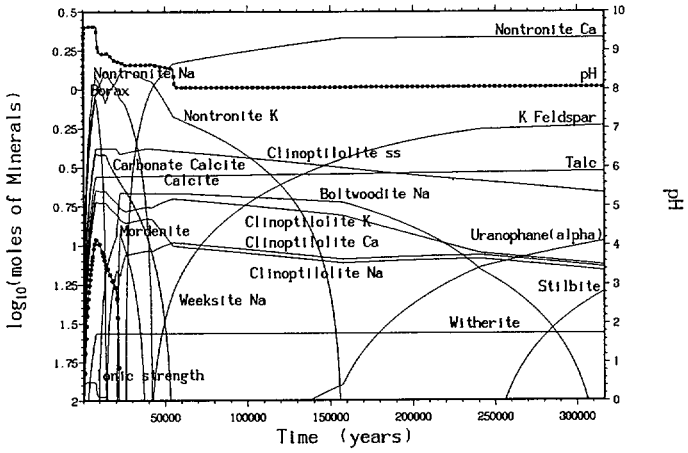


Figure 6-23: EQ6 Run with Weeksite Forming, Run out to 300,000 years

This final plot (Figure 6-23) shows the run that formed weeksite, run all the way out to 300,000 years. It is clear that weeksite forms early in the run, but then goes back into solution as the pH decreases. The minerals that were suppressed in order to form weeksite were chalcedony, cristobalite (alpha) & (beta), coesite, and $SiO_2$(am).

Uranophane was one of the other minerals observed in experimental data, and this plot shows Uranophone (alpha) forming just shy of 150,000 years. The third mineral mentioned in the experimental data, haiweeite, does not form in this run because it is no longer included in the thermodynamic database (Attachment I ).

Thus, in the WP models, very high Si activity is required to make weeksite the stable alteration phase, even when steel is removed from the model. It is doubtful that such high aqueous Si would persist in a degrading WP, due to the large mass of steel corrosion products. Hence the apparent discrepancy between the U phases observed in experiments, and those predicted in the WP models, reflects the very different controls on Si activity in the two systems.

# 7. CONCLUSIONS

The Materials Degradation and Release Model predicts the amounts of fissile materials and neutron absorbers that remain in a WP, during an extended period of aqueous degradation. The predictions are used for evaluation of internal criticality; thus the conservatism of the model is tied to the amounts of fissile materials (Pu and U), neutron absorbers (e.g., Gd) and neutron moderators (e.g., water) that remain in the package. Implicitly, the model also predicts the compositions of the solutions that leave the WP as a function of time, to provide "source terms" for evaluation of external criticality. The model assumes a bathtub scenario, in which the WP is filled with water to a point of overflow. The model normally employs fixed $fO_2$ and $fCO_2$, though sensitivity studies (Ref. 29 and Ref. 35) have been performed to evaluate effects of reducing conditions and redox limited by the competition between degradation and diffusion. In most calculations, the aqueous phase is assumed to be in equilibrium with all solids (corrosion products) that precipitate within the WP.

Implementation of the model was demonstrated with the examples of a Pu-ceramic WP. Degradation rates and drip rates were varied by at least two orders of magnitude. The specific combination of rates, along with the sequence of degradation were chosen to be conservative for either internal or external criticality concerns. For internal criticality, one of the most conservative cases with the highest Gd loss (s10, Table 6-8) was achieved with low steel, average glass and very high fuel (Table 6-6); whereas the most conservative for external criticality with the highest Pu discharged (case s5) was achieved with very low steel, moderately high glass, and very high fuel.

The Materials Degradation Model encompasses a large variety of combinations of glass, fuel and steel degradation rates and mechanisms; the variety of possible combinations makes it impractical to validate the model by comparison against a single analogue or lab experiment. Instead, the validation proceeds by defining the most uncertain and important sub-models; specifically, the sub-models for degradation of glass and actinide ceramics (e.g., spent fuel or Pu-ceramics). The sub-models are validated by comparison against laboratory experiments and archeological analogues.

The glass sub-model is compared against a set of MCC-4 (flow-through dissolution) experiments with an alkaline analogue of DHLW, and by comparison with a corroded archeological glass sample. The glass sub-model predicts the assemblage and approximate amounts of minerals formed in the MCC-4 tests. When kinetic precipitation is added, the sub-model also provides a reasonable prediction of the aqueous Mg concentrations. When applied to the 450-year-old archeological samples, the sub-model predicts the sequence of minerals observed in the glass-soil samples, and provides a plausible mechanism to explain why the in-soil degradation rates exceed those predicted by the MCC-4 tests.

The fuel sub-model is evaluated by comparison against the HBR-3-25 experiments of Wilson (Ref. 75) and the subsequent EQ6 calculations by Wilson and Bruton (Ref. 76). The comparison proceeds in two steps, or levels of model refinement. The first refinement reproduces the modeling of Wilson and Bruton, but takes advantage of available refinements in the thermodynamic database. However, the fundamental assumptions of the Wilson and Bruton calculation (fixed $fCO_2$ and $fO_2$) are retained. Compared to the Wilson and Bruton study, the first refinement achieves much better agreement between the observed and predicted Pu solubilities. The predicted Pu solubility is still ~20 times higher than the observed value; nonetheless, a sensitivity study shows that within this uncertainty, the Pu solubility has little

effect on the predicted performance of the WP. However, the first refinement overpredicts U solubility by about two orders of magnitude.

In the second refinement of the fuel sub-model, more realistic controls are placed on the control of $fO_2$ and $fCO_2$, and the rate of fuel degradation is refined to be consistent with the experimental results. Consequently, the predicted and observed aqueous U concentrations match closely, and the predicted and observed Pu concentrations differ only by a factor of ~5. Given the larger uncertainties in package temperature and the ambient chemical conditions, and the uncertainty inherent in the thermodynamic database, this agreement is quite good. There is also reasonably good agreement between the predicted and observed alteration minerals.

An additional sensitivity study addresses the experimental observation that weeksite forms during the degradation of U-bearing glasses. Weeksite is not predicted in any of the WP degradation scenarios, in which actinides and glass degrade more or less simultaneously; this discrepancy suggests an inaccuracy in the degradation models. It is speculated that weeksite formation requires transient conditions of high Si activity, as might be found in a lab experiment. The sensitivity study confirms this supposition. In a WP containing abundant steel corrosion products, Si activity is likely to be controlled by the formation of Fe-rich clays, so weeksite in unlikely to provide long-term control on U solubility.

Use of the model is currently restricted, by available thermodynamic data, to temperatures of ~25 °C for actinide-bearing systems, and ≤100 °C for simple systems that are composed of major elements (e.g. Ca, Mg, K, Na, Fe, Si and Al). This limitation is not implicit in the model itself, and will be alleviated with future updates of the thermodynamic database. However, it is possible to approximate some temperature effects by selecting a range of rate parameters. The model is restricted to ionic strengths < 4 (preferably, ≤1) by use of the B-dot ionic strength correction. The model outlined in this document is restricted to "bathtub" conditions, but with minor modification, can be applied to drip-through systems (that is, systems in which the aqueous phase is not contiguous and does not fill every void within the package).

## 8. INPUTS AND REFERENCES


1. AP-2.21Q, Rev. 1, ICN 0, BSCN 001. *Quality Determinations and Planning for Scientific, Engineering, and Regulatory Compliance Activities.* Washington, D.C.: U.S. Department of Energy, Office of Civilian Radioactive Waste Management. ACC: MOL.20010212.0018.

2. AP-3.10Q, Rev. 2, ICN 4, ECN 1. *Analyses and Models.* Washington, D.C.: U.S. Department of Energy, Office of Civilian Radioactive Waste Management. ACC: MOL.20010827.0114.

3. AP-3.15Q, Rev. 3, ICN 0. *Managing Technical Product Inputs.* Washington, D.C.: U.S. Department of Energy, Office of Civilian Radioactive Waste Management. ACC: MOL.20010801.0318.

4. AP-SI.1Q, Rev. 3, ICN 01, ECN 02. *Software Management.* Washington, D.C.: U.S. Department of Energy, Office of Civilian Radioactive Waste Management. ACC: MOL.20010705.0239.

5. AP-SV.1Q, Rev. 0, ICN 2. *Control of the Electronic Management of Information.* Washington, D.C.: U.S. Department of Energy, Office of Civilian Radioactive Waste Management. ACC: MOL.20000831.0065.

6. ASM International 1987. *Corrosion.* Volume 13 of *ASM Handbook.* 9th Edition. Materials Park, Ohio: ASM International. TIC: 240704.

7. ASTM A 20/A20M-99a. 1999. *Standard Specification for General Requirements for Steel Plates for Pressure Vessels.* West Conshohocken, Pennsylvania: American Society of Testing and Materials. TIC: 247403.

8. ASTM A 240/A 240M-99b. 2000. *Standard Specification for Heat-Resisting Chromium and Chromium-Nickel Stainless Steel Plate, Sheet, and Strip for Pressure Vessels.* West Conshohocken, Pennsylvania: American Society for Testing and Materials. TIC: 248529.

9. ASTM A 276-91a. 1991. *Standard Specification for Stainless and Heat-Resisting Steel Bars and Shapes.* Philadelphia, Pennsylvania: American Society for Testing and Materials. TIC: 240022.

10. ASTM A 516/A 516M - 90. 1991. *Standard Specification for Pressure Vessel Plates, Carbon Steel, for Moderate- and Lower-Temperature Service.* Philadelphia, Pennsylvania: American Society for Testing and Materials. TIC: 240032.

11. ASTM G 1-90 (Reapproved 1999). 1990. *Standard Practice for Preparing, Cleaning, and Evaluating Corrosion Test Specimens.* West Conshohocken, Pennsylvania: American Society for Testing and Materials. TIC: 238771.

12. Baxter, R.G. 1988. *Defense Waste Processing Facility Wasteform and Canister Description.* DP-1606, Rev. 2. Aiken, South Carolina: E.I. du Pont de Nemours & Company, Savannah River Plant. TIC: 8704.

13. Bear, J. 1988. *Dynamics of Fluids in Porous Media.* New York, New York: Dover Publications. TIC: 217568.

14. BSC (Bechtel SAIC Company) 2001. *EQ6 Calculations for Chemical Degradation of Melt and Dilute Waste Packages.* CAL-EDC-MD-000012 REV 00. Las Vegas, Nevada: Bechtel SAIC Company. ACC: MOL.20010719.0064.

15. BSC (Bechtel SAIC Company) 2001. *EQ6 Calculation for Chemical Degradation of Pu-Ceramic Waste Packages: Effects Updated Waste Package Design and Rates.* CAL-EDC-MD-000009 REV 01. Las Vegas, Nevada: Bechtel SAIC Company. URN-0933.

16. BSC (Bechtel SAIC Company) 2001. *In-Package Chemistry for Waste Forms.* ANL-EBS-MD-000056 REV 00. Las Vegas, Nevada: Bechtel SAIC Company. ACC: MOL.20010322.0490.

17. BSC (Bechtel SAIC Company) 2001. *Technical Work Plan for: Waste Package Design Description for LA.* TWP-EBS-MD-000004 REV 01. Las Vegas, Nevada: Bechtel SAIC Company. ACC: MOL.20010702.0152.

18. BSC 2001. *Software Code: ASPRIN.* V1.0. 10487-1.0-00.

19. Cooper, G.I. and Cox, G.A. 1994. "A Comparative Study of the Natural and Experimental Corrosion of Poorly Durable Potash-Lime-Silica Glasses." *Scientific Basis for Nuclear Waste Management XVII, Symposium held November 29-December 3, 1993, Boston, Massachusetts.* Barkatt, A. and Van Konynenburg, R.A., eds. 333, 525-531. Pittsburgh, Pennsylvania: Materials Research Society. TIC: 213541.

20. Cooper, G.I. and Cox, G.A. 1996. "The Aqueous Corrosion of Potash–Lime–Silica Glass in the Range of 10–250°C." *Applied Geochemistry, 11,* ([4]), 511-521. [Oxford, England]: Elsevier. TIC: 250577.

21. Cox, G.A. and Ford, B.A. 1993. "The Long-Term Corrosion of Glass by Ground-Water." *Journal of Materials Science, 28,* (20), 5637-5647, London, England: Chapman & Hall. TIC: 245170.

22. CRWMS M&O 1996. *Second Waste Package Probabilistic Criticality Analysis: Generation and Evaluation of Internal Criticality Configurations.* BBA000000-01717-2200-00005 REV 00. Las Vegas, Nevada: CRWMS M&O. ACC: MOL.19960924.0193.

23. CRWMS M&O 1997. *Criticality Evaluation of Degraded Internal Configurations for the PWR AUCF WP Designs.* BBA000000-01717-0200-00056 REV 00. Las Vegas, Nevada: CRWMS M&O. ACC: MOL.19971231.0251.

24. CRWMS M&O 1997. *Degraded Mode Criticality Analysis of Immobilized Plutonium Waste Forms in a Geologic Repository.* Predecisional Document. A00000000-01717-5705-00014 REV 01. Las Vegas, Nevada: CRWMS M&O. ACC: MOL.19980422.0911.

25. CRWMS M&O 1998. *EQ6 Calculations for Chemical Degradation of Fast Flux Test Facility (FFTF) Waste Packages.* BBA000000-01717-0210-00028 REV 00. Las Vegas, Nevada: CRWMS M&O. ACC: MOL.19981229.0081.

26. CRWMS M&O 1998. *EQ6 Calculations for Chemical Degradation of PWR LEU and PWR MOX Spent Fuel Waste Packages.* BBA000000-01717-0210-00009 REV 00. Las Vegas, Nevada: CRWMS M&O. ACC: MOL.19980701.0483.

27. CRWMS M&O 1998. *Software Code: EQ3/6.* V7.2b. LLNL: UCRL-MA-110662.

28. CRWMS M&O 1999. *DOE SRS HLW Glass Chemical Composition.* BBA000000-01717-0210-00038 REV 00. Las Vegas, Nevada: CRWMS M&O. ACC: MOL.19990215.0397.

29. CRWMS M&O 1999. *EQ6 Calculation for Chemical Degradation of Pu-Ceramic Waste Packages: Effects of Updated Materials Composition and Rates.* CAL-EDC-MD-000003 REV 00. Las Vegas, Nevada: CRWMS M&O. ACC: MOL.19990928.0235.

30. CRWMS M&O 1999. *One (1) Compact Diskette for Electronic Data for EQ6 Calculation for Chemical Degradation of Pu-Ceramic Waste Packages: Effects of Updated Materials Composition and Rates.* CAL-EDC-MD-000003 REV 00. Las Vegas, Nevada: CRWMS M&O. ACC: MOL.19990923.0238.

31. CRWMS M&O 1999. *Software Code: EQ6, Version 7.2bLV.* V7.2bLV. 10075-7.2bLV-00.

32. CRWMS M&O 2000. *CSNF Waste Form Degradation: Summary Abstraction.* ANL-EBS-MD-000015 REV 00. Las Vegas, Nevada: CRWMS M&O. ACC: MOL.20000121.0161.

33. CRWMS M&O 2000. *Defense High Level Waste Glass Degradation.* ANL-EBS-MD-000016 REV 00. Las Vegas, Nevada: CRWMS M&O. ACC: MOL.20000329.1183.

34. CRWMS M&O 2000. *EQ6 Calculation for Chemical Degradation of Shippingport LWBR (Th/U Oxide) Spent Nuclear Fuel Waste Packages.* CAL-EDC-MD-000008 REV 00. Las Vegas, Nevada: CRWMS M&O. ACC: MOL.20000926.0295.

35. CRWMS M&O 2000. *In-Drift Accumulation of Fissile Material from Waste Packages Containing Plutonium Disposition Waste Forms.* CAL-EDC-GS-000001 REV 00. Las Vegas, Nevada: CRWMS M&O. ACC: MOL.20001016.0008.

36. CRWMS M&O 2000. *Total System Performance Assessment for the Site Recommendation.* TDR-WIS-PA-000001 REV 00 ICN 01. Las Vegas, Nevada: CRWMS M&O. ACC: MOL.20001220.0045.

37. CRWMS M&O 2000. *Unsaturated Zone Flow and Transport Model Process Model Report.* TDR-NBS-HS-000002 REV 00 ICN 02. Las Vegas, Nevada: CRWMS M&O. ACC: MOL.20000831.0280.

38. CRWMS M&O 2000. *Waste Package Degradation Process Model Report.* TDR-WIS-MD-000002 REV 00 ICN 02. Las Vegas, Nevada: CRWMS M&O. ACC: MOL.20001228.0229.

39. CRWMS M&O 2001. *Defense High Level Waste Glass Degradation.* ANL-EBS-MD-000016 REV 00 ICN 01. Las Vegas, Nevada: CRWMS M&O. ACC: MOL.20010130.0004.

40. CRWMS M&O 2001. *EQ6 Calculations for Chemical Degradation of N Reactor (U-metal) Spent Nuclear Fuel Waste Packages.* CAL-EDC-MD-000010 REV 00. Las Vegas, Nevada: CRWMS M&O. ACC: MOL.20010227.0017.

41. Deer, W.A.; Howie, R.A.; and Zussman, J. 1966. *An Introduction to the Rock-Forming Minerals.* New York, New York: John Wiley & Sons. TIC: 245492.

42. DOE (U.S. Department of Energy) 1998. *Design Specification.* Volume 1 of *Preliminary Design Specification for Department of Energy Standardized Spent Nuclear Fuel Canisters.* DOE/SNF/REP-011, Rev. 1. Washington, D.C.: U.S. Department of Energy, Office of Spent Fuel Management and Special Projects. TIC: 241528.

43. DOE (U.S. Department of Energy) 1998. *Total System Performance Assessment.* Volume 3 of *Viability Assessment of a Repository at Yucca Mountain.* DOE/RW-0508. Washington, D.C.: U.S. Department of Energy, Office of Civilian Radioactive Waste Management. ACC: MOL.19981007.0030.

44. DOE (U.S. Department of Energy) 1999. *Waste Acceptance System Requirements Document.* DOE/RW-0351, Rev. 03. Washington, D.C.: U.S. Department of Energy, Office of Civilian Radioactive Waste Management. ACC: HQO.19990226.0001.

45. DOE (U.S. Department of Energy) 2000. *Quality Assurance Requirements and Description.* DOE/RW-0333P, Rev. 10. Washington, D.C.: U.S. Department of Energy, Office of Civilian Radioactive Waste Management. ACC: MOL.20000427.0422.

46. Donnay, J.D.H. and Ondik, H.M. 1972-73. *Crystal Data: Determinative Tables.* Page C-103. Washington, DC: National Bureau of Standards. On Order Library Tracking Number-248645

47. Efurd, D.W.; Runde, W.; Banar, J.C.; Janecky, D.R.; Kaszuba, J.P.; Palmer, P.D.; Roensch, F.R.; and Tait, C.D. 1998. "Neptunium and Plutonium Solubilities in a Yucca Mountain Groundwater." *Environmental Science & Technology, 32,* (24), 3893-3900. [Easton, Pennsylvania]: American Chemical Society. TIC: 243857.

48. Eisenberg, N.A.; Lee, M.P.; Federline, M.V.; Wingefors, S.; Andersson, J.; Norrby, S.; Sagar, B.; and Wittmeyer, G.W. 1999. *Regulatory Perspectives on Model Validation in High-Level Radioactive Waste Management Programs: A Joint NRC/SKI White Paper.* NUREG-1636. Washington, D.C.: U.S. Nuclear Regulatory Commission. TIC: 246310.

49. Firsching, F.H. and Brune, S.N. 1991. "Solubility Products of the Trivalent Rare-Earth Phosphates." *Journal of Chemical Engineering, 36,* 93-95. Washington, D.C.: American Chemical Society. TIC: 240863.

50. Harrar, J.E.; Carley, J.F.; Isherwood, W.F.; and Raber, E. 1990. *Report of the Committee to Review the Use of J-13 Well Water in Nevada Nuclear Waste Storage Investigations.* UCID-21867. Livermore, California: Lawrence Livermore National Laboratory. ACC: NNA.19910131.0274.

51. Huertas, F.J.; Caballero, E.; Jimenez de Cisneros, C.; Huertas, F.; and Linares, J. 2001. "Kinetics of Montmorillonite Dissolution in Granitic Solutions." *Applied Geochemistry, 16,* (4), 397-407. New York, New York: Pergamon. TIC: 250578.

52. International Centre for Diffraction Data 1986. *Mineral Powder Diffraction File, Data Book.* Pages 16-20,28,122,172,241,269,455-456,481,491-492,535-537,770-771,787-789,792,843,861-862,966,1025-1027,1030-1032,1038-1039,1107,1193-1194. Swarthmore, Pennsylvania: International Centre for Diffraction Data. TIC: 243579.

53. Kuchment, L.S.; Demidov, V.N.; Naden, P.S.; Cooper, D.M.; and Broadhurst, P. 1996. "Rainfall-Runoff Modelling of the Ouse Basin, North Yorkshire: An Application of a Physically

Based Distributed Model." *Journal of Hydrology, 181,* (1-4), 323-342. [New York, New York]: Elsevier. TIC: 250551.

54. Latimer, W.M. 1952. *The Oxidation States of the Elements and Their Potentials in Aqueous Solutions.* 2nd Edition. Pages 8, 9, 30, 215, 270-274. New York, New York: Prentice-Hall. TIC: 238748.

55. LL000123351021.117. ANL 94/34 - The Effects of the Glass Surface Area/Solution Volume Ratio on Glass Corrosion: A Critical Review. Submittal date: 01/28/2000.

56. LLNL (Lawrence Livermore National Laboratory) 1998. *Plutonium Immobilization Project Data for Yucca Mountain Total Systems Performance Assessment, Rev. 1.* PIP 98-012. Livermore, California: Lawrence Livermore National Laboratory. ACC: MOL.19980818.0349.

57. McCright, R.D. 1998. *Corrosion Data and Modeling, Update for Viability Assessment.* Volume 3 of *Engineered Materials Characterization Report.* UCRL-ID-119564, Rev. 1.1. Livermore, California: Lawrence Livermore National Laboratory. ACC: MOL.19980806.0177.

58. MO0006J13WTRCM.000. Recommended Mean Values of Major Constituents in J-13 Well Water. Submittal date: 06/07/2000.

59. MO0009THRMODYN.001. Input Transmittal for Thermodynamic Data Input Files for Geochemical Calculations. Submittal date: 09/20/2000.

60. Mon, K. 2001. "CLST IRSR Meeting Summary." E-mail from K. Mon to [J. Nowak] (SNL), February 23, 2001, with attachment. ACC: MOL.20010328.0446.

61. Parrington, J.R.; Knox, H.D.; Breneman, S.L.; Baum, E.M.; and Feiner, F. 1996. *Nuclides and Isotopes, Chart of the Nuclides.* 15th Edition. San Jose, California: General Electric Company and KAPL, Inc. TIC: 233705.

62. Roberts, W.L.; Campbell, T.J.; and Rapp, G.R., Jr. 1990. *Encyclopedia of Minerals.* 2nd Edition. New York, New York: Van Nostrand Reinhold. TIC: 242976.

63. Shaw, H., ed. 1999. *Plutonium Immobilization Project Input for Yucca Mountain Total Systems Performance Assessment.* PIP-99-107. Livermore, California: Lawrence Livermore National Laboratory. TIC: 245437.

64. Shaw, H.F.; Ebbinghaus, B.B.; Bourcier, W.L.; and Gray, L. 2001. *Plutonium Immobilization Project Input for Yucca Mountain Total Systems Performance Assessment.* PIP-01-004, Rev. 4.0. Livermore, California: Lawrence Livermore National Laboratory. TIC: 249220.

65. SN9911T0811199.003. Calculations of Physical and Chemical Properties of Fast Flux Test Facility (FFTF) Waste Package. Submittal date: 11/15/1999.

66. Spahiu, K. and Bruno, J. 1995. *A Selected Thermodynamic Database for REE to be Used in HLNW Performance Assessment Exercises.* SKB Technical Report 95-35. Stockholm, Sweden: Swedish Nuclear Fuel and Waste Management Company. TIC: 225493.

67. Stockman, H.W. 1994. *PP: A Graphics Post-Processor for the EQ6 Reaction Path Code.* SAND94-1955. Albuquerque, New Mexico: Sandia National Laboratories. TIC: 241246.

68. Stout, R.B. and Leider, H.R., eds. 1991. *Preliminary Waste Form Characteristics Report.* Version 1.0. Livermore, California: Lawrence Livermore National Laboratory. ACC: MOL.19940726.0118.

69. Strachan, D.M.; Barnes, B.O.; and Turcotte, R.P "Standard Leach Tests for Nuclear Waste Materials." Scientific Basis for Nuclear Waste Management, Proceedings of the Third International Symposium, Boston, Massachusetts, November 17-20, 1980. Moore, J.G., ed. 3, 347-354. New York, New York: Plenum Press. TIC: 204407.

70. Towe, K.M. and Bradley, W.F. 1967. "Mineralogical Constitution of Colloidal 'Hydrous Ferric Oxides'." *Journal of Colloid and Interface Science, 24,* 384-392. [New York, New York: Academic Press]. TIC: 250230.

71. Turner, D.R. and Pabalan, R.T. 1999. "Abstraction of Mechanistic Sorption Model Results for Performance Assessment Calculations at Yucca Mountain, Nevada." *Waste Management, 19,* (6), 375-388. New York, New York: Pergamon Press. TIC: 246704.

72. Vernaz, E. Y. and Godon, N. 1991. "Key Parameters of Glass Dissolution in Integrated Systems." *Scientific Basis for Nuclear Waste Management XIV, Symposium held November 26-29, 1990, Boston, Massachusetts,* Abrajano, T. A., Jr. and Johnson, L.H., eds. *212,* 19-30. Pittsburgh, Pennsylvania: Materials Research Society. TIC: 203656.

73. Weast, R.C. and Astle, M.J., eds. 1979. *CRC Handbook of Chemistry and Physics.* 60th Edition. 2nd Printing 1980. Boca Raton, Florida: CRC Press. TIC: 245312.

74. Weast, R.C., ed. 1977. *CRC Handbook of Chemistry and Physics.* 58th Edition. Cleveland, Ohio: CRC Press. TIC: 242376.

75. Wilson, C.N. 1988. "Summary of Results from the Series 2 and Series 3 NNWSI Bare Fuel Dissolution Tests." *Scientific Basis for Nuclear Waste Management XI, Symposium held November 30-December 3, 1987, Boston, Massachusetts.* Apted, M.J. and Westerman, R.E., eds. *112,* 473-483. Pittsburgh, Pennsylvania: Materials Research Society. TIC: 203662.

76. Wilson, C.N. and Bruton, C.J. 1989. *Studies on Spent Fuel Dissolution Behavior Under Yucca Mountain Repository Conditions.* PNL-SA-16832. Richland, Washington: Pacific Northwest Laboratory. ACC: HQX.19890918.0047.

77. Wolery, T.J. and Daveler, S.A. 1992. *EQ6, A Computer Program for Reaction Path Modeling of Aqueous Geochemical Systems: Theoretical Manual, User's Guide, and Related Documentation (Version 7.0).* UCRL-MA-110662 PT IV. Livermore, California: Lawrence Livermore National Laboratory. TIC: 205002.

78. Yang, I.C.; Rattray, G.W.; and Yu, P. 1996. *Interpretation of Chemical and Isotopic Data from Boreholes in the Unsaturated Zone at Yucca Mountain, Nevada.* Water-Resources Investigations Report 96-4058. Denver, Colorado: U.S. Geological Survey. ACC: MOL.19980528.0216.

## 9. ATTACHMENTS

I. One Compact Disk (CD) containing the EQ3/6 computer files and Excel spreadsheets.

II. Listing of Files on Compact Disk, 5 pages.

III. Sketch SK-0196 Rev. 3, 5 DHLW/DOE –WP Assembly Configuration for Site Recommendation, 2 pages.

## Attachment II. Listing of Files on Compact Disk

This attachment contains the MS-DOS directory for files placed on the electronic media (Attachment I). The files are of various types:

1. Excel files (extensions = xls).
2. EQ3/6 input files (extension = 3i or 6i).

   ASCII text file: provides input parameters for EQ3/6.
3. EQ3/6 output files (extension = 3o or 6o).

   ASCII text file: provides detailed information about the system at each print point, which is specified by the user in the input file.
4. EQ3/6 pickup files (extension = 3p or 6p).

   ASCII text file: provides a description of the system at the end of that run to be used as an input file for a continuation run.
5. EQ6 Tab-delimited text files (extension = txt).

   *.elem_aqu: total aqueous moles of elements.

   *.elem_min: total moles of elements in minerals.

   *.elem_tot: total moles of elements (aqueous + mineral).

   *.min_info: moles of each mineral.
6. EQ6 binary output file (extension = bin).

   Binary file: provides detailed information about the system at the full numerical precision for *every* time step.
7. EQ3/6 text data files used for the calculations, located in folder "databases", with name 'data0.yme'.
8. Batch files (extension = bat) used to start EQ6 runs.
9. Winzip files (extension = zip).

Below are listed the contents of the DOS directories within the electronic attachment:

The first column is the DOS file name.

The second column lists <DIR> if it is a directory
or gives the files size (bytes) if it is a file.

The third and fourth columns are the date and time of the last update.

The fifth column is the filename.

**Directory of Disk**

| DOS FILE NAME | SIZE (IF A FILE) | DATE | TIME | FILE NAME |
|---|---|---|---|---|
| DATABA~5 | <DIR> | 09-07-01 | 11:45a | databases |
| FUEL2 | <DIR> | 09-07-01 | 11:07a | Fuel2 |
| GLASS | <DIR> | 09-07-01 | 11:08a | Glass |
| J13WSF | <DIR> | 09-07-01 | 11:09a | j13wsf |
| MINERALS | <DIR> | 09-07-01 | 11:05a | Minerals |
| PU199~15 | <DIR> | 09-07-01 | 11:45a | Pu 1999 |
| PU200~17 | <DIR> | 09-07-01 | 11:45a | Pu 2001 |
| 0 file(s) | | 0 bytes | | |

**Directory of F:\databases**

| | | | | | |
|---|---|---|---|---|---|
| DATA0 | YME | 2,658,654 | 08-27-01 | 11:39a | data0.yme |
| 1 file(s) | | 2,658,654 bytes | | | |

**Directory of F:\Fuel2**
(Files used in Section 6.3.2.2)

| | | | | | |
|---|---|---|---|---|---|
| ELEM_AQU | BIN | 13,964 | 08-23-01 | 11:46a | elem_aqu.bin |
| ELEM_AQU | TXT | 22,401 | 08-23-01 | 11:46a | elem_aqu.txt |
| ELEM_M_A | TXT | 21,216 | 08-23-01 | 11:46a | elem_m_a.txt |
| ELEM_MIN | TXT | 21,208 | 08-23-01 | 11:46a | elem_min.txt |
| ELEM_TOT | TXT | 21,221 | 08-23-01 | 11:46a | elem_tot.txt |
| J13FU~18 | XLS | 39,424 | 08-28-01 | 1:32p | j13fuel_081001.xls |
| J13SFUEL | 6I | 30,791 | 08-23-01 | 11:34a | j13sfuel.6i |
| J13SF~22 | 6O | 2,050,574 | 08-23-01 | 11:46a | j13sfuel.6i.6o |
| J13SF~30 | 6P | 33,453 | 08-23-01 | 11:46a | j13sfuel.6i.6p |
| J13SF~32 | 6T | 218,400 | 08-23-01 | 11:46a | j13sfuel.6i.6t |
| J13SF~36 | 6TX | 122,906 | 08-23-01 | 11:46a | j13sfuel.6i.6tx |
| J13SFUEL | BIN | 7,893,328 | 08-23-01 | 11:46a | J13SFUEL.BIN |
| J13SFUEL | TX0 | 46,731 | 08-27-01 | 8:54a | J13SFUEL.TX0 |
| MIN_INFO | TXT | 42,566 | 08-23-01 | 11:46a | min_info.txt |
| 15 file(s) | | 10,578,813 bytes | | | |

**Directory of F:\Glass**
(Files used in Section 6.3.1)

| | | | | | |
|---|---|---|---|---|---|
| CLAY!H2O | 6I | 24,764 | 08-20-01 | 10:50a | clay!H2o.6i |
| CLAY_H2O | 3I | 8,690 | 08-15-01 | 8:36a | clay_h2o.3i |
| CLAY_H2O | 6I | 24,689 | 08-15-01 | 8:41a | clay_H2o.6i |
| ELEM_~14 | XLS | 176,128 | 08-31-01 | 6:57a | elem_Stain00a_staine6a_stai_e6s.xls |
| GLA!CLY0 | 6I | 25,345 | 08-23-01 | 8:51a | gla!cly0.6i |
| GLA!CLY1 | 6I | 25,641 | 08-20-01 | 2:28p | gla!cly1.6i |
| GLA!CLY2 | 6I | 25,614 | 08-20-01 | 1:50p | gla!cly2.6i |
| GLA!CLY3 | 6I | 25,762 | 08-20-01 | 2:50p | gla!cly3.6i |
| GLASCLY0 | 6I | 25,158 | 08-15-01 | 4:45p | glascly0.6i |
| GLASCLY1 | 6I | 25,454 | 08-20-01 | 1:27p | glascly1.6i |
| GLASCLY2 | 6I | 25,649 | 08-20-01 | 1:27p | glascly2.6i |
| GLASCLY3 | 6I | 25,723 | 08-20-01 | 1:27p | glascly3.6i |
| GLASS~32 | XLS | 55,296 | 08-31-01 | 6:57a | glass_archeol.xls |
| MG_ST~34 | XLS | 71,680 | 08-31-01 | 6:57a | Mg_stain_glass_expt.xls |
| STAI!E6S | 6I | 27,485 | 08-13-01 | 7:44p | stai!e6S.6i |
| STAI_E6S | 6I | 27,631 | 08-22-01 | 6:26p | stai_e6s.6i |
| STAIN00 | 3I | 8,644 | 08-02-01 | 4:46p | stain00.3i |
| STAIN00A | 6I | 25,118 | 08-22-01 | 6:26p | stain00A.6i |
| STAIN00B | 6I | 24,647 | 08-02-01 | 9:46p | stain00B.6i |
| STAIN01! | 6I | 24,504 | 08-03-01 | 8:18p | stain01!.6i |
| STAIN01A | 6I | 24,390 | 08-20-01 | 5:14p | stain01A.6i |
| STAINE1A | 6I | 24,538 | 08-13-01 | 1:28p | staine1A.6i |

```
STAINE2A 6I         24,612  08-13-01  1:54p staine2A.6i
STAINE3A 6I         24,612  08-13-01  1:57p staine3A.6i
STAINE4A 6I         24,612  08-13-01  2:07p staine4A.6i
STAINE5A 6I         24,612  08-13-01  2:11p staine5A.6i
STAINE6A 6I         24,612  08-13-01  2:22p staine6A.6i
STAINE6S 6I         27,408  08-13-01  6:03p staine6S.6i
        28 file(s)        903,018 bytes
```

**Directory of F:\j13wsf**

(Files used in Section 6.3.2.1)

```
DECAYE~6 241            10  01-25-00 11:23a decay.eq6.24100
J13WSF13 6I         28,648  08-28-01  2:25p j13wsf13.6i
J13WSF13 6O      1,121,844  08-28-01  2:30p j13wsf13.6o
J13WSF13 6P         30,441  08-28-01  2:30p j13wsf13.6p
J13WSF13 6T         74,563  08-28-01  2:30p j13wsf13.6t
J13WSF13 6TX        75,681  08-28-01  2:30p j13wsf13.6tx
J13WSF13 BAT           371  08-28-01  2:26p j13wsf13.bat
J13WSF13 BIN     3,102,800  08-28-01  2:30p j13wsf13.bin
J13WS~34 TXT        18,436  08-28-01  2:30p j13wsf13.elem_aqu.txt
J13WS~36 TXT        17,507  08-28-01  2:30p j13wsf13.elem_min.txt
J13WS~38 TXT        17,520  08-28-01  2:30p j13wsf13.elem_tot.txt
J13WS~40 TXT        27,265  08-28-01  2:30p j13wsf13.min_info.txt
J13WSF_  6I         28,499  08-04-99  7:57p j13wsf_.6i
J13WSF_  6O      1,105,389  07-20-01 11:50a j13wsf_.6o
J13WSF_  6P         30,099  07-20-01 11:50a j13wsf_.6p
J13WSF_  6T         72,919  07-20-01 11:50a j13wsf_.6t
J13WSF_  6TX        74,020  07-20-01 11:50a j13wsf_.6tx
J13WSF_  BAT           365  07-20-01 11:46a j13wsf_.bat
J13WSF_  BIN     3,093,008  07-20-01 11:50a j13wsf_.bin
J13WS~70 TXT        17,967  07-20-01 11:50a j13wsf_.elem_aqu.txt
J13WS~72 TXT        17,062  07-20-01 11:50a j13wsf_.elem_min.txt
J13WS~74 TXT        17,075  07-20-01 11:50a j13wsf_.elem_tot.txt
J13WS~76 TXT        26,517  07-20-01 11:50a j13wsf_.min_info.txt
J13WSF_  XLS       180,736  08-30-01  2:31p J13WSF_.xls
P52L1~80 XLS        74,752  08-29-01  9:54a p52 L142 loss.xls
P52_L142 6I         44,420  08-28-01  4:00p p52_L142.6i
P52_L142 6O      9,348,863  08-28-01  4:44p p52_l142.6o
P52_L142 BAT           541  08-28-01  3:01p P52_L142.bat
P52_L142 BIN   111,585,016  08-28-01  4:44p p52_L142.bin
P52_~444 TXT        85,121  08-28-01  4:44p p52_L142.elem_aqu.txt
P52_~446 TXT        79,992  08-28-01  4:44p p52_L142.elem_min.txt
P52_~448 TXT        80,005  08-28-01  4:44p p52_L142.elem_tot.txt
P52_~450 TXT       179,352  08-28-01  4:44p p52_L142.min_info.txt
P52AL142 6I         44,568  08-28-01  4:02p p52aL142.6i
P52AL142 6O      9,360,237  08-28-01  5:26p p52al142.6o
P52AL142 BIN   111,553,840  08-28-01  5:26p p52aL142.bin
P52A~814 TXT        85,518  08-28-01  5:26p p52aL142.elem_aqu.txt
P52A~818 TXT        80,365  08-28-01  5:26p p52aL142.elem_min.txt
P52A~820 TXT        80,378  08-28-01  5:26p p52aL142.elem_tot.txt
P52A~822 TXT       180,136  08-28-01  5:26p p52aL142.min_info.txt
        40 file(s)    252,041,846 bytes
```

**Directory of F:\Minerals**
(Files used in Section 6.3.3)

```
F_1_0522 6I          35,958  08-10-01  9:47a f_1_0522.6i
F_1_05~8 6O         943,588  09-04-01  4:50p f_1_0522.6i.6o
F_1_0~12 6P          32,654  09-04-01  4:50p f_1_0522.6i.6p
F_1_0~14 6T         106,340  09-04-01  4:50p f_1_0522.6i.6t
F_1_0~18 6TX         57,117  09-04-01  4:50p f_1_0522.6i.6tx
F_1_0~20 ELE          9,121  09-04-01  4:50p f_1_0522.6i.elem_aqu
F_1_0~22 ELE          8,560  09-04-01  4:50p f_1_0522.6i.elem_m_a
F_1_0~24 ELE          8,552  09-04-01  4:50p f_1_0522.6i.elem_min
F_1_0~26 ELE          8,565  09-04-01  4:50p f_1_0522.6i.elem_tot
F_1A0522 6I          36,031  08-10-01  9:48a f_1a0522.6i
F_1A0~30 6O         885,386  09-04-01  4:52p f_1a0522.6i.6o
F_1A0~34 6P          32,564  09-04-01  4:52p f_1a0522.6i.6p
F_1A0~36 6T          95,420  09-04-01  4:52p f_1a0522.6i.6t
F_1A0~40 6TX         50,522  09-04-01  4:52p f_1a0522.6i.6tx
F_1A0~42 ELE          8,748  09-04-01  4:52p f_1a0522.6i.elem_aqu
F_1A0~44 ELE          8,211  09-04-01  4:52p f_1a0522.6i.elem_m_a
F_1A0~46 ELE          8,203  09-04-01  4:52p f_1a0522.6i.elem_min
F_1A0~48 ELE          8,216  09-04-01  4:52p f_1a0522.6i.elem_tot
F_1B0522 6I          36,030  08-10-01  9:48a f_1b0522.6i
F_1B0~52 6O         879,433  09-04-01  4:54p f_1b0522.6i.6o
F_1B0~56 6P          32,638  09-04-01  4:54p f_1b0522.6i.6p
F_1B0~58 6T          95,420  09-04-01  4:54p f_1b0522.6i.6t
F_1B0~60 6TX         50,522  09-04-01  4:54p f_1b0522.6i.6tx
F_1B0~62 ELE          8,748  09-04-01  4:54p f_1b0522.6i.elem_aqu
F_1B0~64 ELE          8,211  09-04-01  4:54p f_1b0522.6i.elem_m_a
F_1B0~66 ELE          8,203  09-04-01  4:54p f_1b0522.6i.elem_min
F_1B0~68 ELE          8,216  09-04-01  4:54p f_1b0522.6i.elem_tot
F_1C0522 6I          36,104  08-10-01 10:54a f_1c0522.6i
F_1C0~72 6O         907,705  09-04-01  4:56p f_1c0522.6i.6o
F_1C0~78 6P          32,712  09-04-01  4:56p f_1c0522.6i.6p
F_1C0~80 6T          97,890  09-04-01  4:56p f_1c0522.6i.6t
F_1C0~82 6TX         51,921  09-04-01  4:56p f_1c0522.6i.6tx
F_1C0~84 ELE          9,121  09-04-01  4:56p f_1c0522.6i.elem_aqu
F_1C0~86 ELE          8,560  09-04-01  4:56p f_1c0522.6i.elem_m_a
F_1C0~88 ELE          8,552  09-04-01  4:56p f_1c0522.6i.elem_min
F_1C0~90 ELE          8,565  09-04-01  4:56p f_1c0522.6i.elem_tot
F_1D0522 6I          36,177  08-10-01 11:00a f_1d0522.6i
F_1D0~94 6O         921,115  09-04-01  4:57p f_1d0522.6i.6o
F_1D0~98 6P          33,360  09-04-01  4:57p f_1d0522.6i.6p
F_1D~100 6T         103,870  09-04-01  4:57p f_1d0522.6i.6t
F_1D~104 6TX         55,156  09-04-01  4:57p f_1d0522.6i.6tx
F_1D~106 ELE          9,121  09-04-01  4:57p f_1d0522.6i.elem_aqu
F_1D~108 ELE          8,560  09-04-01  4:57p f_1d0522.6i.elem_m_a
F_1D~110 ELE          8,552  09-04-01  4:57p f_1d0522.6i.elem_min
F_1D~112 ELE          8,565  09-04-01  4:57p f_1d0522.6i.elem_tot
F_1E0522 6I          36,176  08-10-01 11:08a f_1e0522.6i
F_1E~116 6O       4,222,609  09-04-01  5:04p f_1e0522.6i.6o
F_1E~130 6P          33,188  09-04-01  5:04p f_1e0522.6i.6p
F_1E~132 6T         291,590  09-04-01  5:04p f_1e0522.6i.6t
F_1E~134 6TX        179,156  09-04-01  5:04p f_1e0522.6i.6tx
F_1E~138 ELE         36,350  09-04-01  5:04p f_1e0522.6i.elem_aqu
F_1E~140 ELE         34,037  09-04-01  5:04p f_1e0522.6i.elem_m_a
F_1E~142 ELE         34,029  09-04-01  5:04p f_1e0522.6i.elem_min
F_1E~144 ELE         34,042  09-04-01  5:04p f_1e0522.6i.elem_tot
FFTF~146 XLS         44,032  09-05-01  9:56a FFTF IA 2001.xls
FFTF~148 XLS        955,904  08-06-01  4:05p fftf_fuel_hws_rev4.xls
        56 file(s)     11,717,896 bytes
```

**Directory of F:\Pu 1999**
(Files used in Section 6.3.2.1; the source is Ref. 40.)

```
PU-CERAM XLS       922,624  09-12-99  4:36p pu-ceram.xls
         1 file(s)        922,624 bytes
```

**Directory of F:\Pu 2001**
(Files used in Section 6.3.2.1; the source is Ref. 18.)

```
A516_R~6 XLS        19,456  01-20-01  5:23p A516_Rate.xls
DENSIT~8 XLS       274,944  08-27-01  4:12p density_pu-ceram.xls
HLW_G~10 XLS        58,368  08-17-01  1:26p HLW_glass REV01.xls
SLEEVE   XLS        15,360  02-06-01  1:59p Sleeve.xls
         4 file(s)        368,128 bytes
```

```
Total files listed:
       145 file(s)    279,190,979 bytes
```

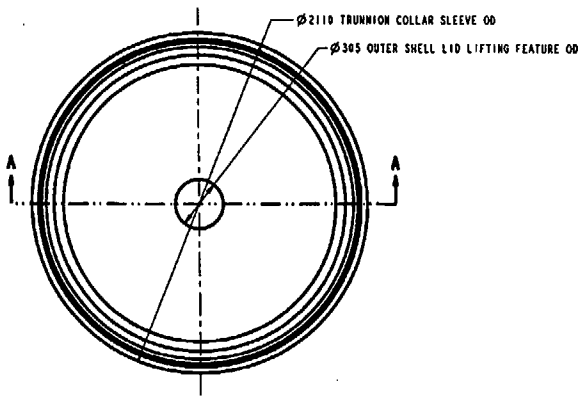


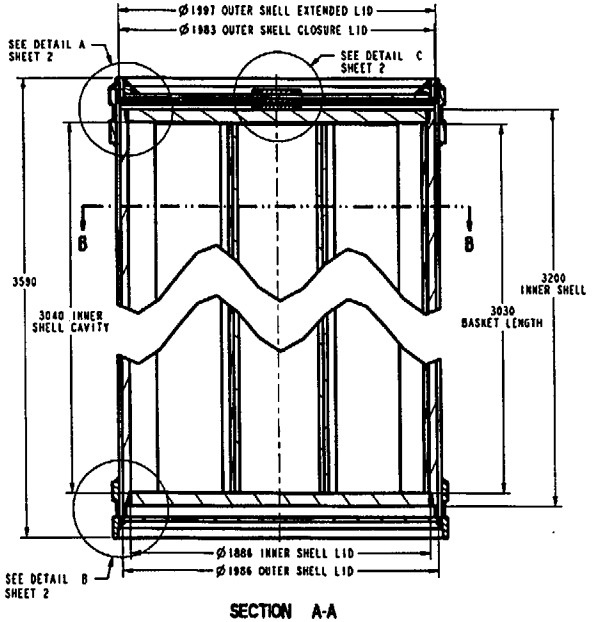


SECTION A-A

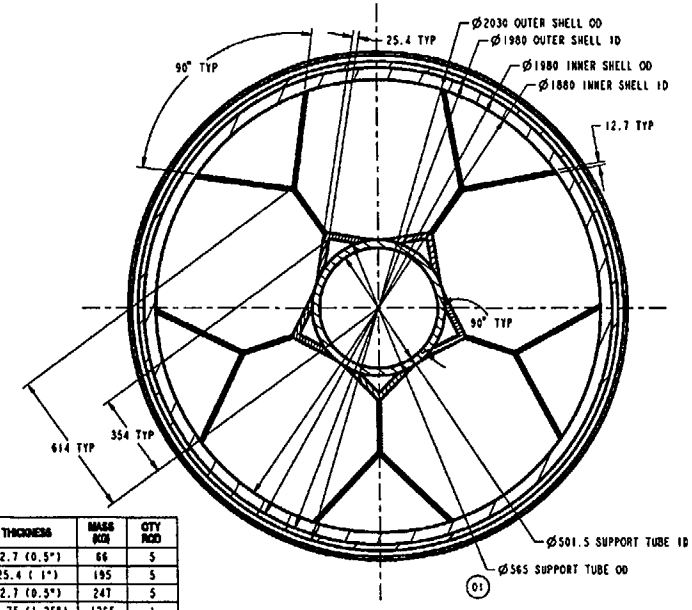


SECTION B-B

| COMPONENT NAME | MATERIAL | THICKNESS | MASS (KG) | QTY PER |
|---|---|---|---|---|
| DIVIDER PLATE | SA-516 K02700 | 12.7 (0.5") | 66 | 5 |
| INNER BRACKET | SA-516 K02700 | 25.4 ( 1") | 195 | 5 |
| OUTER BRACKET | SA-516 K02700 | 12.7 (0.5") | 247 | 5 |
| SUPPORT TUBE | SA-516 K02700 | 31.75 (1.25") | 1265 | 1 |
| INNER SHELL | SA-240 S31600 | 50 | 7621 | 1 |
| INNER SHELL LID | SA-240 S31600 | 80 | 1765 | 2 |
| INNER LID LIFTING FEATURE | SA-240 S31600 | 27 | 12 | 1 |
| OUTER SHELL | SB-575 N06022 | 25 | 4692 | 1 |
| EXTENDED OUTER SHELL LID | SB-575 N06022 | 25 | 172 | 1 |
| EXTENDED OUTER SHELL LID BASE | SB-575 N06022 | 25 | 629 | 1 |
| EXTENDED OUTER LID REINFORCING RING | SB-575 N06022 | 50 | 129 | 1 |
| OUTER LID LIFTING FEATURE | SB-575 N06022 | 27 | 13 | 2 |
| OUTER SHELL FLAT CLOSURE LID | SB-575 N06022 | 10 | 268 | 1 |
| OUTER SHELL FLAT BOTTOM LID | SB-575 N06022 | 25 | 689 | 1 |
| UPPER TRUNNION COLLAR SLEEVE | SB-575 N06022 | 40 | 655 | 1 |
| LOWER TRUNNION COLLAR SLEEVE | SB-575 N06022 | 40 | 642 | 1 |
| INNER SHELL SUPPORT RING | SB-575 N06022 | 20 | 53 | 1 |
| TOTAL ALLOY 22 WELDS | SFA-5.14 N06022 | - | 325 | *** |
| TOTAL 316 WELDS | SFA-5.9 S31680 | - | 133 | *** |
| WASTE PACKAGE ASSEMBLY | - | - | 23380 | 1 |
| HLW GLASS ASSEMBLY | - | - | 2500* | 5 |
| 18" CANISTER SHORT | - | - | 2270** | 1 |
| WP ASSEMBLY WITH SNF | - | - | 38130 | - |

(03) * WASTE ACCEPTANCE SYSTEM REQUIREMENTS DOCUMENT. E00000000-00811-1708-00001 REV 03, DOE/RW-0351. ACC: MOO.19990226.0001. PAGE 18. SECTION 4.2.3.1.A.4.

** UNITED STATES DEPARTMENT OF ENERGY 1998. DESIGN SPECIFICATION FOR DEPARTMENT OF ENERGY STANDARDIZED SPENT NUCLEAR FUEL CANISTERS, VOLUME I. DESIGN SPECIFICATION. REV 01. WASHINGTON D.C.: UNITED STATES DEPARTMENT OF ENERGY. TIC: 241528

*** SEE SK-0197 FOR WELD CONFIGURATION AND MASSES

UNITS: mm

DO NOT SCALE FROM SKETCH

| REVISIONS | | | |
|---|---|---|---|
| REV | DESCRIPTION | DRW BY | DATE |
| 00 | ISSUED APPROVED | DGM | 1/26/00 |
| 01 | IN SECTION B-B Ø 565 SUPPORT TUBE OD "WAS" ID | DGM | 4/21/00 |
| 02 | "MODIFIED" REVISION TABLE, "ADDED" DIMENSION 4 TO DETAIL A, "MODIFIED" CROSS HATCHING ON DETAIL A | BH | 4/25/00 |
| 03 | IN NOTE **, DOE/RW-0351 "WAS" DOE/RW-315P, IN REVISION BLOCK REV 00, 1/26/00 "WAS" 1/25/00, "ADDED" REVISION BALLOONS TO SECTION B-B AND DETAIL "A" | EJC | 6/5/00 |

"FOR INFORMATION ONLY"

# 5 DHLW/DOE SNF - SHORT WP ASSSEMBLY CONFIGURATION FOR SITE RECOMENDATION

SKETCH NUMBER: SK-0196 REV 03 SHEET 1 OF 2

SKETCHED BY: EUGENE CONNELL EJC 06/06/00 SmB 06/06/00 SmB for MJA 06/06/00

DATE: 06/05/00

FILE: /home/pro.library/checkout/sketches/5shtw.short/sk-0196_rev03.dwg

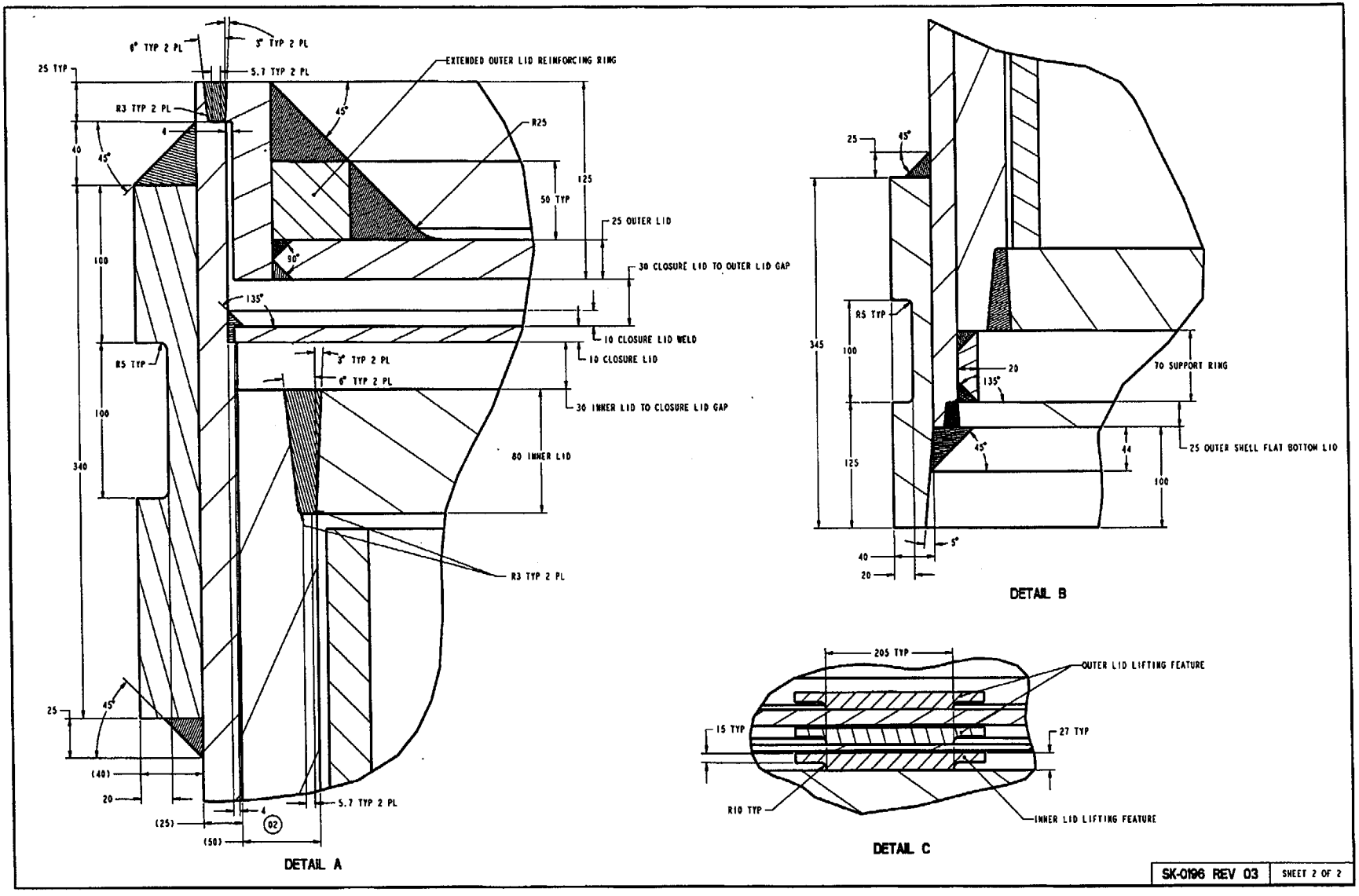
6° TYP 2 PL
3° TYP 2 PL
5.7 TYP 2 PL
EXTENDED OUTER LID REINFORCING RING
25 TYP
R3 TYP 2 PL
4
40
45°
R25
125
50 TYP
25 OUTER LID
90°
30 CLOSURE LID TO OUTER LID GAP
100
135°
10 CLOSURE LID WELD
10 CLOSURE LID
R5 TYP
3° TYP 2 PL
6° TYP 2 PL
30 INNER LID TO CLOSURE LID GAP
100
80 INNER LID
340
R3 TYP 2 PL
25
45°
(40)
20
(25)
4
5.7 TYP 2 PL
02
(50)
DETAIL A
25
45°
345
100
R5 TYP
20
135°
TO SUPPORT RING
125
45°
44
25 OUTER SHELL FLAT BOTTOM LID
100
5°
40
20
DETAIL B
205 TYP
OUTER LID LIFTING FEATURE
15 TYP
27 TYP
R10 TYP
INNER LID LIFTING FEATURE
DETAIL C
SK-0196 REV 03
SHEET 2 OF 2

3

# OFFICE OF CIVILIAN RADIOACTIVE WASTE MANAGEMENT
## CALCULATION COVER SHEET

1. QA: QA
Page: 1 Of: 38

2. Calculation Title
Radiolytic Specie Generation from Internal Waste Package Criticality

3. Document Identifier (including Revision Number)
CAL-EBS-NU-000017 REV 00

| 4. Total Attachments | 5. Attachment Numbers – Number of pages in each |
|---|---|
| 3 | I-1, II (1 + CD-ROM), III-12 |

| | Print Name | Signature | Date |
|---|---|---|---|
| 6. Originator | John A. McClure<br>Georgeta Radulescu | John A. McClure<br>Georgeta Radulescu | 9/25/2001<br>9/28/2001 |
| 7. Checker | Luca J. Gratton (Technical)<br>Kristine Dutton (Compliance) | Luca J. Gratton<br>Kristine Dutton | 9/28/2001<br>9/28/01 |
| 8. Lead | John A. McClure | John A. McClure | 9/25/2001 |

9. Remarks

**Revision History**

| 10. Revision No. | 11. Description of Revision |
|---|---|
| 00 | Initial Issue |

## CONTENTS

## FIGURES

**Page**

## TABLES

## ACRONYMS

| | |
|---|---|
| B&W | Babcock and Wilcox |
| BSC | Bechtel SAIC Company |
| BWR | Boiling Water Reactor |
| CD-ROM | Compact Disc - Read Only Memory |
| CRWMS | Civilian Radioactive Waste Management System |
| CSNF | Commercial Spent Nuclear Fuel |
| DHLW | Department of Energy Owned High Level Waste |
| DOE | U.S. Department of Energy |
| DTN | Data Tracking Number |
| EBS | Engineered Barrier System |
| FEP | Features, Events, and Processes |
| GWd/MTU | GigaWatt days per Metric Ton Uranium |
| $k_{eff}$ | effective neutron multiplication number |
| MGR | Monitored Geologic Repository |
| M&O | Management and Operating Contractor |
| NRC | U.S. Nuclear Regulatory Commission |
| OCRWM | Office of Civilian Radioactive Waste Management |
| PWR | Pressurized Water Reactor |
| SNF | Spent Nuclear Fuel |
| WP | Waste Package |
| YMP | Yucca Mountain Project |

## 1. PURPOSE

The effects of radiation on the corrosion of various metals and alloys, particularly with respect to in-reactor processes, has been discussed by a number of authors (Shoesmith and King 1998, p. 2). Shoesmith and King (1998) additionally discuss the effects of radiation on the proposed Monitored Geologic Repository (MGR) Waste Package (WP) materials. Radiation effects on the corrosion of metals and alloys include, among other things, radiolysis of the local gaseous and aqueous environment to produce both oxidizing and reducing radicals. In particular, radiolysis processes in moist air environments lead to the fixation of nitrogen as NO, $NO_2$, and especially $HNO_3$ (Reed and Van Konynenburg 1988, pp. 393-404). Nitric acid is assumed to be the principal corrosive radiolytic chemical specie and is produced in an irradiated air-water vapor system when the hydroxyl radicals generated from the water vapor convert nitrogen dioxides, that are formed by the radiolytic reaction between nitrogen and oxygen, to nitric acids.

Chemical species produced by radiolysis have been identified in the Disposal Criticality Analysis Methodology Topical Report (DCTR) (YMP 2000, p. 2-2) as a mechanism for accelerating corrosion of the MGR engineered barrier system (EBS). Radiolytic sources of corrosion have also been considered in the screening of processes and issues in the drip shield and WP degradation (Civilian Radioactive Waste Management System [CRWMS] Management and Operating Contractor [M&O] 2001a, Section 6.2.27), Yucca Mountain Project (YMP) features, events, and processes (FEP) No. 2.1.13.01.00. The latter reference dealt specifically with radiolytic effects of gamma radiation on the WP and drip shield, excluding them from further consideration because of low consequence. The potential for chemical interactions within the WP from radiolytic effects was considered insignificant in the Waste Form Degradation Process Model Report (CRWMS M&O 2000c, p. 3-21) and therefore neglected except as a possible perforation mechanism for the Zircaloy cladding (CRWMS M&O 2000c, p. 3-40).

Radiolysis producing a local depression of the pH resulting in localized corrosion of cladding material is included in the localized corrosion model as a special feature, YMP FEP NO. 2.1.02.15.00 (CRWMS M&O 2000d, Section 6.2.5). Neutron and gamma doses considered in the screening decision for this FEP were representative of the residual radionuclide decay only and did not consider the dose from an internal criticality. Although the Zircaloy cladding is resistant to direct attack by nitric acid, cladding destabilization may occur allowing the buildup of metal-halide complexes in solutions that can promote corrosion (CRWMS M&O 2000b, p. II–1). Screening arguments for this corrosion mechanism show that environments conducive to the accumulation of the necessary chemical species are unlikely.

The U.S. Nuclear Regulatory Commission (NRC) has also expressed a concern during key technical information exchanges regarding the effects on criticality consequence evaluations resulting from radiation from the criticality event (Reamer and Williams 2000, p. 6). In particular, their concern is that although Zircaloy has excellent corrosion resistance to nitric acid and hydrogen peroxide, the concentration of these species can be enhanced by radiolysis during an internal WP criticality, potentially accelerating the corrosion effects in the cladding material.

Attachment III contains the text of the white paper responding to the NRC/DOE (U.S. Department of Energy) DOE Criticality Key Technical Issue regarding radiolytic enhancement of Zircaloy corrosion rates resulting from an internal WP criticality. The white paper documented a scoping calculation of the radiolytic generation potential for nitric acid and an estimate of the consequences with respect to corrosion rates of Zircaloy. The chemical environment conducive to enhanced corrosion rates was identified and compared with possible conditions resulting from a static criticality. Based upon the scoping calculation results, radiolytic contributions to enhanced corrosion rates from criticality events could not be screened out from consideration. Mitigating effects from the chemical interactions, however, may reduce possibilities for accelerated Zircaloy corrosion. A detailed geochemical calculation of such factors was outside the scope of the initial calculation. It should be noted, however, that the radiolytic production rate of nitric acid during a static criticality event from the detailed calculation (Section 6 of this document) is within 10% of the rate from the scoping calculation (Attachment III). Thus, consequences relating to accelerated corrosion rates for Zircaloy derived from the detailed geochemistry calculation are not expected to differ significantly from the scoping calculation, i.e., a potential exists for lowering the pH of the WP environment but scavenging effects may prevent sufficient accumulation of nitric acid to affect corrosion rates.

The purpose of this calculation is to provide a detailed calculation the potential for generation of radiolytic species during a postulated static criticality event in a WP. The consequences of any radiolytic specie generation, estimated in Attachment III, will be addressed in a revision to this calculation.

This calculation is done in accordance with the *Technical Work Plan for: Waste Package Design Description for LA* (License Application) (BSC [Bechtel SAIC Company] 2001a, Section 3). Details of this activity are in Section 3, Tasks for Work Scope 2, Disposal Criticality Analysis Methodology Development. The work plan calls for resolution of all items in the revised DCTR for which NRC acceptance is sought. The calculational method, input description, and results from this calculation are given in the following sections.

## 2. METHOD

Radiolytic production of particular chemical species depends upon the radiation environment, the chemical components present, and the physical environment where the radiolytic reactions are occurring. However, the yield of any given chemical species is characterized by a single parameter, "G", identified as the G-factor (Reed and Van Konynenburg 1991, pp. 1396-1403). The "G" value represents the number of molecules of a chemical species produced per 100 eV of absorbed radiation energy in the volume containing the irradiated environment. Measurements of the "G" factor for production of nitrogen dioxide (one-to-one production ratio for nitric acid) from mixed neutron-gamma radiation range from approximately 0.5 to 2.5 molecules/100 eV of absorbed energy (Reed and Van Konynenburg 1991, p. 1399). The value used in this calculation is 1.0 (Assumption 3.3) and this value is also assumed to apply to neutron irradiation (Assumption 3.3). The acid production rate scales linearly with the "G" factor and the uncertainty in the factor expressed in Section 6 as range of possible molar quantities of nitric acid generated. The "G" value of 1.0 was chosen for this calculation to be consistent with other radiolytic acid production calculations discussed in Section 5.

For this calculation, a 21-pressurized water reactor (PWR) WP, containing commercial spent nuclear fuel (CSNF) assemblies, was assumed to have failed and subsequently partially filled with water. The steel basket structure was assumed to have fully degraded with the degradation products settling to the bottom of the WP. Hematite ($Fe_2O_3$) is assumed to be the only iron-bearing degradation product formed from the original basket material (Assumption 3.1). This is consistent with previous studies (CRWMS M&O 1997, Section 7.1.1) that showed that replacement of hematite by goethite had little effect on criticality. In a separate suite of evaluations, the contribution to the degradation product volume from diaspore generated by oxidized aluminum from the thermal shunt plates is also considered. The packing fraction of the hematite, or the hematite-diaspore mixture, was assumed to be 0.58 (Assumption 3.2), with the remaining space filled with water. For evaluations involving mixtures, complete reaction of the Fe and Al in the donating structures provides a mole fraction of 0.8439 (mass fraction = 0.9350) for the hematite in the degradation product mixture material. Degradation products were assumed to be present outside the fuel pins in assemblies below the degradation product-water mixture level, but not within the guide tube and instrument tube spaces of those assemblies. The water level above the degradation product-water mixture was assumed to extend sufficiently high to maintain criticality, leaving an air-water vapor space at the top of the WP. The radiant energy deposition in the air-water vapor space was calculated with the MCNP code (Briesmeister, 1997) using the KCODE option and tracking the transport of both neutron and gamma particles. The gamma interactions include photon and electron processes leading to dissociation of the gas molecules and generation of nitric acids in the air-water vapor space.

A KCODE calculation provides the combined estimates (track length, collision, and absorption) of $k_{eff}$ for the waste package (Briesmeister 1997, p. 2-153). Additionally, the code collects information about events that occur during the calculation in set of variables known as tallies. A series of these tallies have been specified in the MCNP input decks to obtain estimates for the following physical quantities:

1. Total, neutron, and gamma energy depositions, in MeV, in the moist air regions of the waste package
2. Average energy released per fission for the waste package
3. Average number of neutrons released per fission for the waste package
4. $k_{eff}$ for each of the SNF regions: the fuel pins surrounded by degradation products (lower region), the fuel pins surrounded by water (middle region), and the fuel pins surrounded by moist air (top region) (see Figure 5.4 for region definition).

Information is collected for both gamma and neutron events using "f6" and "f4" tally types that are defined as

f6 energy deposition averaged over a cell in MeV/g
f4 flux averaged over a cell in particles/cm$^2$.

The MCNP results for the specified tallies are provided per fission neutron.

## 2.1 ENERGY DEPOSITION

The combination of the "f6" tally card and an "sd" segment divisor card that sets the mass divisors of the cells to unity provides the track length estimate of cell energy deposition, in MeV. The cell energy deposition is the integral over the cell volume, time range, and particle energy range from the total reaction rate in the cell multiplied by the heating response, as shown in Equation 1 (Briesmeister 1997, p. 2-72)

$$ED = \rho_a \int_V \int_t \int_E \sigma_T(E)\Phi(\vec{r}, E, t)H(E)dEdtdV \qquad \text{Eq. 1}$$

where:

ED = energy deposition (MeV)
$\rho_a$ = atom density (atoms/barn-cm)
$\sigma_T(E)$ = total microscopic cross-section (barn)
$\Phi(\vec{r}, E, t)$ = particle flux (neutrons or photons/cm$^2$s)
H(E) = heating response (MeV)
V = cell volume (cm$^3$)
E = neutron or photon energy (MeV)
t = time (s).

The f6 tally is equivalent to a f4 track length estimate of cell flux modified by energy-dependent multipliers, which consist of the particle total reaction rate number and the heating number on a fm card (tally multiplier, Briesmeister 1997, p. 2-73). The reaction numbers used as multipliers are –1 (total cross section) and –4 (average heating number) for neutrons and –5 (total cross section) and –6 (photon heating number) for photons (Briesmeister 1997, p. 3-77). This equivalent tally has been specified in the MCNP calculations for verification purposes.

## 2.2 TRACK LENGTH ESTIMATOR FOR $k_{eff}$

The track length estimator for $k_{eff}$ provides an estimate for the integral shown in Equation 2. This estimator has been specified in the MCNP input using an "f4:n" (neutron) tally card, an "fm" card that contains the –6 (total fission cross section) and –7 (number of neutrons released per fission) reaction multipliers, and an "sd" card (volume multiplier) that sets the fuel region volume to unity (Briesmeister 1997, pp. 2-151 and 2-163) given by

$$k_{eff} = \rho_a \int_{V}\int_{t}\int_{E} \Phi(\vec{r}, E, t)\,dE\,dt\,dV \sum_{k} f_k \bar{\nu}_k(E)\sigma_{fk}(E) \qquad \text{Eq. 2}$$

where:

$f_k$ = atomic fraction for nuclide k
$\sigma_{fk}(E)$ = microscopic neutron fission cross section (barn) for nuclide k
$\bar{\nu}_k(E)$ = average number of prompt or total neutrons produced per fission by the collision nuclide at the incident neutron energy.

## 2.3 AVERAGE NUMBER OF NEUTRONS RELEASED PER FISSION

The average number of neutrons released per fission for the system is calculated as the ratio of total neutrons released in fission events to the fission reaction rate, as shown in Equation 3

$$\nu_{avg} = \frac{\rho_a \int_{V}\int_{t}\int_{E} \Phi(\vec{r}, E, t)\,dE\,dt\,dV \sum_{k} f_k \bar{\nu}_k(E)\sigma_{fk}(E)}{\rho_a \int_{V}\int_{t}\int_{E} \sigma_f(E)\Phi(\vec{r}, E, t)\,dE\,dt\,dV} \qquad \text{Eq. 3}$$

where:

$\sigma_f(E)$ = total microscopic fission cross-section (barn).

The numerator of the fraction is evaluated using the track length estimator for $k_{eff}$, as described in the previous section. The f4 tally (track length estimator for cell flux) and the –6 multiplier provide an estimate for the total fission reaction rate, which represents the denominator of the fraction.

## 2.4 AVERAGE ENERGY RELEASED PER FISSION

The average energy released per fission is calculated using the ratio of the estimated total fission energy released to the fission reaction rate, as shown in Equation 4

$$Q_{avg} = \frac{\rho_a \int_{V}\int_{t}\int_{E} \Phi(\vec{r}, E, t)\,dE\,dt\,dV \sum_{k} f_k \sigma_{fk}(E)\bar{Q}_k(E)}{\rho_a \int_{V}\int_{t}\int_{E} \sigma_f(E)\Phi(\vec{r}, E, t)\,dE\,dt\,dV} \qquad \text{Eq. 4}$$

where:

$Q_{avg}$ = average energy released per fission (MeV/fission)
$Q_k(E)$ = average energy produced per fission by the collision nuclide at the incident neutron energy.

The numerator of the fraction is evaluated using the f4 tally and the –6 and –8 (fission energy) multiplier. The denominator is evaluated as described in the previous section.

Control of the electronic management of data is accomplished in accordance with the process control evaluation for technical work plan of this calculation (BSC 2001a).

## 3. ASSUMPTIONS

3.1 It is assumed that the steel in the basket assembly and fuel assembly end fittings is fully degraded. Hematite ($Fe_2O_3$) and Diaspore (ALO(OH)) are assumed to be the only degradation products remaining from the steel internals. The rational for this assumption is that these minerals have a very low solubility whereas other degradation products with higher solubilities are more likely to be transported out of the WP. This minimizes the amount of neutron absorber materials in the WP which is conservative. This assumption is used in Sections 2 and 5.

3.2 It is assumed that the porosity of packed particles resulting from degradation of the steel and aluminum internal structure of a 21 PWR WP is 42%. The rationale for this assumption is that measurements of the porosity of compacted granular materials (sand) was limited to approximately 42% before onset of container distortion (CRWMS M&O 1998b, p. 15). This assumption is used in Sections 2, 5, and 6.

3.3 It is assumed that the "G" factor for radiolytic production of nitric acid has the same value for neutron radiation as for gamma radiation. The rationale for this assumption is that radiolytic specie production is proportional to the absorbed energy rather than the effective dose. This assumption is used in Sections 2, 5, and 6.

3.4 It is assumed that the spacing between fuel assemblies in an asymmetric arrangement (resting on the WP) is 0.25 cm. The rationale for this assumption is that degradation products from the basket structure remaining between assemblies will prevent direct contact between assemblies This assumption is used in Sections 5 and 6.

3.5 It is assumed that the stainless steel inner shell of the WP is not degraded. The rationale for this assumption is that it is conservative. Degradation products from the WP shell would increase the total volume of the hematite in the WP, thus decreasing the moist air space available for radiolytic reactions. This assumption is used in Sections 5 and 6.

3.6 It is assumed that the Babcock and Wilcox (B&W) Mark B 15x15 fuel design used for this calculation is representative of the fuel types anticipated for potential disposition in the MGR. The basis for this assumption is this assembly type has been used for WP source term (CRWMS M&O 1999a, Section 3) and radiolysis calculations (BSC 2001b, Section 5.2). This assumption is used in Section 5.

3.7 It is assumed that the instrument tube in a B&W Mark B fuel assembly is the same length as the fuel pins. The rationale for this assumption is that it is conservative allowing slightly more moderator within the assemblies immersed in the degradation products. This assumption is used in Section 5.

# 4. USE OF COMPUTER SOFTWARE AND MODELS

## 4.1 COMPUTER SOFTWARE

### 4.1.1 MCNP

The MCNP code (CRWMS M&O 1998c), qualified according to Office of Civilian Radioactive Waste Management (OCRWM) procedure AP-SI.1Q, *Software Management*, was used to calculate the effective neutron multiplication factor ($k_{eff}$) of the system and radiant energy deposition in the vapor space of the WP. The software specifications are as follows:

- Software name: MCNP
- Software version/revision number: Version 4B2
- Software tracking number (CSCI): 30033 V4B2LV
- Computer type: Hewlett Packard (HP) 9000 Series Workstations
- Computer processing unit number: Software is installed on the CRWMS M&O workstation "bloom" whose CRWMS M&O Tag number is 700887.

The input and output files for the various MCNP calculations are contained on a compact disk-read only memory (CD-ROM) (Attachment II) with the files documented in Attachment I. The calculation spreadsheets described in Sections 5 and 6 and included in Attachment II are such that an independent repetition of the calculations may be performed.

The MCNP software used was:

(a) appropriate for the calculation of criticality and radiant energy deposition (MCNP is a Monte Carlo computer program designed for criticality calculations and for tracking neutron and gamma radiation)

(b) used only within the range of validation (benchmark cases used in validation the code include a number of critical configurations involving $UO_2$ fuels and shielding configurations involving neutron and gamma particle transport CRWMS M&O 1998a)

(c) obtained from the Software Configuration Management in accordance with appropriate procedures.

### 4.1.2 Excel

- Title: Excel
- Version/Revision Number: Microsoft® Excel 97 SR-2
- This software is installed on a personal computer running Microsoft Windows 95 with CRWMS M&O Tag number 113136.

Microsoft Excel for Windows, Version 97 SR-2, was used in this calculation to translate the input data into the correct format and units using standard mathematical expressions and operations. It was also used to reformulate and display results. The user-defined formulas, inputs, and results are documented in sufficient detail to allow an independent repetition of computations. Thus, Microsoft Excel is used only as a worksheet and not as a software routine. Microsoft Excel is an exempt software product according to OCRWM procedure AP-SI.1Q, *Software Management*.

## 4.2 MODELS

None used.

## 5. CALCULATION

As stated in Section 1, the purpose of this calculation is to evaluate the potential for production of radiolytic nitric acid during a postulated criticality event involving intact PWR CSNF in a degraded basket configuration inside a 21-PWR WP. The PWR CSNF used in the calculation were B&W 15x15 PWR assemblies (Assumption 3.6) having a five wt% initial $^{235}U$ enrichment, 30 GWd/MTU (GigaWatt-days/metric ton uranium) burnup, and a 25,000 year radionuclide decay period.

The reference design for the repository (CRWMS M&O 2000a, Section 1.7.1) features a line loading of WPs, a drip shield with no backfill, emplacement of the WPs on a corrosion resistant pallet with a nominal spacing of ten centimeters between WPs, resting on an invert filled with crushed tuff. The principal components of this design are illustrated by the drift segment shown in Figure 5.1. The 21-PWR WP configuration that is the basis for MCNP representation used in this calculation is illustrated in Figure 5.2. Descriptions of the MCNP representation of the WP, fuel assemblies, and other data used in the calculation are given in the following sections.

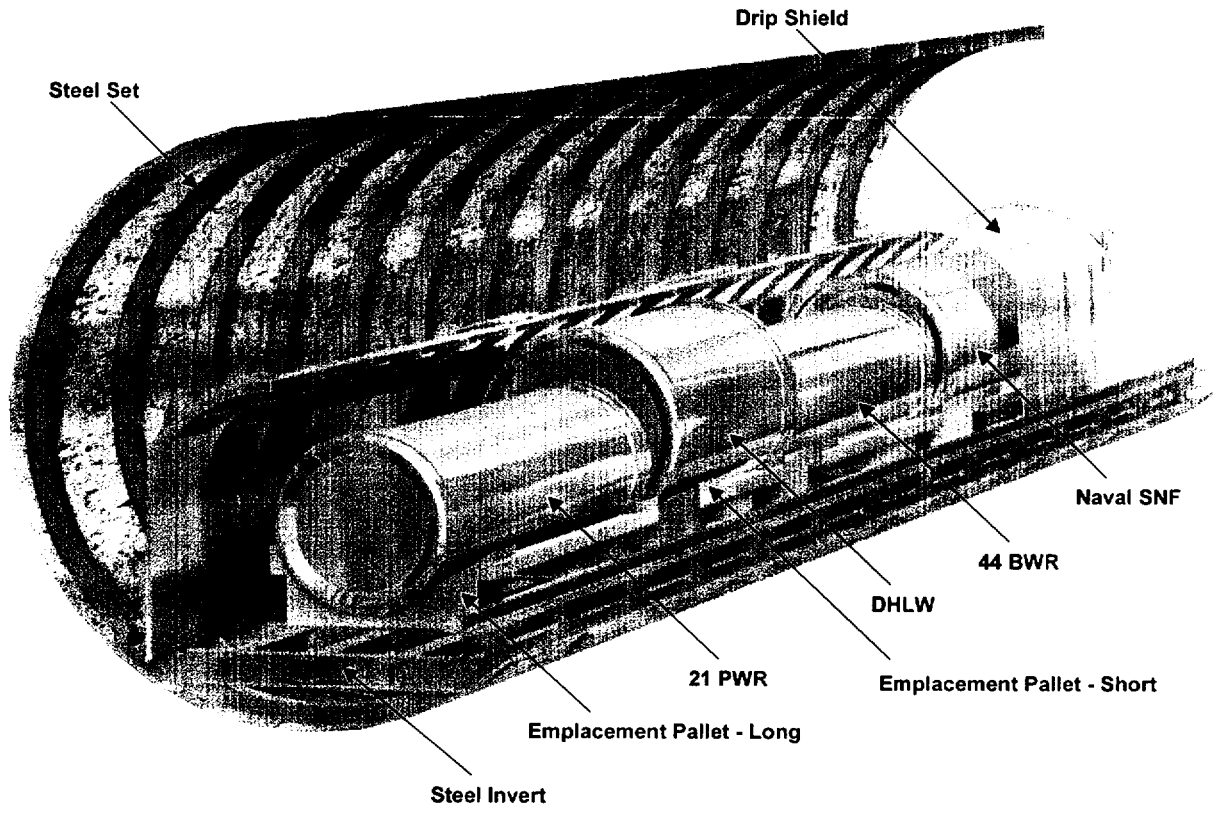


Figure 5.1. MGR Drift Segment Showing Waste Packages, Pallets, and Drip Shield

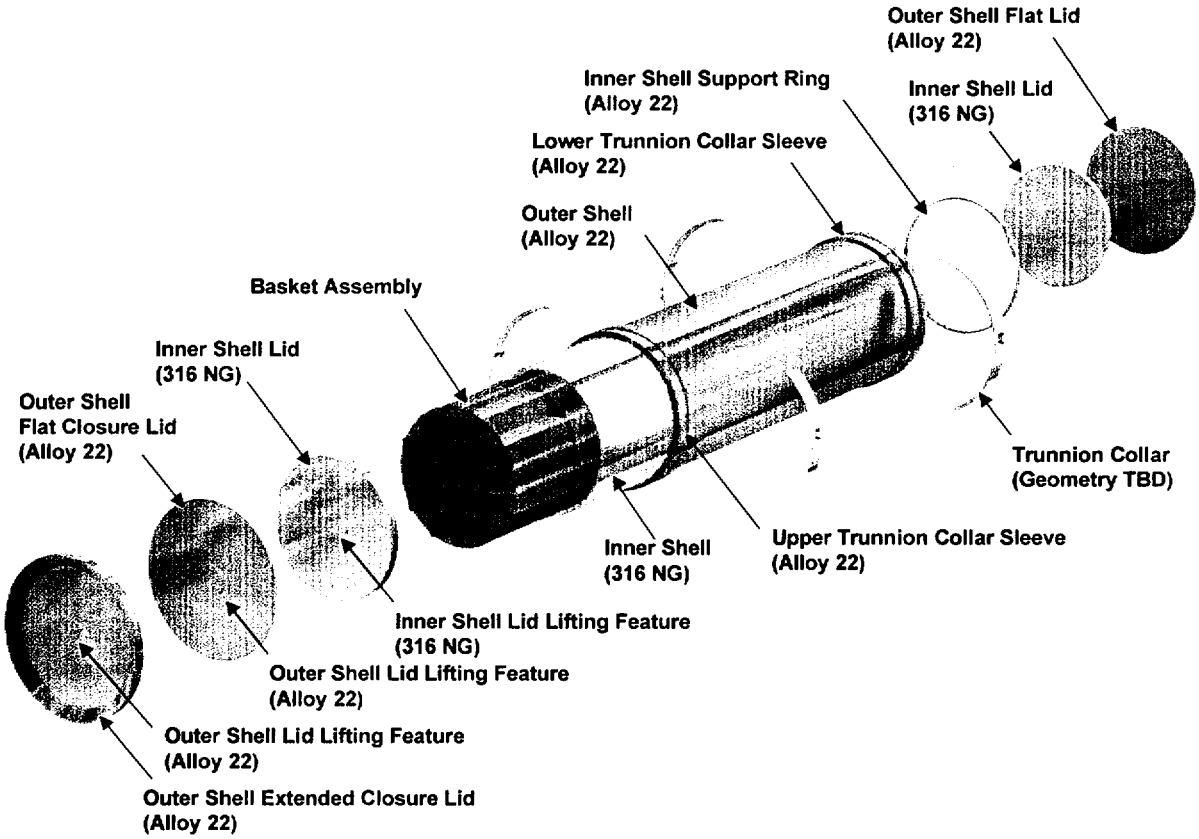


Figure 5.2. 21-PWR Waste Package Assembly Configuration

## 5.1 LIST AND STATUS OF INPUT DATASETS

The document tracking numbers (DTN) used in this calculation are listed in Table 5.1. These DTNs are all qualified-verification level 2, for uses not supporting the principal factors.

Table 5.1. Summary List of Input DTNs

| Input | Content |
|---|---|
| DTN: MO0003RIB00071.000 | Physical and Chemical Characteristics of Alloy 22 |
| DTN: MO0003RIB00076.000 | Physical and Chemical Characteristics of Type 316N Grade Stainless Steel |
| DTN: MO9906RIB00048.000 | Waste Package Material Properties: Waste Form Materials |
| DTN: MO9906RIB00054.000 | Waste Package Material Properties: Structural Materials |

## 5.2 INPUT DESCRIPTION

### 5.2.1 21-PWR Waste Package

The 21-PWR WP, illustrated in Figure 5.2, consists of an inner shell of 316 NG stainless steel for strength, an outer shell of corrosion resistant Alloy 22, inner shell lids of 316 NG stainless steel, outer shell lids of Alloy 22, and the basket assembly of 516 carbon steel containing embedded Neutronite absorber plates. The WP geometry and dimensions of the WP are listed in Table 5.2. For this calculation, the basket assembly is assumed to be fully degraded (Assumption 3.1). Products resulting from the degradation of the basket are assumed to be in a settled configuration which is the most reactive configuration. Gross CSNF assembly (DOE 1987, p. 2A-31 – 2A-45) and WP component (CRWMS M&O 2000e, Attachment I) masses and materials are listed in Table 5.3.

Table 5.2. Waste Package Dimensions

| Parameter | Value | Units | Radius | Basis |
|---|---|---|---|---|
| Inner Shell OD | 152.4 | cm | 76.2 | CRWMS M&O 2000e, Attachment I |
| Inner Shell ID | 142.4 | cm | 71.2 | CRWMS M&O 2000e, Attachment I |
| Inner Shell Length | 477.5 | cm | - | CRWMS M&O 2000e, Attachment I |
| Inner Shell Lid Diameter | 142.0 | cm | 71.0 | CRWMS M&O 2000e, Attachment I |
| Inner Shell Lid Thickness | 9.5 | cm | - | CRWMS M&O 2000e, Attachment I |
| Outer Shell OD | 156.4 | cm | 78.2 | CRWMS M&O 2000e, Attachment I |
| Outer Shell ID | 152.4 | cm | 76.2 | CRWMS M&O 2000e, Attachment I |
| Outer Shell Length | 501.5 | cm | - | CRWMS M&O 2000e, Attachment I |
| Outer Shell Lid Diameter | 152.7 | cm | 76.35 | CRWMS M&O 2000e, Attachment I |
| Outer Shell Lid Thickness | 1.0 (top flat)<br>2.5 (base and extension) | cm | - | CRWMS M&O 2000e, Attachment I |
| Total Waste Package Length | 516.5 | cm | - | CRWMS M&O 2000e, Attachment I |
| Inner Shell Cavity Volume | $7.30212 \cdot 10^6$ | $cm^3$ | - | inner shell dimension data in this table |

Table 5.3. Components and Material Inventories for Waste Package

| Components | Mass (kg) | Material | Basis |
|---|---|---|---|
| Outer WP Shell and Lids | 4880 | Alloy 22 | CRWMS M&O 2000e, Attachment I |
| Inner WP Shell and Lids | 11109 | Stainless Steel 316 | CRWMS M&O 2000e, Attachment I |
| Basket Tubes, Sideguides, Cornerguides and Stiffeners | 5723.68 | A 516 Carbon Steel Grade 70 | CRWMS M&O 2000e, Attachment I |
| Fuel Basket Plates A, B and C | 2064 | Neutronit A 978 | CRWMS M&O 2000e, Attachment I |
| Fuel Basket Plates D and E | 336 | SB 209 Aluminum 6061 | CRWMS M&O 2000e, Attachment I |
| Assembly Nozzle – Top (/assbly) | 7.480 | Stainless Steel CF3M | DOE 1987, p. 2A-32 |
| Assembly Nozzle – Bottom (/assbly) | 8.160 | Stainless Steel CF3M | DOE 1987, p. 2A-32 |
| Assembly Spring Retainer (/assbly) | 0.910 | Stainless Steel CF3M | DOE 1987, p. 2A-32 |
| Assembly Upper End Plugs (/assbly) | 0.060 | Stainless Steel 304 | DOE 1987, p. 2A-32 |
| Assembly Lower Nuts (/assbly) | 0.150 | Stainless Steel 304 | DOE 1987, p. 2A-32 |
| Assembly Upper Nuts (/assbly) | 0.510 | Stainless Steel 304L | DOE 1987, p. 2A-32 |
| Assembly Spacer – Plenum (/assbly) | 1.040 | Inconel 718 | DOE 1987, p. 2A-32 |
| Assembly Spacer – Bottom (/assbly) | 1.300 | Inconel 718 | DOE 1987, p. 2A-32 |
| Assembly Spacers – Core (/assbly) | 4.900 | Inconel 718 | DOE 1987, p. 2A-32 |
| Holddown Spring (/assbly) | 1.800 | Inconel 718 | DOE 1987, p. 2A-32 |
| Assembly Instrument Tube (/assbly) | 0.640 | Zircaloy 4 | DOE 1987, p. 2A-32 |
| Assembly Guide Tubes (/assbly) | 8.000 | Zircaloy 4 | DOE 1987, p. 2A-32 |

### 5.2.2 B&W Mark B Intact Fuel Assembly

The representations of the B&W 15x15 Mark B PWR fuel assembly in the calculations use nominal specifications and parameters (DOE 1987, p. 2A-32 – 2A-35 and Punatar 2001, p. 2-4 – 2-10). Intact assembly specifications and dimensions are provided in Table 5.4. Assembly dimensions are given primarily in English units and converted into metric units. The number of digits in the corresponding metric value column is a result of the direct units conversion and is not indicative of precision. These parameters are used as input to the degradation product inventory calculations (see Attachment II), the MCNP $k_{eff}$ searches, and collision density calculations (Attachment II). The initial assembly heavy metal (i.e., U) inventory specified in Table 5.4 differs by less than 3% from the value used for definition of the fuel composition (CRWMS M&O 1999a, p. 23, Table 12) used for calculating the 30 GWd/MTU burnup and 25,000 year decay isotopic of the fuel assemblies, and is therefore acceptable for use in these calculations of system mass and volume (Attachment II). The WP shell dimensions (CRWMS M&O 2000e, Attachment I) given in Table 5.2 are also input to the calculations as necessary.

Table 5.4. Mechanical Parameters of the B&W 15x15 Mark B Fuel Assembly

| Parameter | Value | Units | Metric | Units | Radius | Basis |
|---|---|---|---|---|---|---|
| Fuel Rods | 208 | /assbly | 208 | /assbly | - | DOE 1987, p. 2A-33 and 2A-45 |
| Fuel Rod Positions on an Assembly Side | 15 | /side | 15 | /side | - | Punatar 2001, p. 2-5, Table 2-2 |
| Guide Tubes | 16 | /assbly | 16 | /assbly | - | DOE 1987, p. 2A-32 and 2A-44 |
| Instrumentation Tubes | 1 | /assbly | 1 | /assbly | - | DOE 1987, p. 2A-32 and 2A-44 |
| Total Guide + Instrument Tubes | 17 | /assbly | 17 | /assbly | - | sum of guide and instrument tubes |
| Clad, Guide and Instrument Tube Material | Zircalloy-4 | | Zircalloy-4 | | - | Punatar 2001, p. 2-5, Table 2-2 |
| Fuel Pellet OD[a] | 0.3686 | in | 0.936244 | cm | 0.468122 | Punatar 2001, p. 2-5, Table 2-2 |
| Active Fuel Rod Length | 141.8 | in | 360.172 | cm | - | Punatar 2001, p. 2-5, Table 2-2 |
| Total Fuel Rod Length | 153.687 | in | 390.366 | cm | - | Punatar 2001, p. 2-15 |
| Fuel Clad OD | 0.430 | in | 1.0922 | cm | 0.5461 | Punatar 2001, p. 2-5, Table 2-2 |
| Clad Wall Thickness | 0.0265 | in | 0.06731 | cm | - | DOE 1987, p. 2A-33 and 2A-45 |
| Fuel Clad ID[a] | 0.377 | in | 0.95758 | cm | 0.47879 | Punatar 2001, p. 2-5, Table 2-2 |
| Fuel Clad End Cap Thickness | 0.2811 | in | 0.714 | cm | - | Punatar 2001, p. 2-15 |
| Fuel Rod Pitch | 0.568 | in | 1.44272 | cm | - | Punatar 2001, p. 2-5, Table 2-2 |
| Guide Tube OD | 0.530 | in | 1.3462 | cm | 0.6731 | Punatar 2001, p. 2-10 |
| Guide Tube Wall Thickness | 0.016 | in | 0.04064 | cm | - | difference between outer and inner radii |
| Guide Tube ID | 0.498 | in | 1.26492 | cm | 0.63246 | Punatar 2001, p. 2-10 |
| Guide Tube Length | 156.313 | in | 397.035 | cm | - | Punatar 2001, p. 2-10 |
| Instrument Tube OD | 0.544067 | in | 1.38193 | cm | 0.69097 | Punatar 2001, p. 2-10 |
| Instrument Tube Wall Thickness | 0.051534 | in | 0.13090 | cm | - | Difference between outer and inner radii |
| Instrument Tube ID | 0.4410 | in | 1.12014 | cm | 0.56007 | Punatar 2001, p. 2-10 |
| Instrument Tube Length | 153.5 | in | 389.890 | cm | - | Punatar 2001, p. 2-10 |
| Fuel Assembly Height | 165.625 | in | 420.6875 | cm | - | DOE 1987, p. 2A-31 and 2A-43 |
| Mass of U | 1022.12 | lbm /assbly | 463.63 | kg /assbly | - | DOE 1987, p. 2A-31 and 2A-43 |

| Parameter | Value | Units | Metric | Units | Radius | Basis |
|---|---|---|---|---|---|---|
| Fuel Assembly Width | 8.536 | in | 21.68144 | cm | - | DOE 1987, p. 2A-31 and 2A-43 |
| Fuel Assembly Pitch | 9.6693(sym) 8.6344(asym) | in | 24.560(sym) 21.93144(asym) | cm | - | Assumption |
| Fuel Assembly Volumetric Displacement | $5.2297 \cdot 10^3$ | $in^3$ | $8.570 \cdot 10^4$ | $cm^3$ | - | Assembly pin, guide and instrument tube data in this table |

NOTE: Table 5.3 entries do not reflect significant digits where necessitated by unit conversions.
[a] OD (outside diameter), ID (inside diameter)

### 5.2.3 Material Compositions and Density

Material compositions and mass densities used in number density and degradation product volume calculations are listed in Table 5.5. The Neutronit A 978 composition used in calculations neglects the 2.2 (wt %) Mo, with assignment of the Mo content to Fe. The isotope $^{95}Mo$ is a principal isotope (YMP 2000, p. 3-34, Table 3-3) that has a natural abundance of 15.92 (atom %) and a ground state thermal neutron capture cross section of 110 (b) (Parrington et al. 1996, p. 31). The neglect of Mo in the basket plates contributes to conservative assessment from a neutronic standpoint, as the Mo does not contribute to parasitic neutron capture.

Table 5.5. Material Specification for the Waste Package Container and Fuel Hardware

| A 516 Carbon Steel Grade 70 | | | | | | |
|---|---|---|---|---|---|---|
| Mass Density ($kg/m^3$) | | | | | | Basis |
| 7850 | | | | | | ASME[a] 1998, Section II-A, SA-20, p. 67 |
| Composition (wt %) | | | | | | Basis |
| Carbon (max) | 0.27 | Manganese | 1.025 | Phosphorus (max) | 0.035 | ASME 1998, Section II-A, SA-516, p. 925 |
| Silicon | 0.275 | Sulfur (max) | 0.035 | Iron (balance) | 98.36 | |

| Stainless Steel CF3M | | | | | | |
|---|---|---|---|---|---|---|
| Mass Density ($kg/m^3$) | | | | | | Basis |
| 8000 | | | | | | SS 316N mass density from DTN: MO0003RIB00076.000 |
| Composition (wt %) | | | | | | Basis |
| Carbon (max) | 0.03 | Chromium | 19.0 | Manganese (max) | 1.5 | SAE 1993, p. 141. Additional 2.5 (wt %) Mo, with equivalent reduction for Fe, incorporated in mass balance. |
| Molybdenum | 2.5 | Nickel | 11.0 | Phosphorus (max) | 0.04 | |
| Silicon (max) | 1.50 | Sulfur (max) | 0.04 | Iron (balance) | 64.39 | |

| Stainless Steel 302 | | | | | | |
|---|---|---|---|---|---|---|
| Mass Density (kg/m$^3$) | | | | | | Basis |
| 7940 | | | | | | SS 304 mass density from DTN: MO9906RIB00054.000 |
| Composition (wt %) | | | | | | Basis |
| Carbon (max) | 0.15 | Chromium | 18.0 | Manganese (max) | 2.0 | SAE 1993, p. 251 |
| Nickel | 9.0 | Phosphorus (max) | 0.045 | Sulfur (max) | 0.03 | |
| Silicon (max) | 1.0 | Iron (balance) | 69.775 | | | |

| Stainless Steel 304 | | | | | | |
|---|---|---|---|---|---|---|
| Mass Density (kg/m$^3$) | | | | | | Basis |
| 7940 | | | | | | DTN: MO9906RIB00054.000 |
| Composition (wt %) | | | | | | Basis |
| Carbon (max) | 0.08 | Chromium | 19.0 | Manganese (max) | 2.0 | DTN: MO9906RIB00054.000 |
| Nickel | 9.25 | Nitrogen (max) | 0.1 | Phosphorus (max) | 0.045 | |
| Sulfur (max) | 0.03 | Silicon (max) | 1.0 | Iron (balance) | 68.495 | |

| Stainless Steel 304L | | | | | | |
|---|---|---|---|---|---|---|
| Mass Density (kg/m$^3$) | | | | | | Basis |
| 7940 | | | | | | DTN: MO9906RIB00054.000 |
| Composition (wt %) | | | | | | Basis |
| Carbon (max) | 0.03 | Chromium | 19.0 | Manganese (max) | 2.0 | DTN: MO9906RIB00054.000 |
| Nickel | 10.0 | Nitrogen | 0.1 | Phosphorus (max) | 0.045 | |
| Sulfur (max) | 0.03 | Silicon (max) | 0.75 | Iron (balance) | 68.045 | |

| Stainless Steel 316 | | | | | | |
|---|---|---|---|---|---|---|
| Mass Density (kg/m$^3$) | | | | | | Basis |
| 7980 | | | | | | SS 316L mass density from DTN: MO9906RIB00054.000 |
| Composition (wt %) | | | | | | Basis |
| Carbon (max) | 0.08 | Chromium | 17.00 | Manganese (max) | 2.00 | ASME 1998, Section II-A, SA-240, p. 366 |
| Molybdenum | 2.50 | Nickel | 12.00 | Phosphorus (max) | 0.045 | |
| Silicon (max) | 0.75 | Sulfur (max) | 0.03 | Nitrogen (max) | 0.10 | |
| Iron (balance) | 65.495 | | | | | |

| Neutronit A 978 | | | | | | |
|---|---|---|---|---|---|---|
| Mass Density (kg/m$^3$) | | | | | | Basis |
| 7760 | | | | | | Kugler 1996, p. 17 |
| Composition (wt %) | | | | | | Basis |
| Boron (min) | 0.75 | Carbon (max) | 0.04 | Chromium | 18.5 | Kugler 1996, p. 14 and ASTM A887-89, p. 2 |
| Cobalt (max) | 0.2 | Nickel | 13.0 | Iron (balance) | 67.51 | |

| Alloy 22 | | | | | | |
|---|---|---|---|---|---|---|
| Mass Density (kg/m$^3$) | | | | | | Basis |
| 8690 | | | | | | DTN: MO0003RIB00071.000 |
| Composition (wt %) | | | | | | Basis |
| Carbon (max) | 0.015 | Chromium | 21.25 | Cobalt (max) | 2.5 | DTN: MO0003RIB00071.000 |
| Iron | 4.0 | Manganese (max) | 0.5 | Molybdenum | 13.5 | |
| Phosphorus (max) | 0.02 | Silicon (max) | 0.08 | Sulfur (max) | 0.02 | |
| Tungsten (max) | 3.0 | Vanadium (max) | 0.35 | Nickel (balance) | 54.765 | |

| Inconel 718 | | | | | | |
|---|---|---|---|---|---|---|
| Mass Density (kg/m$^3$) | | | | | | Basis |
| 8190 | | | | | | DTN: MO9906RIB00054.000 |
| Composition (wt %) | | | | | | Basis |
| Aluminum | 0.5 | Carbon | 0.04 | Chromium | 19.0 | DTN: MO9906RIB00054.000 |
| Columbium | 5.13 | Manganese | 0.18 | Molybdenum | 3.05 | |
| Nickel | 52.5 | Silicon | 0.18 | Sulfur | 0.008 | |
| Titanium | 0.9 | Iron (balance) | 18.512 | | | |

| Zircaloy 4 | | | | | | |
|---|---|---|---|---|---|---|
| Mass Density (kg/m$^3$) | | | | | | Basis |
| 6560 | | | | | | DTN: MO9906RIB00048.000 |
| Composition (wt %) | | | | | | Basis |
| Chromium | 0.1 | Iron | 0.21 | Oxygen | 0.125 | DTN: MO9906RIB00048.000 |
| Tin | 1.45 | Zirconium (balance) | 98.115 | | | |

| SB 209 Aluminum 6061 | | | | | | |
|---|---|---|---|---|---|---|
| Mass Density (kg/m$^3$) | | | | | | Basis |
| 2700 | | | | | | DTN: MO9906RIB00048.000 |
| Composition (wt %) | | | | | | Basis |
| Chromium | 0.195 | Copper | 0.275 | Iron (max) | 0.7 | DTN: MO9906RIB00048.000 |
| Manganese (max) | 0.15 | Magnesium | 1.0 | Silicon | 0.6 | |
| Titanium (max) | 0.15 | Zinc (max) | 0.25 | Aluminum (balance) | 96.68 | |

NOTE: Minor differences exist between the compositional specifications for Stainless Steel 302, Stainless Steel 316 and Neutronit A 978 in Table 5.5 and in the mass balance calculations (Attachment II, File "21-PWR-EDAII-A-0914_cor.xls", Sheet "Vol-Mass"). These compositional specifications have no effect on the degradation product compositions, because neither the plenum spring nor inner WP shell materials are degraded in the assessments.
[a] American Society of Mechanical Engineers.

Isotopic and elemental atomic weights are given in Table 5.6. Table 5.7 defines the CSNF composition for a nominal LEU PWR assembly with an initial fissile enrichment of 5.0 (wt %), 30 GWd/MTU burnup, and 25,000 years of post-irradiation isotopic decay (CRWMS M&O 1999b, Disk 3, File "Waste.Stream.E2.R1.B7.cut", TBV-4111). This combination of high initial enrichment and relatively low burnup is not representative of the average assembly in the PWR commercial waste stream, and is conservative because it contributes to a high reactivity attribute. The assembly definition taken for the source term calculation uses an initial heavy

metal inventory of 475 kg (CRWMS M&O 1999a, p. 23, Table 12) , which differs from the specification in Table 5.3 by less than 3%. The isotopic inventories specified in Table 5.7 are based on the assembly definition of CRWMS M&O 1999a (p. 23, Table 12).

Table 5.6. Isotopic and Atomic Weights

| Isotope or Element | Atomic Weight (amu) or (g/mole) | Basis |
|---|---|---|
| H | 1.00794 | Parrington et al. 1996, p. 62 |
| O | 15.9994 | Parrington et al. 1996, p. 63 |
| Al | 26.981538 | Parrington et al. 1996, p. 63 |
| Fe | 55.845 | Parrington et al. 1996, p. 62 |
| $^{95}$Mo | 94.905841 | Parrington et al. 1996, p. 31 |
| $^{99}$Tc | 98.9062545 | Audi and Wapstra 1995, p. 22 |
| $^{101}$Ru | 100.905581 | Parrington et al. 1996, p. 31 |
| $^{103}$Rh | 102.905504 | Parrington et al. 1996, p. 31 |
| $^{109}$Ag | 108.904756 | Parrington et al. 1996, p. 31 |
| $^{143}$Nd | 142.909810 | Parrington et al. 1996, p. 37 |
| $^{145}$Nd | 144.912569 | Parrington et al. 1996, p. 37 |
| $^{147}$Sm | 146.914894 | Parrington et al. 1996, p. 36 |
| $^{149}$Sm | 148.917180 | Parrington et al. 1996, p. 36 |
| $^{150}$Sm | 149.917272 | Parrington et al. 1996, p. 36 |
| $^{152}$Sm | 151.919729 | Parrington et al. 1996, p. 36 |
| $^{151}$Eu | 150.919846 | Parrington et al. 1996, p. 36 |
| $^{153}$Eu | 152.921226 | Parrington et al. 1996, p. 36 |
| $^{155}$Gd | 154.922619 | Parrington et al. 1996, p. 36 |
| $^{233}$U | 233.039627 | Parrington et al. 1996, p. 49 |
| $^{234}$U | 234.040945 | Parrington et al. 1996, p. 49 |
| $^{235}$U | 235.043922 | Parrington et al. 1996, p. 49 |
| $^{236}$U | 236.045561 | Parrington et al. 1996, p. 48 |
| $^{238}$U | 238.050785 | Parrington et al. 1996, p. 48 |
| $^{237}$Np | 237.048166 | Parrington et al. 1996, p. 48 |
| $^{239}$Pu | 239.052156 | Parrington et al. 1996, p. 48 |
| $^{240}$Pu | 240.053808 | Parrington et al. 1996, p. 48 |
| $^{241}$Pu | 241.056845 | Audi and Wapstra 1995, p. 61 |
| $^{242}$Pu | 242.058737 | Parrington et al. 1996, p. 48 |
| $^{241}$Am | 241.056822 | Parrington et al. 1996, p. 48 |
| $^{243}$Am | 243.061374 | Parrington et al. 1996, p. 48 |

Table 5.7. CSNF Composition

| Isotope | Mass (g/assbly) | Number Density $(b \cdot cm)^{-1}$ |
|---|---|---|
| $^{16}O$[a] | 6.39E+04 | 4.6628E-02 |
| $^{95}Mo$ | 3.52E+02 | 4.3307E-05 |
| $^{99}Tc$ | 3.29E+02 | 3.8840E-05 |
| $^{101}Ru$ | 3.31E+02 | 3.8302E-05 |
| $^{103}Rh$ | 2.07E+02 | 2.3488E-05 |
| $^{109}Ag$ | 2.72E+01 | 2.9163E-06 |
| $^{143}Nd$ | 4.20E+02 | 3.4316E-05 |
| $^{145}Nd$ | 3.14E+02 | 2.5301E-05 |
| $^{147}Sm$ | 1.33E+02 | 1.0570E-05 |
| $^{149}Sm$ | 2.10E+00 | 1.6466E-07 |
| $^{150}Sm$ | 1.32E+02 | 1.0281E-05 |
| $^{152}Sm$ | 5.52E+01 | 4.2426E-06 |
| $^{151}Eu$ | 9.29E+00 | 7.1875E-07 |
| $^{153}Eu$ | 4.22E+01 | 3.2222E-06 |
| $^{155}Gd$ | 1.79E+00 | 1.3491E-07 |
| $^{233}U$ | 5.08E+00 | 2.5453E-07 |
| $^{234}U$ | 1.82E+02 | 9.0801E-06 |
| $^{235}U$ | 1.21E+04 | 6.0110E-04 |
| $^{236}U$ | 3.24E+03 | 1.6027E-04 |
| $^{238}U$ | 4.43E+05 | 2.1729E-02 |
| $^{237}Np$ | 6.82E+02 | 3.3594E-05 |
| $^{239}Pu$ | 1.40E+03 | 6.8382E-05 |
| $^{240}Pu$ | 5.80E+01 | 2.8212E-06 |
| $^{241}Pu$ | 1.98E-05 | 9.5908E-13 |
| $^{242}Pu$ | 1.00E+02 | 4.8238E-06 |
| $^{241}Am$ | 5.97E-04 | 2.8918E-11 |
| $^{243}Am$ | 1.58E+00 | 7.5902E-08 |

NOTE: data in Table 5.7 use exponential notation: e.g., $1.0 \cdot 10^{-3} = 1.0E-03$
isotopic mass inventories from CRWMS M&O 1999b, Disk 3, File "Waste.Stream.E2.R1.B7.cut"
[a] $^{16}O$ mass inventory satisfies $UO_2$ composition. see Attachment II, File "fuel_comp.xls", sheet "25,000"

### 5.2.4 Degradation Product Inventories

Degradation product inventories and characteristics are summarized in Table 5.8. Calculations for the hematite and diaspore volumes and masses are made in Attachment II, File "21-PWR-EDAII-A-0914_cor.xls", Sheet "Vol-Mass", assuming a 58% solid volume fraction in the degradation product mixture. The 58% solid volume fraction is derived from compacted granular material and represents an upper bound on the solid fraction (Assumption 3.2). Degradation product volumes and masses are converted to number densities in Attachment II, File "deg_comp.xls", Sheet "Number_Densities."

Table 5.8. Degradation Product Inventories and Characteristics

| Hematite Only | | | |
|---|---|---|---|
| Solid Product Volume Fraction (%) | Mixture Mass Density[a,b] ($g/cm^3$) | | Volume[b] ($cm^3$) |
| 58 | 3.4592 | | 3.4209E+06 |
| Fe Density[c] $(b \cdot cm)^{-1}$ | Al Density[c] $(b \cdot cm)^{-1}$ | O Density[c] $(b \cdot cm)^{-1}$ | H Density[c] $(b \cdot cm)^{-1}$ |
| 2.29228E-02 | 0.00000E+00 | 4.84239E-02 | 2.80795E-02 |
| Configuration | Degradation Product Mixture Height[d] (cm) | | Water Level Height[d] (cm) |
| Symmetric | 13.62160 | | 36.2 |
| Asymmetric | 19.90699 | | 71.2 |

| Hematite and Diaspore | | | |
|---|---|---|---|
| Solid Product Volume Fraction (%) | Mixture Mass Density[a,b] ($g/cm^3$) | | Volume[b] ($cm^3$) |
| 58 | 3.3899 | | 3.7871E+06 |
| Fe Density[c] $(b \cdot cm)^{-1}$ | Al Density[c] $(b \cdot cm)^{-1}$ | O Density[c] $(b \cdot cm)^{-1}$ | H Density[c] $(b \cdot cm)^{-1}$ |
| 2.14338E-02 | 1.28589E-03 | 4.87622E-02 | 2.93654E-02 |
| Configuration | Degradation Product Mixture Height[d] (cm) | | Water Level Height[d] (cm) |
| Symmetric | 22.02201 | | 47.0 |
| Asymmetric | 27.95594 | | N/A |

NOTE: some data in Table 5.8 use exponential notation: e.g., $1.0 \cdot 10^{-3}$ = 1.0E-03
[a] nominal water density of 1.0 (g/cc), see Table 6.1
[b] see Attachment II, File "21-PWR-EDAII-A-0914_cor.xls", Sheet "Vol-Mass"
[c] see Attachment II, File "deg_comp.xls", Sheet "Number_Densities"
[d] height from WP axis elevation.

## 5.3 MCNP REPRESENTATION OF 21-PWR WASTE PACKAGE

A principal assumption for this calculation (Assumption 3.1) is that the steel components (basket assembly and fuel assembly end fitting) are completely degraded with only the Hematite and (optionally) Diaspore remaining in the WP. The fuel assemblies, with Zircaloy cladding and spacer grids, remain intact. The MCNP representation of the assemblies is thus limited to the fuel pins, guide tubes, and instrument tubes. The assembly descriptions consist of four axial zones, partially disjoint, that are based upon the fuel composition distribution. One zone includes the fuel pin end caps and spacers, the second zone includes the gas plenums and springs, the third zone contains the active fuel region, and the last zone contains only the guide tubes which extend beyond the fuel pins. This configuration is illustrated in Figure 5.3.

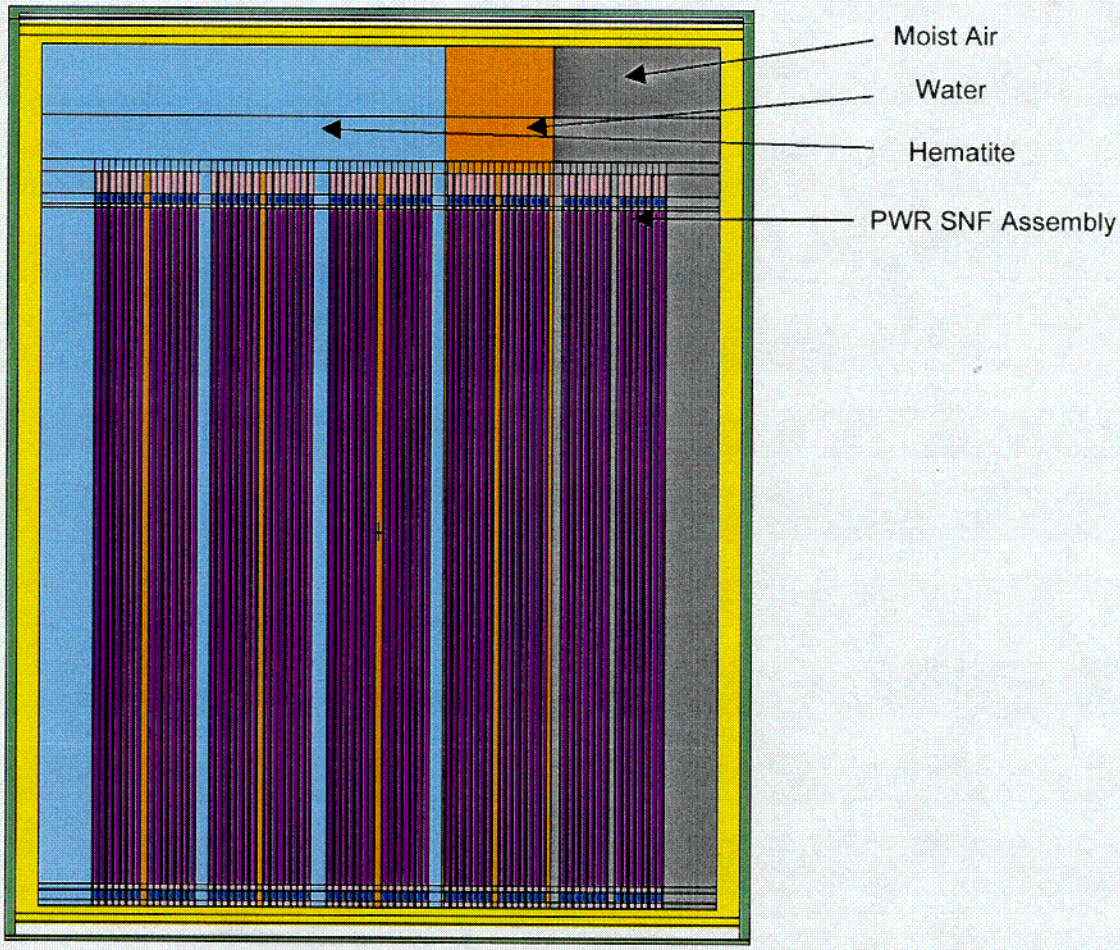


NOTE: Drawing not to scale.

Figure 5.3. Waste Package Vertical Cross Section

At the time of original repository emplacement, the CSNF assemblies occupy the basket bays illustrated in Figure 5.2. Two MCNP representations of the 21-PWR WP and fuel assemblies were constructed, one configuration having a symmetric crosssectional arrangement of fuel assemblies and the second with an asymmetric arrangement. These representations are illustrated in Figures 5.4 and 5.5, respectively. The symmetric configuration is very conservative with respect to the criticality potential of the WP.

Configurational subclasses were defined for the radiolysis calculations based on the maintenance of the original assembly spacing with respect to the package horizontal crossectional plane. In the symmetric case (Figure 5.3), the original relative assembly spacing was maintained, averaging 24.56 cm for the assembly pitch throughout the basket structure, despite basket plate, thermal shunt and fuel tube degradation. The absolute assembly locations are frozen at the original design positions allowing no vertical or horizontal displacements, with

C03

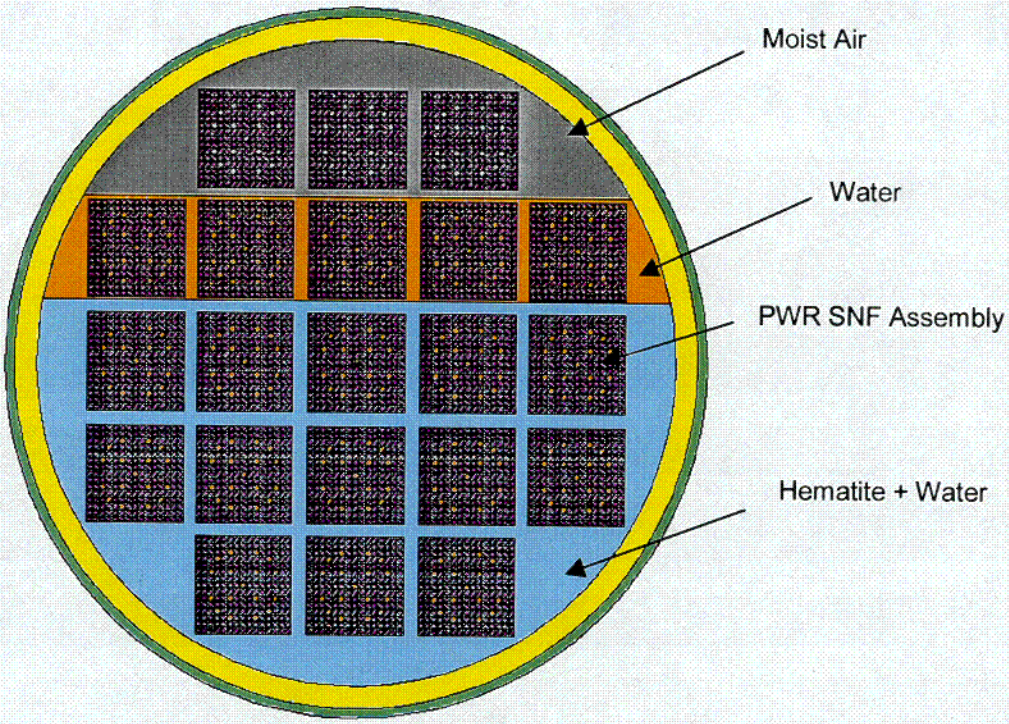


Figure 5.4. Symmetric Configuration: Hematite Degradation Product

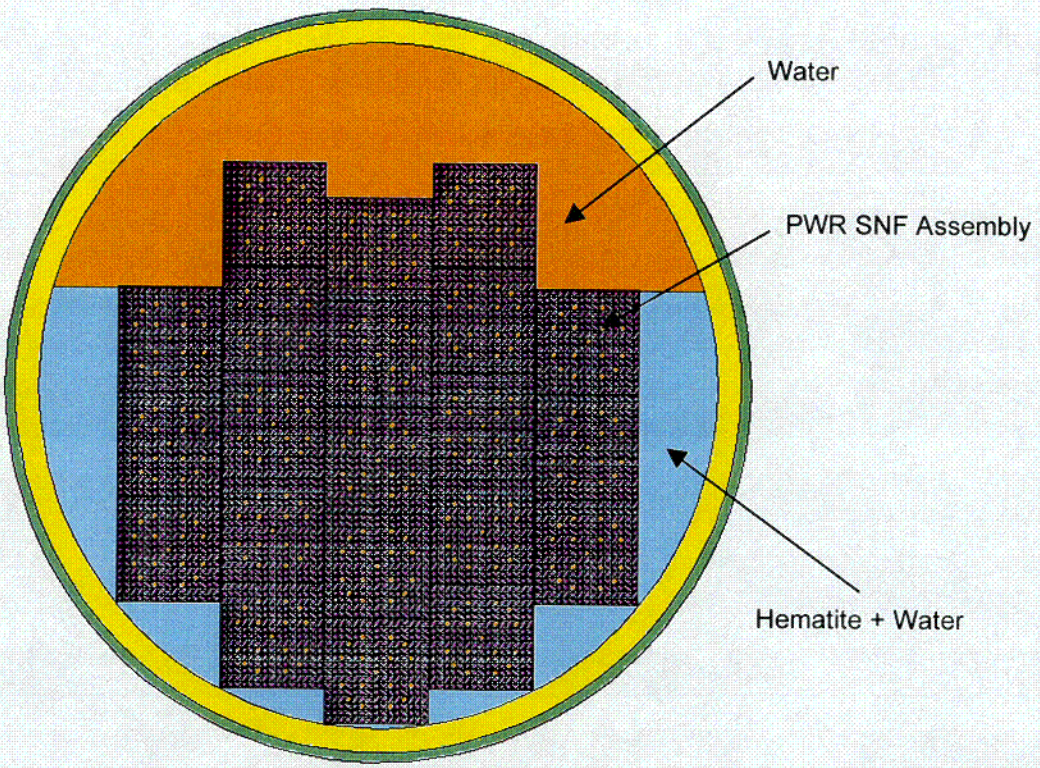


Figure 5.5. Asymmetric Configuration: Hematite Degradation Product

C 04

the degradation product mixture occupying the assembly interstices and the available waste package cavity void space. Degradation products were excluded from the interior of the guide tubes and instrument tubes since, in the horizontal position, there is little likelihood these products will enter the tubes. The maintenance of original assembly positions is a bounding configuration for the determination of $k_{eff}$ because it maximizes the fraction of CSNF assemblies residing above the degradation product mixture line, thereby placing more assemblies in an overlying water moderated region and maximizing the assembly multiplication worths.

The asymmetric configuration (Figure 5.5) accounts for the vertical settling of the assemblies within the WP cavity. The assembly pitch is the assembly width plus a 0.250-cm interstitial separation (Assumption 3.4). Vertical translations of the assemblies from the original positions create five columns of assemblies, with the lowest row of assemblies contacting the surface at the base of the inner WP shell. The resulting spatial distribution of assemblies is asymmetric with respect to the WP cross-section, but still symmetric with respect to the bi-lateral arrangement. The hematite and diaspore degradation product mixture occupies the assembly interstices and the accessible WP cavity void space excluding the assembly guide tubes and instrument tubes.

Configurational subclasses were identified according to assumptions concerning the degradation products remaining in the WP. If all of the steel and aluminum structures within the WP, excluding the shell and closure lids, and exposed assembly hardware are degraded, the hematite displacement volume exceeds the diaspore displacement volume by approximately a factor of 10 (see Attachment II, File "21-PWR-EDAII-A-0914_cor.xls", Sheet "Vol-Mass"). The degradation product mixture definition is varied parametrically to determine the influence of including or excluding the minor Al-bearing fraction of the mixture. In combination with variations for symmetric or asymmetric configurations, parametric variations produce a total of four distinct degraded configurations:

1. symmetric assembly configuration, with hematite only
2. symmetric assembly configuration, with hematite and diaspore
3. asymmetric assembly configuration, with hematite only
4. asymmetric assembly configuration, with hematite and diaspore.

The configurations with Hematite as the only degradation product are illustrated in Figure 5.4 for the symmetric case and Figure 5.5 for the asymmetric case. The symmetric configuration with both Hematite and Diaspore as degradation products is illustrated in Figure 5.6. These figures also show the crosssectional areas occupied by the degradation product mixture, water, and moist air. For the asymmetric configuration, criticality could not be achieved with any moist air space in the WP (Section 6) , and thus radiolytic specie production can not occur for that configuration.

The energy deposition in the air filled region calculated by MCNP is given in units of MeV per fission neutron. This energy must be multiplied by nubar (number of neutrons per fission) and number of fission events occurring in a criticality to obtain the total energy deposition from a

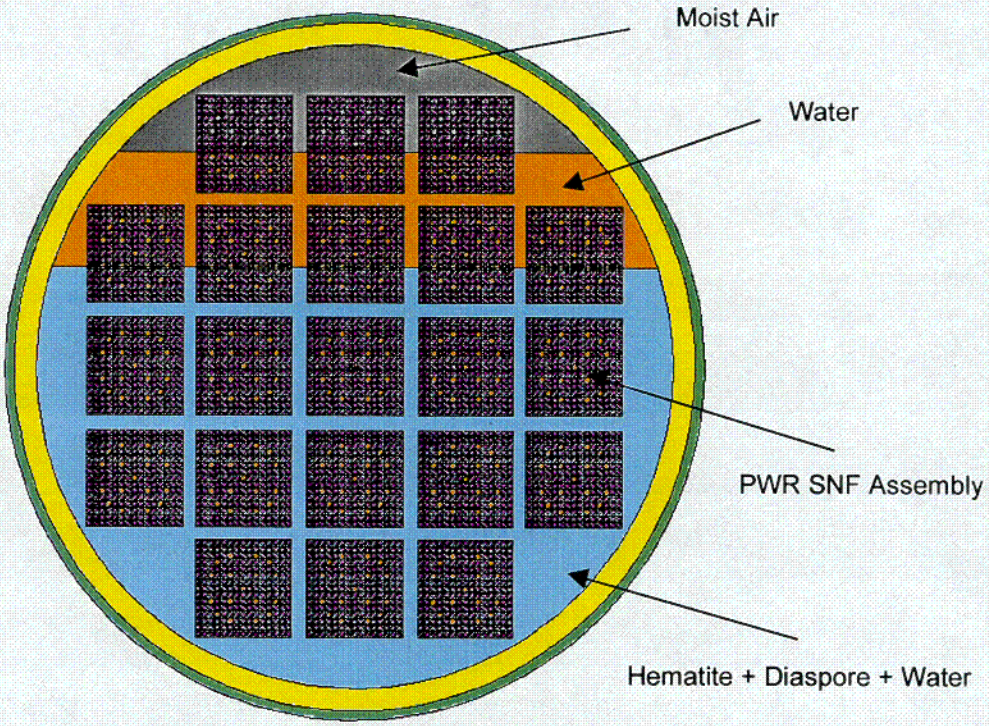


Figure 5.6. Symmetric Configuration: Hematite and Diaspore Degradation Products

postulated criticality. These operations are documented in the spreadsheet file "21-PWR-EDAII-A-0914_cor.xls" (sheet "Tally-result") included in Attachment II.

C05

## 6. RESULTS

This document may be affected by technical product input information that requires confirmation. Any changes to the document that may occur as a result of completing the confirmation activities will be reflected in subsequent revisions. The status of the technical product input information quality may be confirmed by review of the Document Input Reference System database (AP-3.15Q, *Managing Technical Product Inputs.* Section 5.4.1e).

As stated in Section 1, radiolytic specie generation that has any potential for enhancing corrosion rates within a WP requires a critical configuration operating over some period of time. In addition, there must be a void space in the WP containing air and water vapor, sources for the radiolytic radicals that ultimately combing to form nitric acid. Thus the WP configurations identified in Section 5 were screened for having a criticality potential coupled with a void space. The level of the degradation product mixture was fixed since its volume was known and the critical water level above the mixture then determined iteratively. These levels, as given in Table 6.1, are 36.2 cm and 47.0 cm for the symmetric configuration with Hematite only and Hematite plus Diaspore, respectively. The asymmetric configuration was near criticality with Hematite only but the water level at the top of the WP leaving no space for radiolytic specie production. With both Hematite and Diaspore as degradation products in the asymmetric configuration, criticality was not possible. The degradation product mixture level, critical water level, and MCNP tally quantities described in Section 2 are summarized in Table 6.1.

The radiant energy deposition, in MeV per fission neutron, in the WP regions filled with moist air for the symmetric configurations are listed in Table 6.2 for the Hematite degradation product case and for the Hematite plus Diaspore case in Table 6.3. The tallies were summed over all of the void locations in the WP with the numbered locations identified in Figure 6.1. It should be noted that regions numbered from two through five consist of the union of lattice all assemblies in the void region.

The radiolytic production of nitric acid for a static criticality averaging one kW is given in Table 6.1 as 7.41E-03 moles/year/kW with Hematite only as the degradation product and 4.07E-3 moles/year/kW with both Hematite and Diaspore as degradation products (Spreadsheet "21-PWR-EDAII-A-0914_cor.xls ", Sheet "Tally-result", Row 162-171). As stated in Section 2, the "G" factor for nitric acid production ranges from 0.5 to 2.5. The "G" value used in deriving the quoted production rate was 1.0 but the results scale linearly with the "G" value. The production rates also scale linearly with time in years and the criticality power level in kW.

Table 6.1. Critical Configuration Parameters

| | Waste Package Configuration | | | |
|---|---|---|---|---|
| | Symmetric-Hematite | Symmetric-Hematite + Diaspore | Asymmetric-Hematite | Asymmetric-Hematite + Diaspore |
| Hematite Level[a] (cm) | 13.62160 | N/A[c] | 19.90699 | N/A |
| Hematite + Diaspore Level | N/A | 22.02201 | N/A | 27.95594 |
| Water Level for the Critical Configuration[a] (cm) | 36.20 | 47.00 | 71.2 | N/A |
| $k_{eff}$ for the Waste Package Lower Region[b] | 0.2217±0.0010 | 0.2799±0.0011 | 0.3789±0.0013 | 0.5881±0.0015 |
| $k_{eff}$ for the Waste Package Middle Region[b] | 0.7289+0.0019 | 0.6846±0.0018 | 0.6157±0.0017 | 0.3401±0.0014 |
| $k_{eff}$ for the Waste Package Top Region[b] | 0.0494±0.0004 | 0.0350±0.0004 | N/A | N/A |
| Track Length Estimator for $k_{eff}$ | 1.0000±0.0018 | 0.9995±0.0018 | 0.9946±0.0017 | 0.9281±0.0017 |
| Combined Estimator for $k_{eff}$ | 0.9995±0.0011 | 1.0009±0.0011 | 0.9945±0.0012 | 0.9285±0.0011 |
| Average Number of Neutrons Released per Fission | 2.5361±0.0091 | 2.5344±0.0091 | N/A | N/A |
| Average Energy Released per Fission (MeV) | 182.3374±0.6564 | 182.3296±0.6564 | N/A | N/A |
| Nitric Acid Production Rate[d] Moles/year/kW | 7.41E-03 | 4.07E-03 | N/A | N/A |

NOTES: [a] The levels of degradation products and water from the waste package center
[b] Track length estimator for $k_{eff}$
[c] Not applicable
[d] "21-PWR-EDAII-A-0914_cor.xls" (sheet "Tally-result")

The specie production rate scales as the number of fissions per unit interval and, thus, linearly for steady-state events. For a one kW average static criticality event extending over 10,000 years (maximum steady state duration assumed for consequence analyses), approximately 74 moles or 4.7 kg of $HNO_3$ could possibly be produced, assuming a "G" factor of 1.0. Uncertainty in the "G" factor results in a range of approximately 37 to 185 moles for the total acid production from such a hypothetical static criticality event.

The 74-mole quantity of $HNO_3$ from the hypothetical static criticality calculation compares to approximately 20moles of $HNO_3$ produced over 90,000 years at < 4 rad/hr from radionuclide decay (BSC 2001b, Section 6).

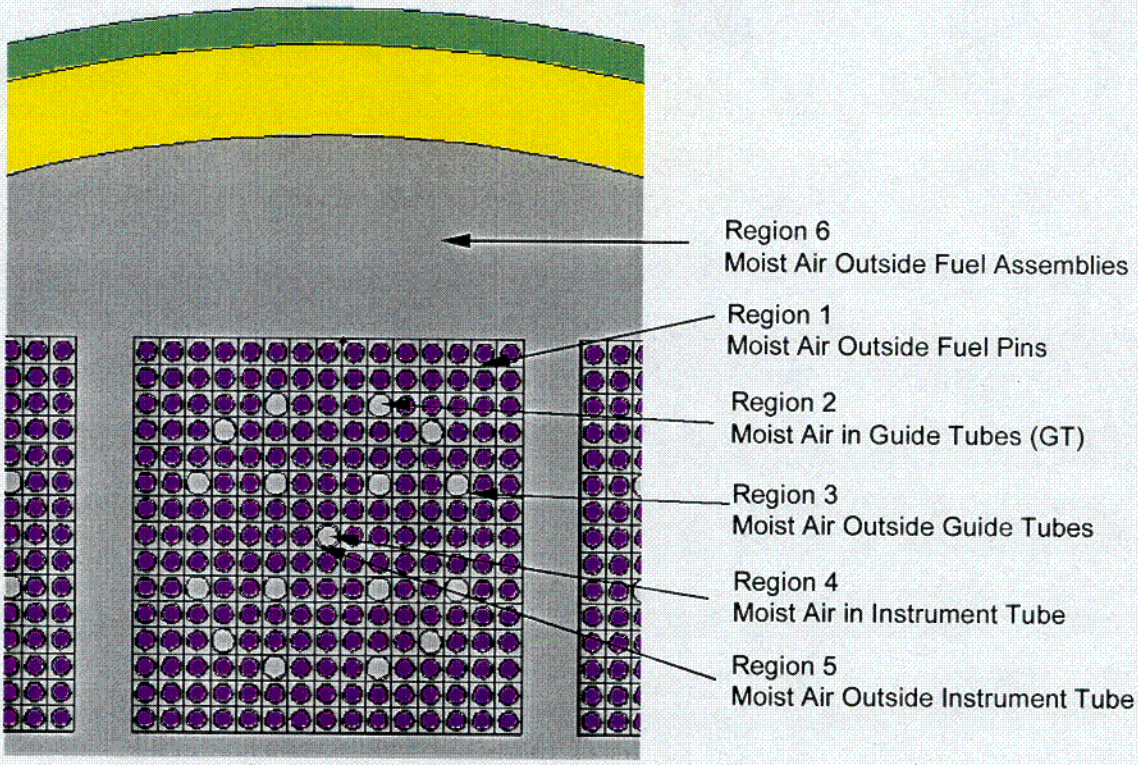


Figure 6.1. Tally Regions in MCNP Calculations

Table 6.2. Energy Deposition for the Symmetric Configuration with Hematite as the Degradation Product

| Moist Air Region | | Total | | Neutron | | Gamma | |
|---|---|---|---|---|---|---|---|
| Axial Location | Radial Location | ED (MeV/neutron) | Relative Error | ED (MeV/neutron) | Relative Error | ED (MeV/neutron) | Relative Error |
| Fuel pin end caps and spacers | 1 | 3.40E-07 | 0.0230 | 2.10E-07 | 0.0245 | 1.30E-07 | 0.0422 |
| | 2 | 2.83E-08 | 0.0426 | 1.83E-08 | 0.0420 | 1.01E-08 | 0.0913 |
| | 3 | 1.45E-08 | 0.0382 | 9.38E-09 | 0.0397 | 5.12E-09 | 0.0776 |
| | 4 | 1.13E-09 | 0.1646 | 7.04E-10 | 0.1670 | 4.26E-10 | 0.3361 |
| | 5 | 5.90E-10 | 0.1222 | 4.08E-10 | 0.1338 | 1.82E-10 | 0.2568 |
| | 6 | 8.63E-07 | 0.0210 | 4.42E-07 | 0.0212 | 4.21E-07 | 0.0349 |
| Fuel pin gas plenums | 1 | 2.63E-07 | 0.0275 | 1.53E-07 | 0.0264 | 1.10E-07 | 0.0532 |
| | 2 | 2.03E-08 | 0.0476 | 1.21E-08 | 0.0479 | 8.20E-09 | 0.0930 |
| | 3 | 1.02E-08 | 0.0428 | 6.39E-09 | 0.0440 | 3.76E-09 | 0.0870 |
| | 4 | 1.03E-09 | 0.1952 | 6.35E-10 | 0.2281 | 3.90E-10 | 0.3539 |
| | 5 | 5.92E-10 | 0.1335 | 3.87E-10 | 0.1330 | 2.04E-10 | 0.2923 |

C06

| Moist Air Region | Total | Neutron | Gamma | | | | |
|---|---|---|---|---|---|---|---|
| Axial Location | Radial Location | ED (MeV/neutron) | Relative Error | ED (MeV/neutron) | Relative Error | ED (MeV/neutron) | Relative Error |
| | 6 | 6.10E-07 | 0.0222 | 3.11E-07 | 0.0225 | 2.99E-07 | 0.0368 |
| Active fuel | 1 | 4.90E-05 | 0.0031 | 3.06E-05 | 0.0036 | 1.84E-05 | 0.0049 |
| | 2 | 3.90E-06 | 0.0047 | 2.55E-06 | 0.0049 | 1.35E-06 | 0.0092 |
| | 3 | 2.04E-06 | 0.0045 | 1.33E-06 | 0.0047 | 7.06E-07 | 0.0088 |
| | 4 | 1.80E-07 | 0.0152 | 1.25E-07 | 0.0151 | 5.46E-08 | 0.0352 |
| | 5 | 1.05E-07 | 0.0129 | 7.38E-08 | 0.0131 | 3.14E-08 | 0.0295 |
| | 6 | 1.03E-04 | 0.0033 | 5.44E-05 | 0.0036 | 4.87E-05 | 0.0053 |
| GT zone without fuel pins | Lattice cells other than GT cells | 1.22E-07 | 0.0467 | 6.83E-08 | 0.0472 | 5.37E-08 | 0.0842 |
| | 2 | 4.89E-09 | 0.0915 | 3.09E-09 | 0.0962 | 1.80E-09 | 0.1812 |
| | 3 | 2.88E-09 | 0.0859 | 1.83E-09 | 0.0989 | 1.05E-09 | 0.1574 |
| | Outside assemblies | 1.88E-07 | 0.0438 | 9.34E-08 | 0.0415 | 9.48E-08 | 0.0731 |
| Top end fittings | Entire | 9.11E-07 | 0.0369 | 4.01E-07 | 0.0375 | 5.09E-07 | 0.0541 |
| Above assemblies | Entire | 8.92E-07 | 0.0429 | 3.71E-07 | 0.0457 | 5.21E-07 | 0.0601 |
| Total | | 1.63E-04 | 0.0029 | 9.12E-05 | 0.0033 | 7.14E-05 | 0.0045 |

Table 6.3. Energy Deposition for the Symmetric Configuration with Hematite and Diaspore as Degradation Products

| **Moist Air Region** | | **Total** | | **Neutron** | | **Gamma** | |
|---|---|---|---|---|---|---|---|
| **Axial Location** | **Radial Location** | **ED (MeV/neutron)** | **Relative Error** | **ED (MeV/neutron)** | **Relative Error** | **ED (MeV/neutron)** | **Relative Error** |
| Fuel pin end caps and spacers | 1 | 2.25E-07 | 0.0270 | 1.30E-07 | 0.0302 | 9.52E-08 | 0.0457 |
| | 2 | 1.53E-08 | 0.0544 | 9.51E-09 | 0.0604 | 5.75E-09 | 0.1028 |
| | 3 | 8.09E-09 | 0.0523 | 4.89E-09 | 0.0607 | 3.20E-09 | 0.0925 |
| | 4 | 1.46E-09 | 0.1352 | 7.29E-10 | 0.1363 | 7.28E-10 | 0.2336 |
| | 5 | 8.31E-10 | 0.1088 | 5.04E-10 | 0.1315 | 3.27E-10 | 0.1878 |
| | 6 | 5.36E-07 | 0.0263 | 2.67E-07 | 0.0271 | 2.69E-07 | 0.0425 |
| Fuel pin gas plenums | 1 | 1.80E-07 | 0.0305 | 9.63E-08 | 0.0316 | 8.37E-08 | 0.0526 |
| | 2 | 1.14E-08 | 0.0613 | 6.53E-09 | 0.0664 | 4.92E-09 | 0.1109 |
| | 3 | 5.83E-09 | 0.0534 | 3.40E-09 | 0.0600 | 2.43E-09 | 0.0953 |
| | 4 | 1.66E-09 | 0.1440 | 1.10E-09 | 0.1784 | 5.52E-10 | 0.2437 |
| | 5 | 6.93E-10 | 0.1197 | 4.07E-10 | 0.1327 | 2.86E-10 | 0.2158 |
| | 6 | 3.85E-07 | 0.0277 | 1.91E-07 | 0.0293 | 1.94E-07 | 0.0447 |
| Active fuel | 1 | 3.19E-05 | 0.0035 | 1.83E-05 | 0.0041 | 1.35E-05 | 0.0054 |
| | 2 | 2.04E-06 | 0.0060 | 1.24E-06 | 0.0064 | 7.93E-07 | 0.0112 |
| | 3 | 1.11E-06 | 0.0056 | 6.69E-07 | 0.0060 | 4.38E-07 | 0.0103 |
| | 4 | 2.76E-07 | 0.0137 | 1.53E-07 | 0.0140 | 1.23E-07 | 0.0250 |
| | 5 | 1.63E-07 | 0.0122 | 8.95E-08 | 0.0122 | 7.37E-08 | 0.0223 |
| | 6 | 5.17E-05 | 0.0044 | 2.72E-05 | 0.0049 | 2.45E-05 | 0.0068 |

| Moist Air Region | | Total | | Neutron | | Gamma | |
|---|---|---|---|---|---|---|---|
| **Axial Location** | **Radial Location** | **ED (MeV/neutron)** | **Relative Error** | **ED (MeV/neutron)** | **Relative Error** | **ED (MeV/neutron)** | **Relative Error** |
| GT zone without fuel pins | Lattice cells other than GT cells | 6.86E-08 | 0.0586 | 3.64E-08 | 0.0622 | 3.22E-08 | 0.0984 |
| | 2 | 2.99E-09 | 0.1185 | 1.67E-09 | 0.1378 | 1.31E-09 | 0.2041 |
| | 3 | 1.39E-09 | 0.1060 | 7.33E-10 | 0.1191 | 6.61E-10 | 0.1799 |
| | Outside assemblies | 1.21E-07 | 0.0540 | 4.77E-08 | 0.0567 | 7.28E-08 | 0.0768 |
| Top end fittings | Entire | 4.62E-07 | 0.0476 | 1.97E-07 | 0.0476 | 2.66E-07 | 0.0695 |
| Above assemblies | Entire | 3.67E-07 | 0.0576 | 1.48E-07 | 0.0616 | 2.19E-07 | 0.0798 |
| **Total** | | 8.95E-05 | 0.0036 | 4.89E-05 | 0.0041 | 4.06E-05 | 0.0054 |

# 7. REFERENCES

## 7.1 DOCUMENTS CITED

Audi, G. and Wapstra, A.H. 1995. *Atomic Mass Adjustment, Mass List for Analysis.* [Upton, New York: Brookhaven National Laboratory, National Nuclear Data Center]. TIC: 242718.

BSC (Bechtel SAIC Company) 2001a. *Technical Work Plan for: Waste Package Design Description for LA.* TWP-EBS-MD-000004 REV 01. Las Vegas, Nevada: Bechtel SAIC Company. ACC: MOL.20010702.0152.

BSC (Bechtel SAIC Company) 2001b. *Gamma and Neutron Radiolysis in the 21-PWR Waste Package.* CAL-MGR-NU-000006 REV 00. Las Vegas, Nevada: Bechtel SAIC Company. ACC: MOL.20010522.0198.

Briesmeister, J.F., ed. 1997. *MCNP-A General Monte Carlo N-Particle Transport Code.* LA-12625-M, Version 4B. Los Alamos, New Mexico: Los Alamos National Laboratory. ACC: MOL.19980624.0328.

CRWMS M&O 1997. *Criticality Evaluation of Degraded Internal Configurations for the PWR AUCF WP Designs.* BBA000000-01717-0200-00056 REV 00. Las Vegas, Nevada: CRWMS M&O. ACC: MOL.19971231.0251.

CRWMS M&O 1998a. *Software Qualification Report for MCNP Version 4B2, A General Monte Carlo N-Particle Transport Code.* CSCI: 30033 V4B2LV. 30033-2003 Rev. 01. Las Vegas, Nevada: CRWMS M&O. ACC: MOL.19980622.0637.

CRWMS M&O 1998b. *Supplemental Criticality Evaluation for Degraded Internal Configurations of a 21 PWR Waste Package.* BBA000000-01717-0210-00022 REV 00. Las Vegas, Nevada: CRWMS M&O. ACC: MOL.19980918.0086.

CRWMS M&O 1998c. *Software Code: MCNP.* 4B2LV. HP. 30033 V4B2LV.

CRWMS M&O 1999a. *PWR Source Term Generation and Evaluation.* BBAC00000-01717-0210-00010 REV 01. Las Vegas, Nevada: CRWMS M&O. ACC: MOL.20000113.0333.

CRWMS M&O 1999b. *Output Files for PWR Source Term Generation and Evaluation.* BBAC00000-01717-0210-00010 REV 01. Las Vegas, Nevada: CRWMS M&O. ACC: MOL.19991111.0702.

CRWMS M&O 2000a. *Total System Performance Assessment for the Site Recommendation.* TDR-WIS-PA-000001 REV 00 ICN 01. Las Vegas, Nevada: CRWMS M&O. ACC: MOL.20001220.0045.

CRWMS M&O 2000b. *Summary of In-Package Chemistry for Waste Forms.* ANL-EBS-MD-000050 REV 01. Las Vegas, Nevada: CRWMS M&O. ACC: MOL.20010129.0134.

CRWMS M&O 2000c. *Waste Form Degradation Process Model Report.* TDR-WIS-MD-000001 REV 00 ICN 01. Las Vegas, Nevada: CRWMS M&O. ACC: MOL. 20000713.0362.

CRWMS M&O 2000d. *Clad Degradation - FEPs Screening Arguments.* ANL-WIS-MD-000008 REV 00 ICN 01. Las Vegas, Nevada. CRWMS M&O. ACC: MOL.20001208.0061.

CRWMS M&O 2000e. *Design Analysis for UCF Waste Packages.* ANL-UDC-MD-000001 REV 00. Las Vegas, Nevada: CRWMS M&O. ACC: MOL.20000526.0336.

CRWMS M&O 2001a. *FEPs Screening of Processes and Issues in Drip Shield and Waste Package Degradation.* ANL-EBS-PA-000002 REV 01. Las Vegas, Nevada: CRWMS M&O. ACC: MOL.2000216.0004.

DOE (U.S. Department of Energy) 1987. *Appendix2A, Physical Descriptions of LWR Fuel Assemblies.* Volume 3 of *Characteristics of Spent Fuel, High-Level Waste, and Other Radioactive Waste Which May Require Long-Term Isolation.* DOE/RW-0184. Washington, D.C.: U.S. Department of Energy, Office of Civilian Radioactive Waste Management. ACC: HQX.19880405.0024.

Kugler, A. 1996. *Bohler Neutronit A976 Sheet and Plate for Nuclear Engineering.* Murzzuschlag, Austria: Bohler Bleche GmbH. TIC: 240558.

Parrington, J.R.; Knox, H.D.; Breneman, S.L.; Baum, E.M.; and Feiner, F. 1996. *Nuclides and Isotopes, Chart of the Nuclides.* 15th Edition. San Jose, California: General Electric Company and KAPL, Inc.. TIC: 233705.

Punatar, M.K. 2001. *Summary Report of Commercial Reactor Criticality Data for Crystal River Unit 3.* TDR-UDC-NU-000001 REV 02. Las Vegas, Nevada: Bechtel SAIC Company. ACC: MOL.20010702.0087.

Reamer, C.W. and Williams, D.R. 2000. Summary Highlights of NRC/DOE Technical Exchange and Management Meeting on Subissues Related to Criticality. Meeting held October 23-24, 2000, Las Vegas, Nevada. Washington, D.C.: U.S. Nuclear Regulatory Commission. ACC: MOL.20001208.0097 through MOL.20001208.0110.

Reed, D.T. and Van Konynenburg, R.A. 1988. "Effect of Ionizing Radiation on Moist Air Systems." *Scientific Basis for Nuclear Waste Management XI, Symposium held November 30-December 3, 1987, Boston, Massachusetts.* Apted, M.J. and Westerman, R.E., eds. *112,* 393-404. Pittsburgh, Pennsylvania: Materials Research Society. TIC: 203662.

Reed, D.T. and Van Konynenburg, R.A. 1991. "Effect of Ionizing Radiation on the Waste Package Environment." *High Level Radioactive Waste Management, Proceedings of the Second*

*Annual International Conference, Las Vegas, Nevada, April 28-May 3, 1991. 2,* 1396-1403. La Grange Park, Illinois: American Nuclear Society. TIC: 204272.

Shoesmith, D.W. and King, F. 1998. *The Effects of Gamma Radiation on the Corrosion of Candidate Materials for the Fabrication of Nuclear Waste Packages.* AECL-11999. Pinawa, Manitoba, Canada: Atomic Energy of Canada Limited. ACC: MOL.19990311.0212.

YMP (Yucca Mountain Site Characterization Project) 2000. *Disposal Criticality Analysis Methodology Topical Report.* YMP/TR-004Q, Rev. 01. Las Vegas, Nevada: Yucca Mountain Site Characterization Office. ACC: MOL.20001214.0001.

## 7.2 INPUT DATA BY DATA TRACKING NUMBER

MO0003RIB00071.000. Physical and Chemical Characteristics of Alloy 22. Submittal Date: 02/25/2000.

MO0003RIB00076.000. Physical and Chemical Characteristics of Type 316N Grade Stainless Steel. Submittal Date: 03/09/2000.

MO9906RIB00048.000. Waste Package Material Properties: Waste Form Materials. Submittal Date: 04/10/2001.

MO9906RIB00054.000. Waste Package Material Properties: Structural Materials. Submittal Date: 04/10/2001.

## 7.3 CODES, STANDARDS, REGULATIONS, AND PROCEDURES

AP-3.12Q, Rev. 0, ICN 4. *Calculations.* Washington, D.C.: U.S. Department of Energy, Office of Civilian Radioactive Waste Management. ACC: MOL.20010404.0008.

AP-3.15Q, Rev. 3. *Managing Technical Product Inputs.* Washington, D.C.: U.S. Department of Energy, Office of Civilian Radioactive Waste Management. ACC: MOL.20010801.0318.

AP-SI.1Q, Rev. 3, ICN 1, ECN 1. *Software Management.* Washington, D.C.: U.S. Department of Energy, Office of Civilian Radioactive Waste Management. ACC: MOL.20010705.0239.

ASME (American Society of Mechanical Engineers) 1998. *1998 ASME Boiler and Pressure Vessel Code.* 1998 Edition with 1999 and 2000 Addenda. New York, New York: American Society of Mechanical Engineers. TIC: 247429.

ASTM A 887-89. 1992. *Standard Specification for Borated Stainless Steel Plate, Sheet, and Strip for Nuclear Application.* Philadelphia, Pennsylvania: ASTM. TIC: 245311.

SAE 1993. *Metals & Alloys in the Unified Numbering System.* 6th Edition. Warrendale, Pennsylvania: Society of Automotive Engineers. TIC: 243414.

## ATTACHMENTS

A list of attachments to this calculation is provided below.

I. List of files on CD-ROM (Attachment II).

II. CD-ROM with data files for calculation.